

ARL66 0118

OFFICE OF AEROSPACE RESEARCH

AD 638530

Contract AF 61(052)-449

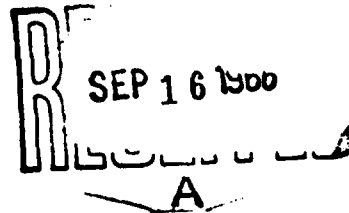
20 April 1966

FINAL REPORT

AN INVESTIGATION OF CRYSTAL
IMPERFECTIONS BY X-RAY DIFFRACTION



By A. R. Lang



CLEARINGHOUSE FOR FEDERAL SCIENTIFIC AND TECHNICAL INFORMATION		
Hardcopy	Microfiche	
\$ 4.00	\$ 1.00	134 <i>12</i>
1 ARCHIVE COPY		

University of Bristol

H. H. Wills Physics Laboratory
Royal Fort
Bristol 2

Best Available Copy

Contract
AF 61(052)-449

20 April 1966

FINAL REPORT

AN INVESTIGATION OF CRYSTAL IMPERFECTIONS
BY X-RAY DIFFRACTION

A. R. LANG

H.H. WILLS PHYSICS LABORATORY
UNIVERSITY OF BRISTOL
BRISTOL 2, ENGLAND

The research reported in this document has been sponsored in whole or in part by the Aerospace Laboratories, OAR, under Contract AF 61(052)-449 through the European Office of Aerospace Research (OAR), United States Air Force.

TABLE OF CONTENTS

	page
1. INTRODUCTION AND DESCRIPTION OF TECHNIQUES	
1.1. The Scope of the Investigation	1
1.2. Plan of this Report	7
1.3. Summary of Experimental Methods	
1.3.1. Apparatus	9
1.3.2. Photographic technique	15
1.3.3. Quality and resolution of X-ray topographs	22
2. STUDIES OF MATERIALS	
2.1. Natural Diamond.	
2.1.1. Types of lattice imperfection in natural diamond	36
2.1.2. Dislocations and trigons	39
2.1.3. Low-relief surface features	40
2.1.4. Precipitates and decorated dislocations	42
2.1.5. X-ray Bragg reflection, 'spike' reflection and ultra-violet absorption topography	42
2.1.6. The structure of nitrogen platelets in diamond	44
2.1.7. Coated diamonds	47
2.1.8. Planar growth defects in diamond	49
2.1.9. Imperfections in Type II diamonds	50
2.1.10. Radiation damage in diamond	52
2.1.11. Abrasion of diamond	54
2.2. Synthetic Diamond	59
2.3. Silicon	
2.3.1. The origin of dislocations in melt-grown silicon	62
2.3.2. Dislocation configurations in a very lightly deformed silicon crystal	64
2.4. Germanium	
2.4.1. Dislocation configurations in melt-grown crystals	66
2.4.2. Deformation of germanium	68
2.4.3. Heavily-doped germanium	70
2.5. Indium Antimonide	
2.5.1. Determination of the absolute configuration of the structure	71
2.5.2. Deformation of indium antimonide	74
2.6. Lithium Fluoride	
2.6.1. Origin of dislocations in lithium fluoride	75
2.6.2. Radiation damage	79
2.7. Magnesium Oxide	82
2.8. Aluminum	83
2.9. Corundum and Ruby	86

	page
2.10. Quartz	
2.10.1. Defects in oscillator-grade quartz	87
2.10.2. Amethyst quartz	95
2.11. Organic Crystals	97
3. X-RAY DIFFRACTION PHENOMENA IN PERFECT CRYSTALS	
3.1. Pendellösung Interference	100
3.2. Coherent Simultaneous Reflection	107
4. DIFFRACTION CONTRAST FROM IMPERFECTIONS IN NEARLY PERFECT CRYSTALS	
4.1. Diffraction Contrast without Interbranch Scattering	109
4.2. Diffraction Contrast with Interbranch Scattering	117
REFERENCES	122
LIST OF REPRINTS	125
REFERENCES	125

ILLUSTRATIONS

Fig. 1. View of Apparatus	following page 9
Fig. 2. Part of Projection Topograph of Plate of Lithium Fluoride, 200 Reflection, MoK α_1 Radiation, X200	" " 33

1. INTRODUCTION AND DESCRIPTION OF TECHNIQUES

1.1. The Scope of the Investigation.

This Report records the main results of a five-year research program. The twin aims of the program were, on the one hand, to advance understanding in the fundamental physics of the diffraction of X-rays by perfect and nearly perfect crystals and, on the other hand, to apply the X-ray topographic technique to a wide variety of problems involving lattice imperfections in crystals. Efforts were made to maintain a balanced, parallel development of both the more theoretical and the more practical aspects of the work. Indeed, in some parts of the research, such as those performed on silicon, germanium and indium antimonide, the study of diffraction phenomena and the analysis of dislocation configurations were pursued simultaneously in the natural course of evolution of the investigation. Whereas it was demonstrated that in many problems X-ray topography may be applied in a quite straightforward manner as a tool for revealing dislocations and other lattice defects, requiring only a minimal reference to the underlying diffraction theory, it was also abundantly shown that a thorough understanding of diffraction theory is necessary if correct interpretations are to be made in the more refined studies, and if X-ray experiments are to be designed to give the maximum information yield. These practical considerations alone would justify a substantial theoretical effort, quite apart from the intrinsic interest of some of the diffraction problems encountered.

Until about eight years ago, it was accepted that the diffraction of X-rays by perfect crystals was adequately described by the theories of Darwin, Ewald and von Laue. (For a readable, introductory account of these theories see James (1948)). They had been tested only in a limited way, firstly by observing that some of the most perfect crystals did give integrated reflections of the low value predicted by theory, and secondly by studying rocking curves obtained with the double-crystal spectrometer and finding that some crystals could exhibit nearly total reflection in a very narrow angular range in the way predicted for the 'perfect' crystal.

(These experiments are reviewed in James (1948) and Compton and Allison (1960)). With the advent of new techniques of high-resolution X-ray topography, and of transmission X-ray topography in particular, new kinds of diffraction experiment were performed which soon revealed phenomena not predicted by the early theories. These phenomena have demanded for their understanding a fresh examination of some of the basic optical assumptions involved in the accepted theories. The required recasting of the 'plane-wave' theories of Ewald and von Laue in the form necessary to take account of the 'coherent spherical wave' illumination of the crystal that applies in most X-ray topographic experiments, and the analysis of many of the effects stemming from this difference in illumination conditions, have been the special contribution of Professor N. Kato in this field. His papers provide the best available background treatments to the theory of X-ray topography. One result of Kato's work has been the demonstration of essential differences between the diffraction conditions of X-ray topography and of thin-film transmission electron microscopy. This and other topics in diffraction theory are discussed in a useful review (Kato, 1963 a).

Since X-ray topographic studies of dislocations form a central theme in the research here described, some brief remarks on the relation between the X-ray method and other methods of rendering individual dislocations visible may be useful. (Several comprehensive reviews of methods of observing individual dislocations are now available, for example, Johnston (1961), Newkirk and Wernick (1962), Amelinckx (1964).)

Dislocations may be made visible optically by 'decoration' techniques in which minute precipitates are formed along the dislocation lines. The precipitates are seen because of their opacity to the radiation used, or by their light-scattering if they are of sub-microscopic size. The method is restricted to materials which are normally transparent to light or at least to radiations in the near infra-red and ultra-violet with which microscope images can be formed. Precipitation on the dislocations obviously changes the state of the crystal lattice profoundly, the process is generally irreversible, and so no sequences of experiments can be made on the same

specimen in order to slow, for example, the multiplication and movement of dislocations.

The etch-pit method is of wider application, since it can be used on both transparent and opaque substances; but for each substance a specific dislocation-etch must be developed. Uncertainty can often arise concerning how truly there is a one-to-one correspondence between etch-pits and dislocation outcrops. Indeed, diffraction methods for observing dislocations may have to be called in to resolve this doubt. The major limitation of the etch-pit method is its restriction to the study of surfaces. The distribution of dislocations within the volume of the specimen can be found by a series of polishing and etching experiments, but this process of course destroys the specimen.

The diffraction methods (electron and X-ray) are much more general in application. The visibility of dislocations arises because the strain field of the dislocation in the crystal lattice causes a significant change in the diffraction behaviour of the crystal regions close to the dislocation compared with regions remote from it. Under properly chosen experimental conditions this 'diffraction contrast' may be made strong, so that a clear image of the dislocation line (strictly, of a certain volume surrounding the line) can be recorded photographically. This contrast does not depend directly upon the chemical nature of the specimen material. It does depend in its detailed manifestations upon the scattering and absorbing powers of the specimen and its thickness, in both the X-ray and electron cases, but these variations are now fairly well understood. Hence the same diffraction theory and interpretative technique may be applied to all crystals. This fortunate circumstance facilitates the speedy application of the diffraction methods to new problems and materials, and to the comparison of dislocation behaviour in different materials.

The electron microscope method of observing dislocations enjoys the great magnifying power of that instrument. The images of dislocations are typically about 100 Angstroms in width. The X-ray topograph, on the other hand, is an unmagnified image of the specimen and must be photomicrographically enlarged, a procedure that is time-consuming and requiring of considerable care in order to get the best results. Moreover,

several factors conspire together to impose a practical resolution limit of about one micron in X-ray topographic work. It follows that X-ray topography cannot compete at all with electron microscopy where resolution is concerned. Its most fruitful fields of application therefore lie especially with crystals of low dislocation density, below 10^6 to 10^7 lines per cm^2 .

Now one of the discoveries emerging from transmission X-ray topography has been the number and variety of crystal species containing specimens with dislocation densities sufficiently low for X-ray topographic observations to be made of individually resolved dislocations within them. Low densities have been found not only in specimens of natural diamond, calcite and quartz, the three species which were reputed as being capable of behaving as perfect crystals, but also in such laboratory-grown materials as metal single crystals. That pure semiconductor crystals should behave as highly perfect crystals, and upon occasion possess vanishingly low dislocation densities, was a not unexpected finding since information on their dislocation densities was available from reliable dislocation etching techniques. It was indeed at the stage of development of semi-conductor crystal-growing when dislocation densities down to about 10^4 lines per cm^2 had been reported that the author turned to examine these materials with his topographic techniques. The aim was to see what point-by-point variations in X-ray reflecting power were produced by local fluctuations in dislocation density when the mean density was as low as 10^4 lines per cm^2 . The result was the discovery that images of individual dislocations could be recorded (Lang, 1958).

Good X-ray topographs of crystals are only obtained when the crystals are carefully handled so that deformation of a major part of the specimen, elastic or plastic, is avoided. The sensitivity with which local damage on crystal surfaces is revealed by X-ray diffraction contrast has formed the basis of X-ray topographic studies of the processes of abrasion, and on the deformation of the substrate by surface deposits. Investigations of abraded surfaces and of fracture surfaces have been

pursued in some detail. The study of strains produced by deliberately applied surface deposits is just beginning. Meanwhile, the domain of materials on which X-ray topographic studies of individual dislocations may be performed continues to expand. Experience suggests that almost any pure, stable compound, organic as well as inorganic, can produce crystals of low dislocation density when these are grown with reasonable care. Thus the properties of dislocations in complex structures are now open to investigation.

Study of the growth history of crystals remains a staple application of X-ray topography. The ability to sample a large crystal volume and present on a single topographic record the variation of imperfection content over a distance in the crystal corresponding to a substantial epoch in its growth history facilitates the correlation of changes in type and density of imperfection with changes in conditions of growth. In studies of natural crystals one may hope to gain an insight into the circumstances under which they grew, circumstances possibly very different from normal laboratory conditions. Diamond has been the natural crystal most extensively examined so far. Natural and synthetic quartz, and the amethyst variety of quartz, have also been investigated to a considerable degree, and they are giving strong indications that they contain defects equalling in interest and complexity those already found in diamond. The development of dislocation configurations during the course of growth of large single crystals has been studied in silicon, lithium fluoride and synthetic quartz. For this investigation, specimens are prepared from slices cut out of a large boule or ingot. Additional information on the origin of imperfections can be gained by comparing crystals grown under conditions differing in a known and carefully controlled way. Except for a series of experiments on aluminum, no research involving the intimate combination of a crystal-growing program with X-ray topographic analysis of the quality of crystals produced has yet been undertaken in the author's laboratory. This deficiency does not arise from any lack of feasibility or usefulness of such a course of research, but simply from a shortage of time and personnel which has tended to concentrate efforts on 'ready-made' crystals, either those produced by

Nature, or by other laboratories.

Two other lines of research whose feasibility has been well demonstrated in exploratory experiments, but which remain to be fully developed in extended research programs, are studies of dislocation motion and of radiation damage. X-ray topography has two notable advantages to offer when employed as the major experimental method in such investigations. Firstly, the experiments can be performed on specimens sufficiently thick to be fully representative of the bulk material. The proximity of surfaces strongly affects dislocation configurations in crystals in which dislocations move easily. It also affects the concentration of defects such as vacancies which are produced on irradiation. A number of cases is known in which experimental methods which look only at surfaces or at thin films fail to give a true picture of conditions in the bulk material, or are strongly suspected of failing to do so. With X-ray topography no such doubts exist. This advantageous characteristic to some extent offsets the low resolution of the X-ray method. Secondly, X-ray topographic experiments, being quite non-destructive, are repeatable at will. It is thus possible to follow stages in the deformation of large specimens. It is also possible to make extended series of experiments on one and the same specimen, involving, say, annealing, neutron irradiation, and step-by-step annealing of radiation damage. Studies of dislocation movements have been made in aluminum, germanium, and, to a lesser degree, in lithium fluoride. Studies of neutron irradiation damage have been performed in some detail on lithium fluoride; similar studies on diamond have commenced.

During the course of the studies of crystal growth and imperfection content, and of deformation and irradiation, a wide variety of phenomena have been observed for the first time. In many cases it would be desirable to follow up these observations by more extensive research. Consequently, few of the lines of investigation described in the following pages can be regarded as fully explored: more often they indicate promise for future profitable work.

1. 2.

Plan of this Report

As already mentioned, the research here reported divides itself roughly into two classes, (a) studies of fundamental phenomena of X-ray diffraction in perfect and nearly perfect crystals, and (b), practical applications of the X-ray topographic techniques to crystal imperfection studies. It would seem logical to commence this Report with a discussion of the fundamentals and then follow with an account of the applications. However, the reverse course has been followed, for the reasons here given. A number of projects falling under the classification "Studies of Materials" have been satisfactorily completed, and a fair proportion of this completed work has been published. This work is described first, so that the major results of the research, from which quantitative and definitive conclusions have been drawn, can be discovered without first traversing discussions of theoretical matters. It is helpful in this connection that, as pointed out in Section 1. 1, practical use of X-ray topographic techniques can often be made without reference to much diffraction theory. At points where the discussions of crystal imperfections presented in Sections 2. 1 through 2. 11 unavoidably involve questions of diffraction theory, cross-references are given to later sections of the Report.

Section 3 deals with a range of diffraction phenomena. These concern aspects of diffraction behaviour characteristic of perfect crystals, and most of them involve those parts of X-ray diffraction theory which have had to be revised or extended as a consequence of X-ray topographic experiments.

The diffraction processes which underlie experimental observations of X-ray diffraction contrast from imperfections are described in Section 4. These important matters have had to be discussed mainly in a rather qualitative and descriptive way, for it is in this branch of the present research that there remain many unfinished investigations and unanswered questions. To simplify the picture, only a limited range of the great variety of diffraction phenomena accompanying the topographic observation of lattice defects is given other than brief mention. It is hoped

that this restriction will enable the general perspective to be grasped more easily, and will help to show that although rigorous and quantitative theory is often still lacking, the general phenomenology of the imaging of lattice defects is reasonably well understood.

About one third of the research done during the period covered by this Report has been published in scientific journals. The majority of papers are concerned with topics falling under Section 2. Thus a number of sub-sections of Section 2 need do little more than serve as introductions to the published papers. Since these papers contain the illustrations without which the work cannot properly be understood, reprints from the journals are included in this Report. For convenience they are bound together at the end of the Report, but they should be considered as an integral part of the text. These eighteen reprints are arranged in sequence in order of date of publication rather than according to topic, but reference to them from any point in the text should be made without difficulty since they have each been numbered on their front page. For brevity, reference to particular points in a published paper included as a reprint will usually be given by citing the reprint number rather than the authors' and journal reference, i.e. 'R18, Fig. 4a' rather than Authier, Rogers and Lang, Phil. Mag. 12 (1965) 547, Fig. 4a'.

The experimental techniques upon which the research is based were developed in the years 1955 to 1958. Developments since then, though important, have been in the nature of refinements rather than radical innovations. Published accounts of the techniques have been brief, and concerned chiefly with the geometrical principles of the diffraction geometry rather than their practical embodiments and the manipulative and photographic procedures they involve. It is thus appropriate to give now a summary of those aspects of the experimental method that have not been published and to explain some of the factors which control the quality and resolution of X-ray topographs.

1. 3. Summary of Experimental Methods

1. 3. 1. Apparatus. A general view of the apparatus is shown in Figure 1. The X-ray source is inside the vertical tower on the left of the picture. On either side of the source are placed the special X-ray goniometers used in topographic studies. Figure 1 shows one of two similar installations: there are four goniometers altogether in operation. The X-ray beam leaving the source is directed along the axis of a lead conduit of rectangular cross-section and then is transmitted through the incident-beam slit assembly located under the lead housing indicated at A in Figure 1. This slit assembly defines both the height and width of the beam. The height is continuously variable and is adjusted by movement of sliding tantalum shutters so as to correspond to the height of the specimen it is desired to investigate. The maximum beam height is about 25 mm. The beam width is determined by which member of a set of pre-set slits is put in position. Standard values of beam width are 12 microns, 100 microns and 175 microns. Factors determining choice of beam width in a particular experiment are discussed below. The distance from the X-ray source to the beam-width defining slit is 40 cm.

The specimen, B in Figure 1, is placed approximately over the rotation axis of the goniometer. This axis is about 4 cm. from the exit slit in the slit assembly at A. The specimen is usually in the shape of a plate and is mounted by wax inside an annulus of lead or aluminum. The annulus is attached to a small bracket fixed to the top of a standard goniometer head. The arcs of the goniometer head allow rotation of the specimen about two horizontal axes by $\pm 30^\circ$. Holes regularly spaced around the annulus enable the specimen to be rotated in its own plane by larger angles. The holes are usually spaced so that this rotation can be made in steps of 30° , 45° or 60° , depending upon the symmetry of the crystal and the number of Bragg reflections it is desired to investigate. The goniometer arcs are attached to circular discs that fit flush into the top of the platform of the traversing mechanism. Surrounding the disc is a 360° scale which enables the plane of the annulus to be set at any desired angle with the direction of the motion of the traversing mechanism.

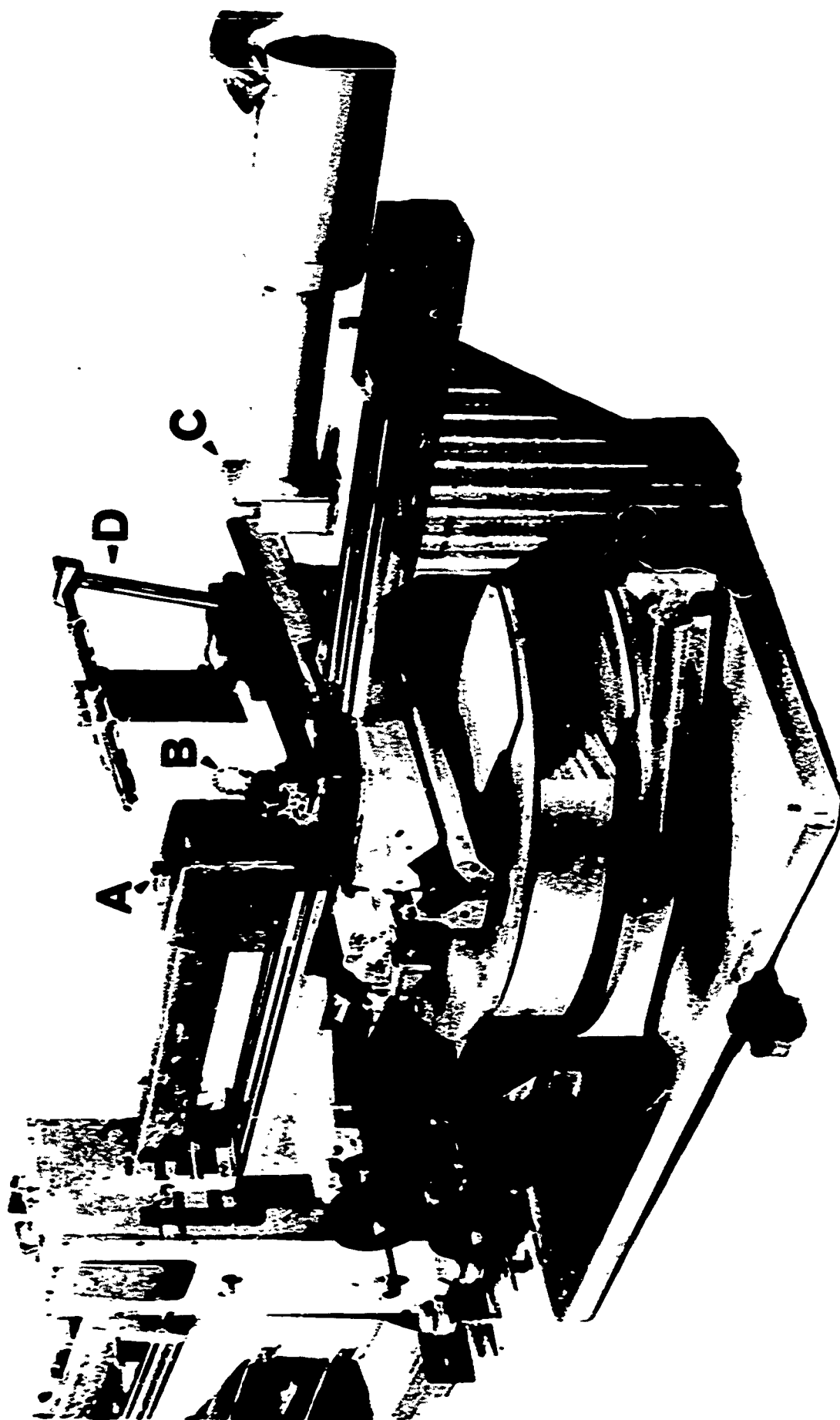


Fig. 1

X-rays diffracted by the specimen are detected by the scintillation counter C in Figure 1. The counter housing slides on the optical ways which top the substantial 'detector-arm' of the goniometer. The bearings of the detector-arm are coaxial with, and surround, those of the central spindle carrying the traversing mechanism. A second arm, called the 'slit-arm', is topped by similar optical ways as those of the detector-arm and it carries the diffracted-beam slit assembly D. The slit-arm is carried by the detector-arm on a sleeve bearing. Thus, the angle between them is variable at will. Usually it is kept at 90° . The counter C and the slit assembly D can be interchanged between the detector-arm and slit-arm if required. This enables high diffraction angles on either side of the direct beam to be recorded.

From the slit assembly D hang a pair of tantalum plates. In the standard topographic techniques it is arranged that the diffracted beam of a given Bragg reflection, and this beam only, passes through the gap between the plates before it reaches the recording photographic emulsion. In order to accomplish the setting of this gap positively and speedily, the assembly D has a number of easily-made adjustments. Firstly, the whole assembly slides on the optical ways of the slit arm and can be clamped in position at any point on the ways. In Figure 1 it is shown drawn right back, away from the X-ray beam, so that the specimen and its mount may be seen. The hanging tantalum plates are provided with small balancing weights (hidden in Fig. 1) which can be adjusted to ensure that they hang in a plane normal to the diffracted beam. The gap between the plates is set by a fine differential screw. After the slits have been set approximately in the right position by sliding the whole slit assembly along the ways of the slit-arm, the fine adjustment of their position to make their gap just straddle the diffracted beam is effected by a micrometer screw. The distance between the hanging slits and the specimen is adjustable over a range of about 2 cm by a spring-loaded screw which rocks the near-vertical supporting shaft about a pivot parallel to the optical ways. Adjustment over a wider range is obtained by unclamping the supporting shaft from its pivot.

The recording medium used in X-ray topography is usually Ilford Nuclear Emulsion. The emulsion, coated on a glass plate $1\frac{1}{2}$ inches by 1 inch, is mounted in a cassette. The cassette stands on the platform of the traverse unit. It is placed between the hanging slits, D, and the counter, C, as near as possible to the former so as to minimise the distance between the specimen and the plate. No cassette was in position when the photograph reproduced in Figure 1 was taken so that the view of the specimen and the hanging slits should not be obstructed.

Similar mechanisms control the angular adjustment of rotation about the goniometer axis for both the central spindle upon which the linear traversing mechanism is fitted and for the cylinder which carries the detector arm. Each rotating member carries large gear wheels of 720 teeth (64 pitch). Radius arms may be latched into the gear teeth at any position. This latching operation sets the angle to the nearest half degree, the angle being read off from a revolution counter. For fine adjustment, tangent screws are used. Attached to the tangent screws are embossed drums $2\frac{1}{2}$ inches in diameter. These may be seen on the left in Figure 1. One revolution of the screw corresponds to 0.1° . The drums are divided into a scale reading from zero to 360, and thus indicate seconds of arc directly. A subsidiary counter, geared to the micrometer spindle, reads in hundredths of a degree. The fine control of angles, performed by easily accessible and controllable drums giving a direct reading in seconds of arc, has proved of inestimable value throughout the use of the goniometers. The performance of the goniometer bearings enables small drum rotations corresponding to fractions of a second of arc to be followed smoothly and faithfully.

The topographic technique most frequently used in the research which is described in this Report is that of the 'projection topograph' (Lang 1959a). In this technique, the specimen is mounted on an accurate linear traversing mechanism and is moved to and fro during the course of the experiment so that it is scanned by the collimated incident beam. The effect is as if a large source of X-rays were present a very long distance from the specimen, ensuring that the whole area of specimen to be

examined is bathed in a uniform, parallel beam. In the projection topograph, Bragg-reflected rays transmitted through the specimen are recorded, and information is gained about the whole interior state of the specimen. The same mechanical arrangement can, of course, be used to study surface reflections from large areas of specimen. The diffraction geometry of reflection scanning techniques, and a variety of their applications using the apparatus of Figure 1, were reported some years ago but have only been published in summary (Lang, 1957a). Reflection scanning topographs have been used in the work described in this Report in instances when surface damage, or the outcrops of defects at surfaces, were the subject of investigation.

The linear traversing mechanism is designed on kinematic principles. The platform carrying the specimen has on its under side five Teflon balls. These ride on a smooth, square-section bar (the near end of which is clearly visible in Figure 1) and on a precision flat (hidden from view in Figure 1). Also attached to the under side of the platform are two plane-ended rods which fit (with about 0.001" clearance) over balls attached to both the spindle end and thimble end of a micrometer head whose barrel is attached to the base of the traversing mechanism. The micrometer is driven by a Synchro through a reduction gear. This Synchro is paired with another Synchro mounted remotely in the Goniometer Control Unit (not shown in Figure 1). The operations of starting, stopping, reversing, changing speed and changing traverse limits are all performed at the Control Unit. This arrangement has the great advantages that (1) the minimum of mechanical and electrical devices is mounted close to the specimen, thus reducing sources of heat and vibration close to the specimen, and (2) no impulses are given to the traversing mechanism, either by reversing-switch contacts, or by handling in gear changing, etc., which might disturb the angular setting, or otherwise upset the specimen. The absence of the requirement to make adjustments on the traversing mechanism itself carries also the incidental advantage of reducing opportunities for accidentally putting hands or fingers in the path of the X-ray beam. Although the motion of the traversing platform is remotely controlled, its position is always accurately known. A revolution counter, reading in thousandths of an inch, is placed in an easily readable position

on the traversing mechanism. The maximum range of scanning is about 23 mm. Since the maximum beam height is about 25 mm it follows that it is possible to scan an area of 25 mm X 23 mm. almost one inch square, on a single topograph.

When the traversing platform is stationary, the 'still' picture obtained is called a 'section topograph'. Indeed, the 'projection topograph' may be regarded as built up from the superimposition of many such 'stills'. The diffraction geometry of the 'section topograph', and some of its applications, have been described (Lang 1957b). Section topographs are often used to examine in detail particular internal features of crystals revealed by projection topographs. It is especially convenient, for this purpose, to be presented with the direct reading of the platform position which is provided by the revolution counter. By this means it is possible to set the position of the platform reproducibly to within a range of 0.0005 inches, which corresponds to the width of the narrowest X-ray beam commonly used in taking section topographs.

The X-ray source used is a Hilger and Watts Ltd. (London, England) Microfocus Unit. The model in the arrangement shown in Figure 1 is 'Y25' and it has the axis of its electron beam vertical. The plane of the target face is horizontal, and in this generator it is facing upwards since the cathode is above it. The cathode is near ground potential, whereas the anode is at high potential and is cooled by oil rather than by water. It follows that the two X-ray beams led off from the ports on either side of the vertical X-ray tube housing are directed slightly above the horizontal plane, the mean take-off angle from the target face being 3° . Since the maximum height of the beam at the specimen is about 25 mm, actual take-off angles range from $1\frac{1}{2}^{\circ}$ at the lowest point of the ribbon beam to $4\frac{1}{2}^{\circ}$ at its top. The X-ray intensity is reasonably constant over this range of take-off angles, but the apparent height of the source varies so that the geometrical resolution is affected, as discussed in Section 1.3.3. In Figure 1 the X-ray tube itself is surrounded by a lead-lined brass box which ensures thorough screening against X-ray leakage from the X-ray tube windows and provides supports

for the front ends of the lead conduits that carry the X-ray beams to the incident-beam slit assemblies of the goniometers

The X-ray tube focus is 1.4 mm long on the X-ray tube target face and is nominally 100 microns wide. It is viewed end-on from the goniometers. Its actual half-width at half maximum intensity appears in practice to be less than 100 microns when the focus is well adjusted. The focus quality depends upon the correct positioning of the filament, focussing hood and target with respect to each other. When the tube is in operation the focus width can be controlled by varying the bias voltage between filament and focussing hood. The design of the X-ray tube and its circuit is essentially that of Ehrenberg and Spear (1951). The tube is continuously pumped so that targets may be changed at will. The following target elements have been used in topographic studies: silver, molybdenum, copper, cobalt and chromium. Experimental targets have been made of tin, antimony and of germanium.

A reliable method of measuring the intensity of diffracted X-rays is essential in order to set up topographic experiments quickly and to estimate exposure times correctly. Scintillation counters are used for this purpose since they offer (1) a large sensitive area, (2) high counting efficiency for all the X-radiations used and (3) high maximum counting rates. A simple but effective counter is shown in Figure 1. The scintillation crystal is a disc of NaI(Th) 25 mm in diameter by 1 mm thick contained in a capsule with a thin beryllium window. The photomultiplier is an E.M.I. Type 9524B, having a 25 mm diameter photocathode. The performance of this photomultiplier is so good that it can be used without a preamplifier. It is connected directly by a single low-capacity screened cable, 4 meters long, to an EKCO Ratemeter Type N624A. This ratemeter contains a stabilised high voltage supply unit, an amplifier of maximum gain 1,000, a discriminator with range 0-100 volts and a linear ratemeter with full scale ranges from zero to 3, 10, 30, 100, 3,000, 10,000, 30,000 and 100,000 counts per second. This division into two ranges per decade has been found very useful. The counter background (X-ray beam off) is about 1 count per second. The counters are reasonably linear in response up to rates of about 30 to 40 thousand counts per second, and they saturate

at about 70,000 counts per second. The rates worked with in the course of setting up topographic experiments usually lie between 10,000 and 50,000 counts per second. Exceptionally small crystals, weak reflections, or highly collimated incident beams may give rates below 1,000 counts per second. When specimens containing a well-developed mosaic structure are being studied it is convenient to use a strip-chart recorder in conjunction with the ratemeter. Individual sub-grains in the specimen can be recognised by the particular reflection peaks they give when the specimen is scanned, and it is possible to set up topographs to study a given sub-grain in several Bragg reflections without the need for trial exposures to check that the sub-grain is in the correct orientation for Bragg reflection. The combination of scintillation counter, ratemeter and strip-chart recorder has, of course, more quantitative applications in the measurement of integrated reflections, angular ranges of reflection, and misorientations between sub-grains.

1.3.2. Photographic technique

In order to produce high quality topographs it is as important to use the most appropriate photographic technique as it is to perform the experiments on suitably designed mechanical apparatus such as that which has been described in Section 1.3.1. In the course of the early X-ray topographic experiments it was found that none of the available X-ray films, whether designed for crystallography or radiography, permitted the full potentialities of the X-ray geometry to be realised. The 'Non-Screen' crystallographic films were much too coarse-grained. The fine-grain 'Kodak Type M' radiographic film, which is used, for example, in the radiography of light alloys, gave much higher resolution but was 16 times slower than the 'Non-Screen' film when used with $\text{AgK}\alpha$ radiation. Various types of dental film, with characteristics intermediate between 'Non-Screen' and 'M' emulsions, were also tried. Attention was then turned to nuclear emulsions, which combine fine grain-size with high stopping power for harder X-rays. Use of Ilford G.5 nuclear emulsion commenced at the end of 1957 and was an immediate success. About a year later, a change was made to the still finer-grained Ilford L.4 nuclear emulsion which had then become routinely commercially available. Ilford L.4 nuclear

emulsions have been used for all serious topographic work since the beginning of 1959.

The chief qualities that make the G. 5 and L. 4 emulsions suitable for X-ray topographic use are a grain-size well below resolution limits of the technique as set by geometrical and other factors, and the availability of a range of thicknesses sufficient to ensure high absorption efficiencies even for the most penetrating radiations likely to be used in X-ray topographic work. An important characteristic of these particular nuclear emulsions is that they are sensitive to low-energy electrons. This is a necessary condition for the efficient recording of X-rays since the actual grain sensitising agents in the emulsion are photoelectrons of usually not more than a few kilovolts energy. Emulsions L. 4 and G. 5 also have a very high concentration of halide so that high stopping power is achieved with the minimum physical thickness of emulsion. The chemical composition of G. 5 and L. 4 emulsions is the same but their grain size is different. The mean diameter of the grains (undeveloped) in these emulsions is 0.27 microns for G. 5 and 0.14 microns for L4. An average chemical analysis of the emulsion in equilibrium with air at normal room temperature with a relative humidity of 58% is, in grams per cc,:

Ag	Br	I	C	H	O	N	S
1.817	1.338	0.012	0.277	0.053	0.249	0.074	0.007

The density is thus 3.828 gm per cc, and the halide content is 3.168 gm per cc. Hence the weight fraction of halide is 83%. Approximate values of the ' $\frac{1}{2}$ value thicknesses', i.e. thicknesses required to absorb half the incident intensity are, for AgK α , 100 microns; for MoK α , 50 microns; and for CuK α , 12 microns. In practice, emulsion 25 microns thick is used for CuK α and all softer radiations, and 50 microns is used in preference to 100 microns for MoK α and AgK α because of its shorter processing time and less risk of emulsion distortion.

One approach to the problem of high resolution in photographic recording is to combine very small grain size with very thin emulsion thickness. This approach is adopted in high-resolution spectrographic

emulsions, for example. In the X-ray topographic case such thin emulsions would be prohibitively inefficient in absorbing the X-rays, under usual experimental conditions. They would also give greater statistical fluctuations in number of developed grains per unit area and a smaller usable photographic density range than the thicker emulsions, two disadvantages which would not be offset by the reduction in scattering and reduction of intercepted lengths of photoelectron tracks which their emulsions should show.

The acceptance of thick emulsions as the standard recording medium restricts the diffraction geometry to techniques in which the emulsion is always placed normal to the diffracted beam. In such cases any distortion of the shape of a crystal face on the topographic image caused by obliquity of the diffracted rays leaving the face must be corrected either by moving the crystal and emulsion at different rates with respect to the X-ray beam, or by rectifying the topograph in the process of photographic enlargement. Both methods have been used with success. The need for setting the emulsion normal to the diffracted beam is of course more severe the thicker the emulsion: one degree off normality would cause a lateral diffusion of the image by nearly 2 microns in a 100 micron thick emulsion. In practice, an optical sighting technique is used to bring the plate cassette (inside which the plate carrying the emulsion is precisely located) to within $\frac{1}{2}^{\circ}$ or less from exact normality to the diffracted beam. The 3" X 1" glass plates on which the emulsion is coated are cut in half before use so that each provides two topographs. $1\frac{1}{2}$ " X 1" in size.

Another complication incurred by use of thick emulsions is the need for long processing and washing times. However, the thickest emulsion used (100 microns) is not so thick as to require the 'temperature cycle' technique to attain reasonably uniform development. It is customary to use what might be called a 'modified temperature cycle' procedure. In this the development is carried out at a constant, low temperature. This is chosen for convenience to be the freezing point of the developer solution. The development time is lengthened by performing the entire

development at this low temperature but the resultant degree of development is fairly uniform throughout the whole emulsion depth. The basis of this procedure is that diffusion times vary little with temperature whereas rate of development increases roughly exponentially with temperature. Diffusion times are proportional to the square of the emulsion thickness.

The developer chosen for use is Kodak D19b. One part of standard strength D19b is mixed with three parts of water. The fixer contains 300 gm sodium hyposulphite plus 30 gm sodium bisulphite per liter. Between developing and fixing, a stop bath of 1% glacial acetic acid is used, and before development the emulsion is soaked in plain water so that it swells to allow rapid diffusion of developer into it. The processing schedule is given in Table 1.3.2 A.

Table 1.3.2. A.

Processing schedule for Ilford nuclear emulsions, times in minutes.

<u>Thickness, microns</u>	<u>25</u>	<u>50</u>	<u>100</u>
Soak	5 -10	10-15	20
Develop	12-30	18-60	30-60
Stop bath	5	10	20
Fix	30	60	120
Wash	60	120	240

The washing is performed in cold, running, filtered water. Drying takes place at room temperature in normal laboratory air, preferably in a muslin-covered box to exclude dust particles which might settle on the wet emulsion.

The reason for the wide range of developing times quoted in Table 1.3.2. A is as follows. One of the admirable characteristics of the Ilford nuclear emulsions is the great range of photographic density over which density is directly proportional to dose of X-rays. Experiments with controlled exposures, using monochromatised characteristic radiations, have shown a strictly linear relationship between density and exposure up to densities of 2 to 2.5. The exposures were made on L 4 emulsion: 25 microns thick exposed to CuK α , 50 microns thick to MoK α and 100

microns thick to AgK α . It has also been found that, for a given exposure, within a very wide range of exposures, the density increases steadily as the development time increases. Now it has been established from much experience that the best conditions both for visual study of topographs under the microscope and also for their photo-micrography are obtained when the 'basic density' of the topograph is about unity. 'Basic density' here refers to the roughly uniform image density produced by areas of crystal free from imperfections. Under this condition the density in images of individual dislocations rises to about two. They are thus visible with high contrast but are still within the linear density range of the emulsion. The actual dose per unit area received by the emulsion in a topographic experiment may vary considerably: special circumstances of the experiment may determine that the exposure be much less or much greater than usual. It is possible, and is indeed customary, to develop all topographs to roughly constant density in the imperfection-free areas; and it follows from what has been said above that this treatment can be extended to exceptional topographs with much smaller or greater exposures than usual. Hence the wide range of development times quoted. Now the nuclear emulsions are relatively insensitive to light. Ilford S (light brown) or F (dark brown) safelights are used, and with them the illumination level is sufficient for an experienced worker to make good estimates of the image density by inspection at stages in the development, and to terminate the development when the desired density is reached. The increase in photographic density produced by lengthening the developing time arises from grain growth in the emulsion, but even with the longest developments used the grain diameter remains below one micron and does not become a factor directly affecting the resolution. What does change between strongly and weakly exposed topographs is of course the number of photons absorbed per unit area, and hence the statistical fluctuations in the number of developed grains per unit area. These fluctuations are a very important factor in determining topographic quality and resolution, and are discussed further in Section 1.3.3 below. To reduce these fluctuations, long exposure times and short development times are favoured.

The nuclear emulsions are stored under refrigeration, and are kept in sealed containers to avoid excessive drying of the emulsions. Since processing is always performed within a few hours of concluding an exposure, no trouble is encountered due to latent-image fading.

Photomicrography of topographs is an exacting process. The apparatus used for this purpose is a Vickers Projection Microscope. This microscope has the path of the specimen-illuminating rays readily accessible. Such accessibility permits variously shaped apertures and variable density masks to be inserted in the illuminating beam and be projected by the sub-stage condenser on to the topograph. A major problem is the wide density range encountered in the average size of field it is required to photograph. These density changes may be due to warping of specimen sub-grains, or varying specimen thickness, for example, and are generally beyond the control of the experimenter. In bad cases it is worthwhile to prepare a slightly out-of-focus enlargement of the topograph on a soft lantern plate and to insert this plate in the illumination system in such a way that it is projected on the topograph with the right reduction in size so as just to match the size of the topograph. It will then partially balance the long-range density variations over the field of interest.

The areas it is desired to include on a given topograph are often greater than 1 mm in diameter. Hence flat-field objectives are used. Since the emulsions to be photographed are quite thick, there is no advantage in using objectives with high numerical apertures since these have only a small depth of focus. Emulsions shrink on processing to about 40% of their undeveloped thickness. Thus some of the information in the emulsion would be lost if the depth of focus were much less than 10, 20 and 40 microns in photography of 25, 50 and 100 micron emulsions, respectively. The wide-field objectives are used without oil immersion, though the topograph itself is always protected by a microscope cover slip, with immersion oil between the glass and the surface of the emulsion. In this way not only is the topograph safely preserved, but light-scattering from small craters and adhering gelatine threads on the emulsion surface is avoided.

The flat-field objectives used are the Zeiss Plan X6.3, N.A. = 0.16; Zeiss Plan X10, N.A. = 0.22; and Cooke Microplan X10, N.A. = 0.25. On a few occasions the Cooke A8464 X20, N.A. = 0.50, has been employed. In Table 1.3.2B are listed the theoretical resolution (given by $\lambda/2N.A.$) and the depth of focus given by the Rayleigh criterion ($\lambda/4\mu \sin^2 \frac{1}{2}\alpha$) for the range of numerical apertures used. The wavelength inserted in these formulae is that of the strong mercury green line, 5,461Å, which is used in visual work. In photography, the combination of film response with the filters used is such as to make dominant the wavelengths around 5,000Å, so the theoretical resolution is then about 10% better. The refractive index of the emulsion is taken as 1.4, and the angle α in the formula for the depth of focus is the semi-angle of the cone of rays in the emulsion.

Table 1.3.2.B

Resolution and depth of field in nuclear emulsions

N.A.	Resolution, microns	Field depth, microns
0.16	1.7	31
0.22	1.2	16
0.50	0.55	3

The figures in Table 1.3.2B agree well with experience: the X6.3 Zeiss objective is best for 100 micron emulsions, the X10 Zeiss or Cooke objectives work well with both 50 micron and 25 micron emulsions. The X20 Cooke objective is used only with 25 micron emulsion and its small depth of focus entails poorer grain density statistics. This loss can be to some extent made good by scanning the objective up and down through the 12 micron thickness of the processed 25 micron emulsion. The Zeiss X6.3 objective gives good quality in fields as large as 3.4 mm in diameter; the corresponding diameter for the X10 flat-field objectives is about 1.2 mm.

Factors such as the length of photoelectron tracks in the emulsion, discussed in Section 1.3.3. below, show that the maximum attainable topographic resolution depends strongly upon the X-ray wavelength.

It gets rapidly poorer for radiations more energetic than MoK α . Thus the three numerical apertures listed in Table 1.3.2B correspond nicely to the maximum values needed for enlarging topographs taken respectively with AgK α , MoK α , and CuK α (and softer) radiations. (Experience has shown that the maximum useful total magnifications obtainable are 150 to 200 with AgK α , 200 to 300 with MoK α , and 400 to 600 with CuK α . The basis of these estimates is discussed fully in Section 1.3.3. below.) The photomicrography is done on to sheet film 12cm X 16.5cm in size which is then printed at magnifications of, say, X2 or X3 to make positive reproductions of the original topographs. A sheet film found generally suitable for micrographic use is Kodak Commercial Fine Grain CF8. This has a long linear range on its density versus log exposure characteristic curve. It also has a gamma that can be varied over a wide range by changing the development conditions.

In another photographic technique pairs of topographs which are stereopairs (for example the hkl and $\bar{h}\bar{k}\bar{l}$ reflections from the same crystal) are enlarged as transparencies and examined in a stereoviewer. These transparencies can also be projected for lecture demonstration purposes, using the Polaroid three-dimensional projection system. For studying stereopairs in the course of research it is usual to examine the original topographs directly under a pair of twin microscopes. For this purpose a pair of similar objectives is used. they may be 3X, 10X or 20X, depending upon the nature of the subject.

1.3.3. Quality and resolution of X-ray topographs.

A more detailed discussion will now be presented concerning various factors which determine the quality and the resolution of X-ray topographs. Firstly some features of the diffraction geometry will be considered.

In the vertical plane, i.e. the plane containing the goniometer axis, the geometric resolution can be calculated according to the simple rule familiar in radiography. Let the distance from source to specimen be a , and from specimen to emulsion be b . Then if the apparent height of the source is h , a point in the specimen will produce an image whose range of diffusion in the vertical direction is $h(b/a)$. The distance a is fixed at

45 cm. At the mean take-off angle of 3° the apparent height of the X-ray tube focus is 70 microns, at the top of the maximum vertical range of illumination of the specimen it is 105 microns, and at the bottom 35 microns. (These figures for a and h follow from the dimensions given in Section 1.3.1.) An average distance from specimen to emulsion is 1 cm. Hence the geometric vertical resolution is 1.5 microns at the mean take-off angle, 2.3 microns at the upper limit of the incident beam and 0.8 microns at its lower limit. When using $\text{CuK}\alpha$ and softer radiations, it is better therefore to avoid using the upper part of the beam; and it is desirable to try and make b less than 1 cm. This effort is barely worthwhile with $\text{MoK}\alpha$ and harder radiations, however, as the discussion following later in this Section will show. Note that there is a slight vertical distortion of the topograph image; the distortion factor is $(a+b)/a$, and is about 2%. This factor need be included only in the more accurate measurements of orientations of dislocations, fault surfaces, etc., on topographs.

The resolution in the horizontal plane, i.e. in the plane of the incident and diffracted rays, involves the angular range of reflection of the crystal and the wavelength spread of the X-ray line used. Firstly, it must be emphasized that topographs of perfect and nearly perfect crystals are recorded with the $\text{K}\alpha_1$ radiation only. Accordingly, the incident beam is sufficiently well collimated to separate completely the Bragg reflections of the α_1 and α_2 components. This collimation is achieved by correct choice of the pre-set beam-width defining slit referred to in Section 1.3.1., and by careful adjustment of the X-ray tube focus.

The contribution of wavelength spread to image diffusion is calculated as follows. Let $d\lambda$ be the wavelength range corresponding to the width at half maximum intensity of the X-ray emission line profile, then the range of Bragg angles corresponding to $d\lambda$ is $d\theta = \tan \theta (d\lambda/\lambda)$. The image of a point in the crystal will be diffused to a width $dx_\lambda = b d\theta$ on the emulsion due to the angular range $d\theta$. Table 1.3.3.A lists the Bragg angles θ , the angular spreads $d\theta$ in seconds of arc, and the values of dx_λ in microns when $b = 1$ cm, calculated for two radiations

and for two interplanar spacings d . Topographs are not often taken of reflections with d greater than $3\frac{1}{2}\lambda$ or less than λ .

Table 1.3.3 A

Image diffusion due to natural wavelength spread

AgK α_1				CuK α_1		
$\lambda = 0.559\text{\AA}$.				$\lambda = 1.540\text{\AA}$.		
$d\lambda = 0.28\text{XU}$.				$d\lambda = 0.6\text{XU}$.		
$d\lambda/\lambda = 5 \times 10^{-4}$				$d\lambda/\lambda = 4 \times 10^{-4}$		
$d, \text{\AA}$.	$d, \text{''}$	$d, \text{''}$	$dx_\lambda, \mu\text{m}$	$d, \text{''}$	$d, \text{''}$	$dx_\lambda, \mu\text{m}$.
3.5	4.6	8.2	0.4	12.7	18	0.9
1	16.2	29	1.4	50.4	99	4.8

Calculations such as those exemplified in Table 1.3.3A show that if Bragg angles larger than about 30° are used (which is not often the case in transmission techniques) then the specimen-to-film distance should be reduced below 1 cm in order to avoid a large contribution to image diffusion from the wavelength spread.

The contribution to image diffusion in the horizontal plane due to the angular range of reflection of the specimen, assuming it behaves as a perfect crystal, can be gauged from the following figures for strong reflections. For weaker reflections the angular range is less, being directly proportional to the integrated reflection. Table 1.3.3B gives the angular widths of reflection at half maximum intensity of some strong reflections in the symmetrical transmission case.

Table 1.3.3 B

Angular widths of reflections at half height, in seconds.

AgK α_1		CuK α_1
Silicon, 220	1.7	5.5
Germanium, 220	3.8	15

From comparison of Tables 1.3.3.A and 1.3.3.B it will be seen that the perfect-crystal angular reflecting range makes much smaller contributions to horizontal diffusion of the image than does the natural

wavelength spread, and can generally be neglected.

Horizontal diffusion of the image will cause more serious loss of resolution if the horizontal scale of the image is compressed by the oblique emergence of diffracted rays from the specimen. Suppose the specimen is in the form of a plate whose horizontal dimension is P , and suppose the Bragg plane used is inclined at an angle α with the normal to the plate. Then, when the deviation 2θ of the diffracted beam and the inclination α are in the same sense about the goniometer axis, the horizontal dimension of the topographic image, P' , is $P \cos(\theta + \alpha)$. Thus the horizontal magnification factor, $\cos(\theta + \alpha)$, is always less than unity. (This applies so long as the standard experimental arrangement is used, in which the diffracted beam is perpendicular to the photographic emulsion and both specimen and emulsion have the same traverse motion.) It is preferable to take topographs with θ and α in opposite senses in order to minimise the horizontal topographic distortion.

When the specimen is in the form of a plate, of thickness t , and is mounted parallel to a plane containing the goniometer axis, then the width, w , of a section topograph image is given by $w = t \sec(\theta - \alpha) \sin 2\theta$, (Lang 1957b). It is customary to mount the specimen plate parallel to the traverse direction in taking projection topographs. When this condition is fulfilled the diffracted beam remains stationary in space during the traverse, and the hanging slits between specimen and emulsion can be set at their minimum gap width. This width is w plus an allowance for the incident beam width. It is highly desirable to keep the gap width as low as possible in order to prevent unwanted Bragg and Laue reflections from reaching the emulsion and also to reduce the background of fluorescence and Compton scattered radiation on the topograph. Of course, in the various techniques of 'limited projection topographs' (R6, Lang 1963a) the gap in the hanging slits is reduced below the above-quoted value of w for the specific purpose of selecting diffracted rays coming from particular layers in the specimen, to the exclusion of others.

Some consideration will now be given to factors affecting the quality and resolution of topographs which depend upon the number and

spatial distribution of developed grains in the nuclear emulsion. These factors are determined by the physical processes accompanying the absorption of radiation in the emulsion, rather than by the diffraction geometry as was the case with the factors considered above. Consequently they are less under the control of the experimenter.

It has been explained in Section 1.3.2. that the need for high absorption efficiency demands the use of thick emulsions rather than the single-grain-layer emulsions often used in high-resolution optical work. In thick emulsions it is necessary to consider the spatial distribution surrounding the primary absorption event of all other following absorption events involving the photoelectrons and fluorescent X-rays into which the incident photon's energy is distributed. Now in the case of CuK α radiation, the energy of which is 8keV, no photoelectrons are produced whose track in the emulsion extends out to a distance greater than about half a micron from its point of origin. Hence absorption of a CuK α photon will either produce a single grain or a clump of perhaps 2 or 3 adjacent grains contained within a volume whose diameter is about half a micron. Such a clump will appear as a single particle at the highest optical magnifications customarily used in enlarging topographs. Hence, in the case of CuK α radiation, and, a fortiori, in the case of softer radiations, there is no significant impairment of resolution by spread of ionisation in the emulsion. The contrary is the case with the radiations harder than CuK α that are commonly employed, MoK α and AgK α . The absorption processes of MoK α and AgK α will now be considered. Both radiations are harder than the K absorption edge of bromine but softer than the K absorption edge of silver. Consequently the ratios of absorption cross-sections in the various electron shells of silver and bromine are the same for both radiations. It is convenient to examine first the behaviour of the primary photoelectron produced in the first step of the absorption process and subsequently the way in which the excited atom in the emulsion loses its energy. For every 100 photons incident upon the emulsion, the relative numbers absorbed by the various shells can be calculated from the known values of absorption coefficients and the 'jump ratio' at the K absorption edge (Compton and Allison, 1960). These numbers appear in

the second column of Table 1.3.3.C. Figures quoted for the radial range and the number of grains along the track are of necessity very rough. By radial range is meant the length of the straight line joining the origin of the photoelectron to the last grain on its track. This is also known as the chord of the track. The value zero means that the photoelectron produces one grain only, at its origin. Along short tracks such as those here considered the electron produces about $1\frac{1}{2}$ grains per micron path, on the average. The range as usually defined is the line integral of the particle trajectory. The radial range (or chord) is of course less, and the difference between the two values becomes greater the lower the electron energy, as the number of high-angle deflections of the electron increased. The figures given in Table 1.3.3.C are based upon experience gained in the present investigation and also upon data obtained in other work with nuclear emulsions, (see, for example, Powell, Fowler and Perkins (1959)). The photoelectron energies are given precisely by the difference between incident photon energy (E_x) and the appropriate absorption edge energy of the absorbing atom ($E_{K,L}$).

Table 1.3.3.C

Absorption processes in nuclear emulsions: characteristics of primary photoelectrons.

Absorption	Relative no. of photons involved	AgK α $E_x=22.1$ keV			MoK α $E_x=17.5$ keV		
		photo- elect. energy, keV	radial range, μ m	no. of grains on track	photo- elect. energy, keV	radial range, μ m	no. of grains on track
Ag L Shell $E_L=3.3$ keV	30	18.8	$2-2\frac{1}{2}$	~ 3	14.2	$1\frac{1}{2}$	~ 2
Br K Shell $E_K=13.5$ keV	60.5	8.6	$0-\frac{1}{2}$	1-2	4.0	0	1
Br L Shell $E_L=1.5$ keV	9.5	20.6	2-3	3-4	16.0	$1\frac{1}{2}-2$	2-3

The spectrum of fluorescent X-rays is the same whether the incident X-rays are MoK α or AgK α . Only a small fraction of the incident photon energy is carried away from the absorbing atom as fluorescent X-radiation. Values of fluorescent yield ($w_{K,L}$) (or of its complement, the internal conversion coefficient (I. C. C.)), are given by Burhop (1952). The relative number of the various fluorescent X-ray photons produced per 100 incident photons, together with their ranges, are listed in Table 1.3.3.D.

Table 1.3.3.D

Absorption processes in nuclear emulsions: number and range of fluorescent X-rays.

Absorbing shell	No. absorbed in shell	No. of fluorescent X-ray photons	Range of fluorescent X-rays, μ m.
Ag, L $w_L=0.1$	30	3	4.1
Br. K $w_K=0.56$	60.5	34	54
Br. L $w_L=0.05$	9.5	0.5	2.5

Now in order for resolution not to be impaired by ionization produced in the absorption of fluorescent radiation, the range of the fluorescent X-rays should either be quite small (not greater than about 1 micron), or sufficiently larger so that the ionization produced is distributed with low average density throughout a volume large compared with the dimensions of image detail it is required to resolve. Only an increase in background occurs in the latter case. Table 1.3.3D shows that the great majority of the fluorescent photons are of comparatively long range, and indeed stand a good chance of escaping from the emulsion before absorption when emulsions of 25 or 50 micron thicknesses are used. The X-rays whose ranges (defined as the reciprocal of the linear absorption coefficient) are 2.5 and 4.1 microns would be quite troublesome

if they were not fortunatel, are

A combination of the data presented in Tables 1.3.3.C and 1.3.3.D provides a picture of the spatial distribution of developed grains. In about 60% of the events in which an incident photon is absorbed the ionization is limited to a volume of diameter about one micron, producing a grain clump effectively at the point of absorption. In the remaining 40% of events most of the energy is carried away by the primary photoelectron; but the probability is high that the remaining energy will be internally converted into Auger electrons so that at least one developed grain will be produced at the point of absorption. When the primary photoelectron has one of the higher energies listed in Table 1.3.3.C the total grain distribution will then have the appearance of a 'chain-shot', but with at most about 3 'links' in the 'chain'. From this picture of the ionization distribution it follows that the resolution limit imposed by spread of ionization in the emulsion may be reasonably assessed to be about 2 - 3 microns with AgK α radiation, and $1\frac{1}{2}$ - 2 microns with MoK α .

Inspection of the topographs shows that very often the dominant factor limiting resolution of fine detail is the presence of a high 'apparent granularity' in the image. This is termed 'apparent' because in fact it has little connection with the actual grain size which is but a fraction of a micron. Rather is it due to statistical fluctuations in the number of developed grains contained within one area element of the emulsion as compared with another. Intensity measurements show that the diffracted beam, even from an intensely reflecting crystal, will deliver but a small number of photons on to each square micron of the emulsion during normal durations of exposure. Moreover, a fundamental obstacle to increasing this dose sufficiently to reduce its relative variance to a low fraction is not so much the long exposures that would be required but that the highest photographic density at which density is still roughly proportional to dose is itself produced by absorption of only a small number of photons per square micron.

The effect of statistical fluctuations may be assessed by dividing the image into equal, small area elements and then determining how small

the elements may be made before a given difference in density between adjacent elements due to a true difference in mean intensity incident upon them is masked by the fluctuations in the number of photons absorbed in each of them during the exposure. A development of this analysis appropriate for X-ray topographs takes into account the fact that the area elements or cells into which the image is divided are not observed just as independent, adjacent pairs during the course of recognition of a pattern. This is particularly true when the aim of the image scrutiny is to detect an exceptional feature in a field where the mean dose has varied only slowly from point to point. The two commonly occurring problems of this type are, firstly, to detect with confidence a small spot where the diffracted intensity received is greater than that in the surrounding area: such a spot could represent the image of an inclusion or precipitate in a matrix of perfect crystal. The second common problem deals with lines: the recognition of a single line on a uniform background, or the resolution of an array of lines, or of a stripe pattern, for example.

Consider first the problem of detecting a small spot. This analysis could be extended to determine the precision with which a given difference in density between spot and surrounding area can be estimated.

Suppose the spot is a disc of diameter D . In the case of a small disc the best magnification to use for its detection is one not so large that the eye cannot easily integrate the intensity over the disc, while still being of course large enough for the eye to resolve comfortably an object the size of the disc. In the case of a large disc, the magnification can be reduced until the area over which the eye integrates corresponds to an area on the topograph image large enough to appear grainless to the eye. The eye compares the average density of the disc with a surrounding area which, in the case of a small disc, may be much larger in area than the disc itself, and, in the case of a large disc, can certainly be taken large enough to appear grainless. Conservatively, the area of the surrounding reference density can be taken to be four times the area of the disc. This would correspond to a surrounding annulus whose width between inner and outer radii was just greater than the radius of the disc. The photographic

density may be assumed to be proportional to the number of photons absorbed per unit area. Let these numbers be n and $n(1 + h)$ in annulus and disc, respectively. Assume that the mean value of n is sufficiently large for the Poisson distribution of observed values of n to be reasonably approximated by a Gaussian distribution.

In the Gaussian distribution the probability of finding a value more than 1.65 times the standard deviation, σ , on one side of the mean is only 1 in 10. Set the condition for confident detection of an excess density in the disc compared with the annulus to be that $n(1 + h) - n$ is greater than $1.65 (\sigma_1 + \sigma_2)$, where σ_1 and σ_2 are the standard deviations of density in disc and annulus. Now, with the magnification chosen so that all photons absorbed in disc and annulus are included in the density integration, it follows that $\sigma_1^2 = n(1 + h)/(1/4\pi D^2)$ and $\sigma_2^2 = n/\pi D^2$. Substitution for σ_1 and σ_2 in the detection condition gives $n^{1/2} = 1.65 \times (1 + 2(1 + h)^{1/2})/\pi^{1/2} h D$. Table 1.3.3E lists values of n , the number of photons absorbed per square micron, for various values of D and h , calculated according to this expression. The lowest value of h , representing only a 3% increase in density, is nearing the lower limit of density differences usually detected in radiography. A doubling of intensity, represented by $h = 1$, is easily achieved in the excess scattering from a localized strain field in a matrix of perfect crystal.

Now, under standard processing conditions, unit density is reached with MoK α radiation when n is about 3. A density of 2, or in extreme cases approaching 3, may be allowed for the density of images of perfect regions, but then the density in imperfect regions is beyond the linear density range. Thus the maximum value of n that can properly be recorded with MoK α is about 8. In the case of CuK α radiation, unit density corresponds to a value of n of about 10, hence $n = 25$ is a practical upper limit. In Table 1.3.3E the combinations of disc size and density that can be confidently detected only with CuK α and softer radiations are indicated by enclosing the relevant n value with single parenthesis. A double parenthesis signifies confident detection also by MoK α .

Table 1. 3. 3.E

Required number, n , of photons absorbed per square micron in surrounding field to ensure the confident detection of a disc, diameter D microns, in which the number of photons absorbed per square micron is 100h% higher than n .

	$h = 0.03$	0.1	0.3	1.0
$D, \mu m$				
1	$\sim 10^4$	$\sim 10^3$	100	(14)
2	2×10^3	196	(25)	((4))
3	$\sim 10^3$	92	(12)	((1.4))
10	88	((8))	((1))	((0.1))
30	(19)	((0.9))	((0.1))	((0.01))

These figures are in good accord with experience. Clearly, the situation with $D = 2\mu m$ and $h = 0.3$ is a border-line case with CuK α , and that with $D = 10\mu m$ and $h = 0.1$ is a border-line case with MoK α .

In the above calculation it has been assumed that the variance in density arises only from the variance in n . There will be contributions to the variance in density from the variance in g , the mean number of grains produced for each absorbed photon, and from the variance in optical absorbing and scattering powers of each grain. For MoK α and AgK α , when g is greater than one, an appropriate formula for the coefficient of variation of density D is

$$\frac{\sigma_D}{D} = n^{-\frac{1}{2}} \left(1 + \frac{\sigma_g^2}{g} \left(\frac{1}{g-1} \right) \right)^{\frac{1}{2}}.$$

The situation is statistically similar to the case of the variation of height of a pulse after one stage of electron multiplication in a photo-multiplier when the mean secondary emission coefficient is equal to g . For a Poisson distribution $\frac{\sigma_g^2}{g}$ is equal to g . The rather conservative detection condition used in Table 1. 3. 3.E should offset effects due to

variation in g . In order to record higher values of n , short development times are used, but it is clearly desirable to avoid stopping development before all sensitized grains are developed. In the case of the harder radiations such incomplete development would effectively increase the variation in g , and in the case of the softer radiations it might involve the loss of effective registration of some incident photons.

Application of this type of analysis to the detection of lines or of stripe patterns follows a similar course to that just outlined. Perhaps the simplest case to consider is the resolution of two close, parallel lines. This problem occurs in practice since under certain diffraction conditions the topograph image of a single dislocation appears as a double line. Knowledge of whether or not the line is double in a particular topograph helps to determine its Burgers vector. Often the central dip in the intensity profile of the line is on the limits of resolution. Detection of the dip is helped by scanning parallel to the line and integrating the density over as long a length of the line as its straightness permits. This length is not likely to be less than 10 microns, and may be much longer in favourable cases. It follows that a dip 1 micron wide with 30% less than peak intensity should be detectable with $\text{CuK}\alpha$, and a similar dip in intensity two microns wide with $\text{MoK}\alpha$.

On the topograph reproduced in Figure 2 there can be recognised the influences of some of the factors discussed in the above paragraphs. The specimen was a cleaved slice of lithium fluoride, etched to remove surface damage, and its final thickness was about 0.4 mm. $\text{MoK}\alpha_1$ was the radiation used. The reflection was 200. The Bragg planes are normal to the specimen plate, and their trace lies parallel to the long edge of the field. The Figure is a positive print. Thus the dislocation lines, which produce an excess of diffracted intensity over that diffracted by the perfect crystal matrix surrounding them, stand out as dark lines on a fairly uniform background. On the original topograph the optical density of the 'perfect crystal' background is about unity, and at the centres of the dislocation images it is between 2 and 3. The feature of interest in the field shown is the array of dislocations stretching from the top left



Fig.2 Lithium Fluoride X 200

to bottom right of the picture. These are part of a low-angle boundary that has been intersected by the surfaces of the specimen plate. Along the top margin of the array the dislocations are outcropping at the specimen surface facing the nuclear emulsion, the outcrop along the bottom margin of the array is at the specimen surface facing the X-ray source. This distinction can be made from a study of the details of the dislocation images. The structure of dislocation images will be discussed later in this Report. It is sufficient to point out here that the relatively large breadth and asymmetric tail of the images of the 'random' dislocations remote from the low-angle boundary arises from the basic diffraction processes producing diffraction contrast and not from laxity of control of instrumental factors in the X-ray optics. When dislocations lie closely side-by-side, as in the low-angle boundary, the mutual cancellation of their long-range strain fields causes their images to sharpen considerably. Indeed they shrink to the point where geometrical resolution, photoelectron track lengths, and statistical fluctuations all play a part in determining how closely-spaced an array can become yet still be clearly resolved on the topographs. On the Figure the apparent granularity of the 'uniform' background can be noticed, and it would become obtrusive if the magnification were substantially increased. Thus a magnification of X 200, as employed in this Figure, is approaching the maximum useful value. The 'scale' of the granularity is roughly one micron, which corresponds to the optical resolution limit with which the topograph was photomicrographed, a numerical aperture of 0.22 having been used, (see Table 1.3.2E). In the array, dislocations spaced apart by 5 microns are easily seen as individual lines. In places where the ratio of peak density to background density is at least 2:1 a dip in density between two dislocations spaced apart by only 3 microns can be adequately recognised, and thus the dislocations be satisfactorily individually resolved. This performance is in accord with the predictions of Table 1.3.3E and the discussion following it. The topograph reproduced in Figure 2 was selected as a fair example of a case when, in the region of interest where the dislocations are closely spaced, the optical density is not far from the optimum value, and the contributions to the limitation of resolution from:

all sources, viz., geometrical, 'pure' diffraction effects, photoelectron ranges, and statistical fluctuations, are all nicely balanced. It is not possible to state a categorical value for the 'resolution limit' on topographs, since the performance in resolution is so dependent upon the type of pattern present in the image, and the particular features of it which it is desired to resolve. By now it will be realised, however, that several factors work together to raise a strong barrier to obtaining resolution limits lower than 1 micron. This micron limit can be achieved with careful technique using CuK α and softer radiations. The range of maximum useful magnifications follows accordingly: values are given in Table 1.3.3.F. Figures in this Table are admittedly rough, but they do represent the fruit of experience.

Table 1.3.3.F

Maximum useful magnifications and resolution limits of X-ray topographs taken with various radiations.

	Resolution limit, μm	Maximum useful magnification
AgK α	2	150 - 200
MoK α	1 - 2	200 - 300
CuK α	1	400 - 600
CoK α , CrK α	1	600 - 800

2. STUDIES OF MATERIALS

2.1. Natural Diamond.

2.1.1. Types of lattice imperfection in natural diamond.

In many respects diamond is a most suitable crystal for X-ray topographic studies. Its low X-ray absorption permits specimens up to several millimetres thick to be easily penetrated by MoK α and AgK α radiations, and enables X-ray topographs of large crystals to be taken satisfying the condition $\mu t \sim 1$ (μ is the linear absorption coefficient, t the specimen thickness). When this condition is satisfied the interpretation of topographic images is much simpler than in the high-absorption case, in particular, it is easy to obtain information about the spatial distribution of imperfections in the specimen when the absorption is low. Also, diamond crystals are mechanically strong and chemically stable. They are easy to mount for either X-ray or optical examination without risk of elastic or plastic deformation of the specimen as a whole, or of localized damage to its surfaces through abrasion or chemical attack. Much more important than these practical considerations, however, is the fact that diamond is one of the most intensively studied crystals of a single chemical element. Many years of research on its mosaic structure, electron density distribution, optical properties (in ultra-violet, visible and infra-red regions), electron spin resonance, cleavage, hardness, surface topography and counting properties have raised more questions than have been convincingly answered, and have repeatedly revealed a dependence of these properties upon the crystal texture, i. e. upon the state of crystal perfection. Such a situation indicates that X-ray topography should be a close adjunct, if not a principal method of examination, in any realistic and critical investigation on the texture-sensitive properties of diamond. There has been no abatement of interest in diamond in recent years; and in two new lines of work in particular, radiation damage and laboratory-produced plastic deformation, it is to be hoped that X-ray topography will play an important role. Both old-established problems concerned with the growth and morphology of natural diamond, and newly arisen questions concerning imperfections in man-made diamonds, have received illumination from

X-ray topographic studies. The wide scope of present day research on the physical properties of diamond is indicated by a recent review volume (Berman 1965). This contains a chapter on X-ray topography by Frank and Lang (1965) dealing especially with applications to studies of diamonds.

The accepted classification of diamonds is into the common Type I, which are more or less absorbing in the ultra-violet below the visible region, and the rarer Type II which transmit down to about 2,200 Å. It is not possible to say from inspection of an X-ray topograph whether the specimen is Type I or Type II, but associations between certain forms of lattice imperfection and the optical type have been demonstrated. It has certainly been shown that the hitherto prevalent notion that Type II diamond has a lower lattice perfection than Type I is an unjustifiable generalization: this conclusion was a by-product of the investigation described in Section 2.1.5. It has also been amply demonstrated that great variations of density of lattice imperfections from point-to-point within a given crystal can be accompanied by correspondingly large variations in optical properties. This finding alone would justify the routine X-ray topographic survey of crystals intended for use as specimens in optical, electrical and other studies.

Lattice imperfections which can be individually resolved on X-ray topographs of diamond can be broadly divided into inclusions and precipitates, dislocations and lamellar imperfections. These three classes of imperfection of course also occur in other crystals, and examples of them will be described in the following sections; but their manifestations in the case of diamond, so it has been found, often take characteristic forms which are of direct relevance to problems peculiar to this crystal. Inclusions, which are bodies accidentally incorporated during growth, may or may not be visible optically. They may or may not produce detectable strain in the diamond matrix surrounding them (the strain being detected either by optical birefringence or, more sensitively, by X-ray diffraction contrast). They may or may not introduce dislocations by lattice closure errors in the matrix enveloping them. However, generation of dislocations by inclusions is very common. Indeed, the very great majority of dislocations in diamond originate on inclusions. A frequent occurrence is a

radiating pattern of dislocations, the radiant point being roughly at the center of the stone and doubtless coinciding with the nucleus from which the crystal grew. Even in cases when a central mote cannot be clearly seen at the radiant such a configuration strongly suggests heterogeneous nucleation of the crystal. When, on the other hand, a distribution of localised strain concentrations is seen from which no dislocations run out in the direction of growth towards a crystal face, then it is likely that these strain centers are due to precipitates which have formed after growth. This interpretation is reinforced when, as is often the case, some of these strain concentrations are seen strung along dislocations which radiate from the center of the crystal. A remarkable example of precipitation, including the decoration of dislocations by precipitates, is described in Section 2.1.4.

The lamellar defects usually take the form of sheets of enhanced diffracting power, and they are interpreted as marking layers of abnormal interplanar spacing due to local concentrations of impurity. Such sheets frequently clearly lie on what were once the growing faces of the crystal. When, as is often the case, much of the crystal volume is occupied by a sequence of these sheets, they provide a direct 'stratigraphic record' of the growth history of the crystal. A study of this stratigraphy reveals that many diamonds have had a complex history of growth, solution, and regrowth. Possibly the rounded forms outlined by layers of enhanced diffracting power which are sometimes observed may indicate both solution surfaces and fronts marking the limits of inward diffusion of some impurity. Rather rarely do lamellar defects on a growth horizon contain a resolvable raft of dislocations. On the other hand, dislocations nucleated at such a horizon and subsequently grown in to the crystal along directions roughly normal to the advancing growth front are quite often observed.

The composition surfaces of twins in diamond often contain lattice imperfections producing long-range strain. Other types of fault surface have been recognised, and appear to be stacking faults (see Section 2.1.8.)

Whether or not defects such as precipitates or dislocations may be resolved individually in a particular region of specimen, a statistical

measure of the departure from the ideally perfect state can still be obtained from the intensity of the integrated reflection or from the visibility of Pendellosung["] fringes (see Sections 3 and 4). Type I diamonds, upon which most topographic work has been done, are known to contain a large density of impurity platelets up to about 1,000 Å in diameter (their distribution and structure are discussed in Sections 2.1.5 and 2.1.6). Yet these diamonds often behave as highly perfect crystals. Type II diamonds, on the other hand, which are free of platelets, can exhibit some strange and extreme forms of lattice distortion. A brief report of the latter is given in Section 2.1.9.

The natural surfaces of diamond are covered by scratches and ring cracks which produce intense diffraction contrast. Artificially cut and polished surfaces can be deliberately damaged by indentation or abrasion. It is found that surface damage can be revealed more sensitively by X-ray topography than by optical methods, and such X-ray studies (described in Section 2.1.11) can throw light on the mechanism of wear of diamonds.

2.1.2. Dislocations and trigons.

This work represents a good example of a study in which features of the surface topography of a crystal, which can be studied by optical microscopy, have been correlated with internal lattice defects made visible by non-destructive X-ray examination. The surface features in question are called trigons, depressions bounded by equiangular triangles, which are found on the natural octahedral faces of the majority of diamonds. A characteristic of natural trigons is that their orientation is opposite to that of the face upon which they appear: consequently their vertices point away from the corners of the crystal face on which they lie. Several different trigon types exist: a description of their morphology, and a classification of them, are given in R7 (Lang 1964a). The most important division of types of trigons is between those that are flat-bottomed and those that are pyramidal. The latter were proved to coincide with dislocation outcrops. On the other hand, no special association of flat-bottomed trigons with dislocations was found. As this investigation of trigons is fully described in R7, only a few points need be mentioned here.

The work provides very strong support for the explanation of pyramidal trigons as being etch-pits produced by some process in Nature. Observations made since the paper R7 was written have done nothing but confirm the conclusions drawn in that paper. Buried trigons are sometimes observed: these are taken as evidence of an etching epoch in the growth history of a diamond. The detailed study of the association of pyramidal trigons with dislocation outcrops and the attempts to find the Burgers vectors of these dislocations were made very difficult by the low visibility of the dislocation images and the obscuring effects of surface damage. A case exists for repeating some of the work on diamonds from which surface damage has been at least in part removed by etching, such etching having proceeded not too deeply so as to make unclear the location of natural pyramidal trigons. It might then be possible to establish conclusively whether there is a dependence of the slope of the sides of pyramidal trigons upon the orientation of Burgers vector of the dislocation associated with them. This dependence was not proved in the work reported in R7. The geometrical perfection of natural trigons shows that the etching process active in Nature had a remarkable specificity and efficiency as a dislocation etch. It would be desirable to be able to reproduce the process in the laboratory, and an essential part of such a study would be a comparison of etch-pit distributions with X-ray topographs. The surface used for such work could either be a polished one, or a natural face containing dislocation outcrops that had not been already naturally etched to produce trigons. Diamonds with apparently un-etched faces have been encountered in the course of the studies here reported.

2.1.3. Low-relief surface features.

Optical microscopic studies of the surfaces of numerous diamonds handled in the course of X-ray topographic investigations have provided much evidence that the surfaces of the great majority of diamonds have been subjected to processes of dissolution. In such cases all traces of the final growth stages have been obliterated. The rare examples encountered of crystals which do not show solution features are of special interest since there is the possibility then that the present surface may be the final growth surface of the specimen. Two such specimens have been

extensively studied. One had surfaces unusually flat and featureless but contained a number of stacking-fault defects in a layer down to about 70 microns below the present surface; these defects will be discussed in Section 2.1.8. The other stone had on one face four pyramidal, terraced hillocks of very low relief. It was also a trigon-free, but not dislocation-free specimen. The configuration and state of bunching of the terraces strongly suggested that they represented steps advancing from the pyramid centers and not receding to them, and hence that they were growth steps rather than etch steps. This specimen has been illustrated and discussed in Frank and Lang (1965). Since that description was written further careful X-ray topographic studies have been made to verify that the pyramid apices do not coincide with outcrops of dislocations originating deep within the crystal. These studies also showed that the diamond had a somewhat imperfect 'skin', perhaps a few microns thick, which diffracted more intensely than the bulk of the crystal. Step width and height measurements made by phase-contrast microscope indicated that the thickness of the fine-stepped pyramidal layer was only about 2 microns. It thus appears most likely that the final stages of growth have been preserved on this crystal, but that the material deposited in this stage was not as perfect as the bulk of the crystal.

The phase-contrast microscopy was performed without silvering the surface of the stone, yet by careful adjustment of the optics and the use of the highest photographic contrast, steps of height less than 10 Angstroms were revealed. This height estimate was made by comparing the visibility of fine steps and coarse steps on the same face, and between the latter coarse steps and steps of roughly known height inside trigons on another stone. In the regions where the steps were closely spaced, their average width was about 10 microns. This figure, taken in conjunction with an average step height of 10 Å, gives a pyramid slope of about 1 in 10^4 . This slope remained constant up to 2 mm from the apex of one of the pyramids. Two of the pyramid apices were located at a crystal edge, a likely place for a growth-promoting contact with another solid to occur.

2.1.4. Precipitates and decorated dislocations.

As pointed out in Section 2.1.1, the relationship between the dislocation configuration and the distribution of strain-producing centers usually shows whether the latter are inclusions, i.e. foreign particles accidentally incorporated into the growing diamond, or precipitates which have formed in the interior of the crystal behind the growth front. One case of precipitation attracted attention because the precipitates were, in the aggregate, visible optically, producing a cloudy region about 3 mm in diameter within an otherwise good quality stone about 5 mm in diameter. The work on this diamond is described in R4 (Shah and Lang 1963). It was found that dislocation-line segments lying within the zone of precipitation were strongly decorated by precipitates, but were not detectably decorated outside this zone. A remarkable feature of the distribution of the precipitates was their extension in finger-like regions radiating in $\langle 110 \rangle$ directions from the center of the crystal. A speculation was put forward that such a distribution might arise if in its early stages the diamond had grown as a cubo-octahedron.

2.1.5. X-ray Bragg reflection, 'spike' reflection and ultra-violet absorption topography.

Rather more than 25 years ago the study of diffuse X-ray reflections from crystals began to receive serious attention. In the earliest work a clear differentiation was not always made between cases when a distribution of reflecting power away from lattice points in reciprocal space arose from some static disorder of the crystal lattice or was due to scattering by acoustic waves in the lattice. This uncertainty applied for a time to the comparatively strong extensions of reflecting power in $\langle 100 \rangle$ directions about certain reciprocal lattice points of diamond which were discovered by Raman and Nilakantan in 1940. Lonsdale and colleagues showed in the following years that these $\langle 100 \rangle$ 'spike' reflections were not thermal diffuse reflections, but that they were 'texture-sensitive' effects, varying from diamond to diamond. It was not until 1956 that a reasonable explanation of the observed diffraction effects was proposed, by Frank (1956), who drew upon the close resemblance of these effects to those produced by the precipitates (known as Guinier-Preston zones) which

develop in age-hardening alloys such as $Al + 4\%Cu$. Frank showed that precipitate platelets on cube planes, satisfying certain conditions with respect to the lattice displacement they produced normal to those planes, could account for the 'spikes'. The difficulty presented by Frank's theory, that no suitable impurity element was known to be present in sufficient quantity to produce precipitates generating 'spikes' of the intensity observed, was removed by Kaiser and Bond's discovery in 1959 that nitrogen was present as a major impurity in the common Type I diamonds. Kaiser and Bond found, moreover, that there was a direct proportionality between nitrogen content and the strength of the chief characteristic ultra-violet and infra-red absorptions of Type I diamond. Now the early studies of diamond 'spike' reflections had found that Type II diamonds (which are substantially nitrogen-free) did not show 'spikes'; but at the time the work reported here was begun it was not known whether there was any regular dependence between 'spike' intensity and strength of the Type I absorption. To investigate this dependence was a major aim of the present work, and the essential need to make the investigation point-by-point in diamond crystals, i. e. by topographic methods, was soon demonstrated by the display of great non-uniformity, in some specimens, of both optical absorption and spike-reflecting power, as well as of the lattice imperfection content revealed by standard X-ray topographic techniques. The special optical and X-ray techniques required for this work, the experimental results obtained, and the conclusions drawn from them, have been fully reported (Takagi and Lang 1964, R9) and only a few comments need be added here. While Takagi and Lang's investigation was in progress Evans and Phaal (1962) succeeded in taking transmission electron micrographs of Type I diamonds which revealed the presence of precipitate platelets lying on cube planes. This confirmed Frank's hypothesis more directly than could be done by X-ray topography, but it could not prove that the platelets contained nitrogen. However, taking the work of Evans and Phaal in conjunction with Takagi and Lang's finding that spike-reflecting power and ultra-violet absorption are associated with each other, point-by-point, and applying Kaiser and Bond's relationship between nitrogen concentration and ultra-violet absorption, it appears extremely

likely that, in regions where the platelets are the major lattice imperfection present, the great bulk of the nitrogen resides in the platelets. The X-ray topographs underline the importance of considering the overall lattice imperfection content when discussing the distribution and state of aggregation of the nitrogen: in all regions where high ultra-violet absorption and high spike intensity were measured the local density of dislocations was negligible. On the other hand, some local regions of highly perfect crystal were found that were also so ultra-violet transparent as to be regarded as Type II diamonds. Thus the previously accepted belief that the Type II optical characteristics were accompanied by poor lattice perfection was shown to be too broad a generalization. There remains much scope for further investigation of the lattice perfection of dislocation-free regions of diamond as a function of platelet concentration. Among other results of Takagi and Lang's work were the finding that where platelet precipitation was present it had occurred with equal density on all cube planes and bore no relation to the local growth direction. Also, boundaries between regions of high and low ultra-violet absorption could be extremely sharp. These boundaries were always associated with growth stratifications revealed by normal X-ray topographs. Thus it appears that variations in platelet concentration correspond to variations in concentration of grown-in impurity, and no detectable diffusion of impurity between crystal growth and the precipitation of the impurity has occurred.

2.1.6. The structure of nitrogen platelets in diamond.

Some years ago Elliott (1960) proposed a structure for the nitrogen impurity platelets precipitated in Type I diamond. This model was accepted until Lang (1964 b, R11) pointed out not only that Elliott had based his model upon the expansion due to the platelet being equal to $1/12$ of the edge of the diamond face-centered cell, instead of $1/3$ of the edge as the 'spike' diffraction data suggested as being the likely minimum value, but also that the bending configuration in his model would probably not produce any expansion at all.

The alternative structure proposed by Lang (1964b, R11) contains

a double layer of nitrogen atoms replacing a single carbon layer parallel to a cube plane. It is not easy to prove that this model is correct since its atomic structure within a diamond cannot be resolved directly, and it cannot exist separately from the diamond matrix. The best that can be done is to check that it does not conflict with observations, such observations being made on as wide a variety of properties as possible. The model is structurally plausible, and no better one has yet been suggested. Experimental data which may be used to test the model can be drawn from the following fields, (a) X-ray 'spike' reflections, including low-angle scattering, (b) electron microscope diffraction contrast of platelet images, (c) lattice parameter measurements, (d) density measurements, and (e) optical measurements. Some aspects of these will now be discussed briefly.

Agreement with (a) formed the starting-point for building the platelet model, though the wide range of displacement possibilities compatible with the 'spike' evidence should be borne in mind as has been discussed by Frank (Proc Phys. Soc. Lond 84 1964 44), and Lang (1964b).

Small-angle scattering close to the direct beam can be regarded as a special case of 'spike' reflection, that about the zero order reflection. No small-angle scattering by platelets has been detected, despite a diligent search. This is in accord with Lang's model in which the platelet cell has the same electron density as a normal cell.

In (b), the electron microscope diffraction contrast study, there appears, superficially, to be some difficulty. The measurements of displacements of the diamond lattice on either side of platelets made by James and Evans (1965), using the method of Ashby and Brown (1963), gave values ranging from 0.15 to 1.2 Å, whereas Lang's model requires a displacement in units of not less than 1.2 Å. There are, however, a number of factors that could have introduced error into James and Evans' results. Most of them act in such a way as would make their derived values of displacement less than the true value, quite possibly by a factor of two or more. Thus the range of values they obtained could well be interpreted as being a spread, due to experimental uncertainties, about a

modal value which, due to systematic error, is about half the true value. In Ashby and Brown's experiments the specimens were several extinction distances thick and fairly highly absorbing. In James and Evans' experiments the diamonds were only one or two extinction distances thick and were quite lightly absorbing. This difference made it more critical in the latter's experiments that the specimen should be set exactly at the Bragg angle: deviation from this condition would lead to apparently smaller displacements than the true ones. Also, the diffraction theory applied assumed that the divergence of the incident electron beam on the specimen was small compared with the angular range of Bragg reflection by the specimen. This condition was not fulfilled in the case of the diamond 400 reflection with which James and Evans obtained most of their results; and again error leading to a displacement value smaller than the true one would thereby arise.

With respect to (c) it should be noted that one effect of the precipitation of platelets on cube planes in an otherwise perfect matrix is to cause the lattice parameter derived from a given interplanar spacing to vary systematically as a function of the indices of reflection. This prediction (Lang 1964b) has serious implications in accurate lattice parameter measurements on diamond. It awaits experimental test.

Introduction into diamond of nitrogen platelets having the structure here proposed will not change its density. Kaiser and Bond in fact found no change in density with increasing nitrogen concentration. More recently other workers have reported precise density measurements on a variety of diamonds and have found a very small spread of density values.

Regarding the optical properties of this nitrogen platelet model, little positive can yet be said in support or against it. Conventional calculations of infra-red absorption properties have been concerned only with the behaviour of individual impurity atoms. There is a strong need for a theoretical investigation of the behaviour of a sheet of impurity atoms, aggregated in a structure such as that proposed for the nitrogen platelet. A similar situation arises in the ultra-violet. It is reasonable to suppose that nitrogen atoms precipitated in plates ranging up to several

tenths of a wavelength in diameter will behave differently optically than if they were distributed at random in the matrix.

From what has been said above it is clear that much work still needs to be done before full confidence in describing the state of aggregation of nitrogen impurity in diamond will be achieved. However, the structure here proposed stands a good chance of survival.

2.1.7. Coated diamonds.

Coated diamonds are of importance both scientifically and commercially. The commercial importance stems from the fact that they are of wide occurrence and indeed represent a high proportion of the output from some mining areas. The material of the coat, though mainly diamond, is filled with fine dust-like particles of a micron or less in size, and it is fairly translucent, but not transparent. It effectively screens the core from visual inspection. The core material is usually white diamond of good quality, though frequently badly cracked. The cracks may contain a film of coat material. The fraction of the total volume occupied by good quality core, and the distribution of cracks within the core, are characteristics of a stone that can easily be discovered by X-ray topographic examination. Such examination might well be worthwhile as a routine commercial operation, to find which coated stones contain a core which it would be profitable to separate from its coat. However, the intention of the investigation here reported (Kamiya and Lang 1965a, R12) was more to study the fundamental properties of the coat, its lattice imperfections and impurity content, than just to demonstrate the ability of X-ray topography to identify coat and core material. Since coated stones are common, an understanding of the process of their growth is of importance in connection with the study of diamond genesis as a whole. The present work showed that the growth mode in diamond coat had much in common with that which can be induced in various crystals by causing them to grow in the presence of a colloidal dispersion of foreign material. Such dispersions (in the solution, or in the melt) can cause spherulitic growth. Diamond coat can be regarded as an early stage in spherulitic growth. The transition from normal growth to the fibrous growth of the

coat usually occurs quite sharply, at any rate locally. The transition may occur at a core surface showing evidence of solution, indicating that the growth process was not continuous from core to coat.

Much interest attaches to identification of the impurity material in the coat. Optical spectroscopic methods have failed to do this. Kamiya and Lang (1965a) applied high-resolution X-ray absorption topography, taking advantage of the fact that local high concentrations of impurity occur in bands in the coat. By comparing the X-ray absorption of various wavelengths, an idea of the atomic number of the impurity can be obtained, and certain elements can be definitely identified and assayed. One such element is iron, whose presence can be sensitively detected by comparing the difference in absorption of $\text{CoK}\alpha$ and $\text{CoK}\beta$ radiations. In the present work it was found that iron was not a major impurity in the coat. The experiments showed that the major impurity elements responsible for the absorption were either quite light, with atomic numbers up to and including titanium (elements such as magnesium, aluminum, silicon, potassium and calcium, probably in combination with each other and with oxygen), or were elements relatively heavy, with atomic numbers greater than the first transition series. Maximum local impurity concentration estimates were about 0.7% MgO or SiO_2 , or a few tenths of 1% of a heavier element such as zirconium. In the presence of such non-ferrous absorbers, the upper limit of the concentration of iron was reckoned to be 0.03%.

Quite recently an account of an electron micro-probe X-ray spectrographic examination of a coated diamond has been published (Seal 1966). This found inclusions in the coat containing silicon and oxygen. One inclusion contained potassium and calcium. No iron was reported. These findings provide good confirmation of Kamiya and Lang's interpretation of their X-ray absorption data.

2.1.8. Planar growth defects in diamond.

In Section 2.1.1. it was mentioned that lamellar defects are of frequent occurrence in diamond. Usually these take the form of fairly extensive sheets of extra diffracting power lying parallel to what was once a growth surface of the diamond. Sometimes they can be traced right round the diamond, forming a complete shell. Sometimes they occur only as the trace of one face, or as the incomplete trace of one face. This localisation may arise from their being the relict of a once continuous shell, most of which had been removed during an epoch of solution in the diamond's history, or from their having been formed only on a particular area of the growing face where there was a local concentration of impurity, growth having occurred under conditions not permitting this impurity to be diffused or carried uniformly around the whole growing surface. Localisations of both types have been observed. In this Section there will be described a quite different type of localised defect, one which is more strictly crystallographically oriented, lying parallel to a $\{111\}$ plane, such plane being inclined at $70\frac{1}{2}^{\circ}$ to the local octahedral growth surface. This defect behaves as a fault surface with a well-defined fault vector, in every way similar to a stacking fault. These stacking-fault type defects are probably quite rare. They have only been observed in one stone which otherwise was of exceptionally high lattice perfection. Apart from one completely grown-in defect which took the form of a regular tetrahedron about 115 microns in edge length, all the plane defects (about 10 in number) outcropped at the surface of the crystal. Some took the form of equiangular triangular sheets with one edge lying in the crystal surface. Others were trihedra composed of three triangular sheets on the three $\{111\}$ -type planes inclined to the crystal surface. The latter formed an open pyramid cutting the crystal surface in an equilateral triangle, with the pyramid apex about 30 microns below the crystal surface. The resemblance of these features to the defects observed by electron microscopy in epitaxially grown layers of silicon on silicon (e.g. Booker 1964) is extremely close, even to the occurrence of single triangles and of trihedra, but not of dihedra. The nature of the defects is doubtless the same in both cases: a stacking fault is nucleated at the crystal growth surface when a small

triangular island of wrongly stacked material is laid down, and then, as the crystal continues growth, it propagates outwards along $\{111\}$ planes inclined to the growth surface. An account of the work done on these defects has been published (Lawn, Kamiya and Lang, 1965, R17). The interest of this work is twofold. Firstly, the fault surfaces which outcrop at the crystal surface are probably in material which was crystallised during the final stages of growth of the crystal. They are thus of significance in providing evidence of conditions at the conclusion of growth. Optical examination of the faces of the stone did not reveal any etch features. Dislocation outcrops were not accompanied by trigons. It is likely that this diamond had not been etched, or if so, only very lightly. Such diamonds are rare.

Secondly, the analysis of the diffraction contrast from the planar defects, which required topographic experiments of the highest refinement obtainable, applied diffraction theory to derive as much information as possible concerning the nature of the defects. A development of dynamical diffraction theory was worked out in order to explain the diffraction effects produced by the interior tetrahedral defect. This involved the explanation of types of diffraction image of which no counterpart would be observable in electron microscopy. Agreement between theory and experiment was very good. In the case of the single triangular fault surfaces it was found possible, despite their small size, to resolve and study separately both the 'area contrast' they produce in certain reflections and the 'line contrast' from their bounding partial dislocations that appeared in other reflections. They were found to be bounded by Frank sessile dislocations.

2.1.9. Imperfections in Type II diamonds.

Type II diamonds have a bad reputation as regards lattice perfection. On the other hand, the work described in Section 2.1.5. showed that Type II optical characteristics are not necessarily linked with a mosaic structure. There do exist, however, certain curious types of mosaic structure among Type II diamonds which involve considerable lattice misorientations. It is likely that the presence of some crystals of this sort among the small fraction classified as Type II out of the total population of diamonds has had the effect of lowering the reputation of this class as a whole. Little

quantitative work has been done on the characterisation of the mosaic structures exhibited by Type II diamond, either by high-resolution topography or by any other method. The observations recorded here involved only a few samples, and the conclusions drawn are only tentative.

The range of misorientations involved is quite large, up to several tenths of a degree in some cases. The linear scale of the misoriented regions is small, down to the limits of X-ray topographic resolution. Hence these diamonds can approach the completely imperfect mosaic crystal in character and have a correspondingly high integrated reflecting power.

It appears possible to divide these mosaic diamonds broadly into two classes, (a) those which exhibit a strong and characteristic birefringence pattern and (b), those which exhibit little birefringence. Class (a) are readily detected as a consequence of their birefringence, whereas the high degree of lattice misorientation in class (b) would not be suspected before X-ray examination. The characteristic birefringence of class (a) has been studied by Ramachandran (1946), and by Freeman and van der Velden (1952). The Indian workers refer to it as a 'geometric' or 'laminar' birefringence pattern: a good descriptive term for this birefringence pattern is 'tatami', after the Japanese rice-straw mat. Tatami patterns resemble closely the stress birefringence patterns in deformed transparent crystals such as the halides (in silver chloride, for example, as described by Nye (1949)). In one tatami diamond examined in the present work the pattern showed laminations with traces parallel to the octahedral planes, but with one set of laminations dominant. The pattern was similar to that given by plastically deformed crystals with intersecting slip systems, one such system being dominant. X-ray topographs enable the actual misorientations to be mapped, though this is a somewhat tedious operation. The topographs show quite sharp lattice curvatures to be present. In class (b) the crystal appears broken up into cells. The distribution of orientations of the cells has not yet been analysed. The relationship between misorientation and position in the specimen does not obviously resemble that exhibited by the tatami diamond, class (a). In class (b) sharp lattice

curvatures ranging over distances of several microns do not seem to be present. The tentative explanation of the mosaic structures of classes (a) and (b) is that diamonds of class (a) have undergone plastic deformation, and that class (b) are annealed and polygonised class (a) diamonds.

2.1.10. Radiation damage in diamond.

Because so much study has been concentrated on various physical properties of diamond over the years, and so much data have been accumulated (though not necessarily fully explained and understood), there is a good case for investigating the effects of irradiation on diamond, both to discover what new properties are exhibited by irradiated diamond and to trace how the behaviour of undamaged diamond is modified by a progressive increase in radiation damage. Such an investigation includes the determination of to what extent the original state may be recovered after annealing. Much of the work done to date on radiation-damaged diamond has been concerned with the changes in optical absorption in the visible and infra-red regions, and in the electron spin resonance spectrum. Most of the experiments have been performed on Type II diamonds because these are purer than Type I diamonds. Strong Type I diamonds contain more than 1×10^{20} atoms of nitrogen per cc. As far as is known, the concentration of other impurity elements in gem-quality diamonds does not generally exceed about 10^{18} atoms per cc. Since, however, the majority of the nitrogen atoms in Type I diamonds are segregated in platelets (see Sections 2.1.5. and 2.1.6) the diamond matrix in Type I stones may well have on average no more impurity dispersed on an atomic scale than Type II. Hence there may be no great difference between Type I and Type II stones as far as the reactions in the bulk of the crystal between the radiation, the diamond structure and the impurities are concerned. (It would be desirable to investigate whether in fact there is a difference between Type I and Type II diamonds as regards the density changes occurring upon irradiation, and the degree of recovery of original density after annealing.) Optical and electron spin resonance studies may indeed be simplified by using Type II stones, but it should be borne in mind that gem-quality Type II diamond is apparently prone to severe lattice distortions and misorientations not exhibited by Type I stones assessed visually to be of as good a quality (see Section 2.1.9.).

It is regrettable that the Type II diamonds whose behaviour after irradiation has been reported in the literature were not examined X-ray topographically so that their lattice imperfections could be recorded.

The diffraction phenomena exhibited by radiation-damaged crystals depend upon the range of the damaging radiation, and whether the whole specimen has been irradiated or only a geometrically well-defined part of it (defined, for example, by an aperture in a radiation shield). If the range of the damaging radiation is less than the specimen thickness, or if part of the specimen is shielded from the radiation, there will be gradients of radiation damage. Since the most common macroscopic manifestation of radiation damage is a dilation, it follows that a single crystal which contains a gradient of radiation damage will also contain a strain gradient. Strong diffraction contrast can be produced locally where the strain gradient exists. Even if the whole specimen receives a uniform dose of damaging radiation, strain gradients may be produced near the surfaces if decomposition products can diffuse towards the surfaces and escape. The effects of radiation damage in diamond should be less complicated than in some materials, such as halides. The crystal structure of diamond is simple. It consists of the single element carbon which does not retain radioactivity after irradiation. Its cross-section for both high energy and thermal neutrons is small so that large specimens may receive a very uniform dose of such radiations. It is not to be expected, in the case of diamond, that the atomic rearrangements occurring during damage or during recovery from damage should be influenced by the proximity of surfaces, but no proper test for strain-gradients at surfaces of irradiated diamond has yet been performed by X-ray topography. On an atomic scale, the processes of radiation damage by fast neutrons in diamond must certainly be complex: the carbon atoms recoiling under impact by such neutrons may have energies up to 10^5 electron volts. This energy is dissipated in many steps, involving different processes.

A notable feature of neutron irradiated diamond is the large decrease in density it can suffer without exhibiting any marked deterioration of the

sharpness of its X-ray diffraction spots as seen in Laue or rotation patterns. Such density decreases may be up to about 4%, corresponding to a linear expansion of over 1%.

This resilience of the diamond structure to radiation damage by neutrons has not only been confirmed by X-ray topographic studies but has been shown to include the maintenance of a high degree of long-range order in the crystal lattice.

Studies have been made of natural octahedral diamonds, of edge length about $2\frac{1}{2}$ mm, which had been irradiated in the Pluto reactor of the Atomic Energy Research Establishment, Harwell. This work was done in collaboration with Dr. E. M. Wilks of the Clarendon Laboratory, Oxford. The fast neutrons had energies up to 10 Mev and the temperature of the specimens during irradiation was about 35°C. Two specimens which were examined in detail had received, respectively 2×10^{19} fast nvt, and 1.4×10^{18} fast plus 1×10^{19} slow nvt. The density decrease of the former specimen was more than 1%. Topographs of both specimens showed diffraction contrast due to (a) surface damage, (b) dislocations radiating from the center of the crystal and (c) sheet-like layers of imperfection. Although considerable lattice imperfection was present, no special diffraction feature was exhibited that could be definitely assigned to radiation damage. It was remarkable how strong the diffraction contrast of individual dislocations remained. This showed that coherence between the incident and Bragg reflected X-rays was maintained over at least some tens of microns. Thus, on the scale of a micron and above, the lattice expansion that had occurred had been extremely homogeneous and isotropic, so that the long-range order of the lattice had been little disturbed. There was some indication, however, that stresses at localised surface damage had been partially relieved.

2.1.11. Abrasion of diamond.

Diamond is the hardest known natural crystal. Upon its great hardness and its resistance to abrasion rest its value in industry as a cutting tool and as a wear-resistant die for wire-drawing. The strong orientation dependence of its mechanical properties when tested under

certain conditions, and the reputed variability and inhomogeneity of diamonds with respect to their mechanical properties, are essentially problems of crystallography and crystal-lattice perfection. Towards the understanding of these, X-ray topography is beginning to make a significant contribution. At the least, X-ray topography can perform a useful service through examining and classifying specimens, and by helping to correlate and rationalise diverse observations. It can proceed further, however, and provide valuable clues to the nature of the mechanisms active on an atomic scale which are involved in the abrasion of diamond.

The simplest method of testing diamond is the scratch test. This shows that diamond will scratch every other naturally occurring substance. It is thus placed first on Moh's hardness scale. Scratch tests on diamond can be made by dragging a diamond stylus over a flat polished diamond surface: these do not reveal the strong anisotropy of resistance to abrasion that is found in some other types of test. Another method of measurement of diamond hardness is the indentation test; in this a small indenter, usually itself made of diamond and having a spherical contour, is pressed into a flat diamond surface so as to form ring cracks. Moderate anisotropy of cleavage properties is demonstrated by ring-cracks; octahedral planes are the preferred cleavage planes. These indentation experiments, in which large cracks a good fraction of a millimeter in length are propagated, are relevant to the study of ring cracks on natural diamond surfaces (which are geometrically similar though usually not larger than a few tens of microns), and to the shattering of diamond tools. Shattering, however, can be minimised by proper mounting and careful use of tools. On the other hand, surface wear, i.e. the gradual removal of material from the working surfaces, is an unavoidable consequence of use, and is much in need of scientific study. The degree of abrasion hardness of diamond has been studied by various workers. One old-established method is to hold the stone flat against a rapidly rotating cast-iron disc (known as a scaife) which is charged with a mixture of oil and diamond powder. The rate of wear is obtained from the rate of loss of weight of the diamond. A newer and more interesting

method is to use the micro-abrasion technique. In this the edge of a small double-conical, rotating, cast-iron wheel is pressed into the surface of the diamond. The wheel is about $\frac{1}{2}$ inch in diameter, its cross-section profile has an included angle of 110° , and it rotates at between 5,000 and 10,000 r.p.m. It may be charged with olive oil and diamond powder about 1 micron in diameter. Alternatively, diamond-bonded wheels may be used. Elastic deformation and wear of the periphery of the wheel, together with some vibration during rotation, have the effect of rounding the profile of the cut produced on the diamond so that it takes the form of a shallow ellipsoidal segment. Its depth and shape can be measured with great accuracy by multiple-beam optical interferometry. Such measurements, combined with phase contrast microscopy, also indicate how smooth is the surface of the cut. Typical cut dimensions are length 0.6 mm, width 0.15 mm, and depth 3 microns. Other advantages of the micro-abrasion technique are that several cuts may be made on the surface of a single stone to examine its uniformity of hardness, and the cuts may be made on areas whose orientation is known precisely. A combined X-ray topographic and micro-abrasion study has been made on several diamonds, the micro-abrasion work being performed by Dr. E.M. Wiiks of the Clarendon Laboratory, Oxford. Some X-ray topographic studies of artificially produced ring cracks have also been performed.

The information provided by X-ray topographic examination of micro-abrasion cuts and ring cracks is as follows. (a) A full topographic survey of the specimen (which can be performed both before and after the mechanical damage is introduced) shows what grown-in lattice strains and imperfections are present in the stone and how they interact with the artificially produced damage. There is evidence that abrasion resistance is affected by impurity layers in the crystal. Such layers can be mapped by X-ray topography. Similarly, stress concentrations at inclusions or precipitates, which are likely to influence crack propagation, can also be mapped.

(b) When the load producing a crack is removed, the surfaces of the crack may close together sufficiently to make the crack invisible

optically. X-ray topographs can show the full depth of cleavage by detecting the loss of coherence between rays diffracted from either side of the crack. They show the lattice damage remaining when the two surfaces of the crack collapse together and do not heal.

(c) By use of a finely-collimated incident beam and by taking topographs with the specimen's angular setting varied over a range about the setting for maximum Bragg reflection, misorientations of damaged material by more than a fraction of a minute of arc are readily detected and mapped. Such misorientations are observed at ring cracks, for example.

(d) Topographs taken with different reflections can find the direction of displacement in the strain field produced by the indentation or abrasion.

(e) The combined evidence of topographs taken with different radiations and with different reflections enables a picture to be built up of both the tilt and dilation components of the strain-field. Exact analysis is difficult, but experience with the study of strain fields of dislocations provides helpful analogies.

(f) If plastic deformation has occurred through the propagation of dislocations along slip-planes then this can be detected provided that the dislocations have moved a distance of roughly 10 microns or more.

It will be appreciated from the foregoing that the information obtained by X-ray topographs not only complements that gained by optical methods but also provides an independent variety of data. The sensitivity of the X-ray methods is sufficient to detect surface damage due to abrasion when nothing can be seen either by multiple-beam interferometry or by phase-contrast micrography. Very small amounts of strain, deep in the crystal, can be detected on topographs by the bending of Pendellösung fringes (see Sections 3.1. and 4.1.) The X-ray topographs are insensitive to irregularities of surface contour, especially in the case of diamond which absorbs X-rays lightly. Tilts of lattice planes parallel to the crystal surface can be detected more sensitively by diffraction contrast

than by measurement of surface contour.

Some specific findings relating to microabrasion cuts will now be summarised. The topographs of cuts on cube, dodecahedral and octahedral faces show interesting differences, but the general pattern is similar for these three faces, and for 'hard' and 'soft' directions on each face. Within the abraded area there appear striae in the direction of motion of the abrading wheel. The average width of striae is a few microns. Using soft X-radiation such as Cu K α and Cr K α these striae can sometimes be resolved into strings of individual micro-cracks. Although these cracks are lined up into striae, the variation of their diffraction contrast with orientation of the diffraction vector does not vary markedly. The most notable feature in the diffraction contrast pattern is the intense concentration of strain (more strictly, of strain gradients) around the periphery of the cut. This peripheral diffraction contrast is especially intense at the end of the cut at which the rotating wheel enters the cut. Topographs taken with the diffraction vector making various angles with the long axis of the cuts show that the strain at the periphery is mainly a lattice rotation about an axis lying in the crystal surface and tangential to the periphery of the cut. By taking transmission topographs with Cu K α radiation which is appreciably absorbed in traversing thicknesses of 1 - 2 mm of diamond it is possible to determine the sense of the lattice rotation by noting the difference in the distribution of diffraction contrast between hkl and $\bar{h}\bar{k}\bar{l}$ topographs. (This utilises the phenomenon of 'energy-flow refraction' in conjunction with the Borrmann effect, see Section 4.1.)

All these observations are compatible with the following model. The abraded area is covered by microcracks of the order of 1 micron depth. Imperfect healing of these cracks after removal of load, and the trapping of debris within them, result in production of a thin layer in a state of uniform compressive stress. This produces an outwardly directed surface traction at the periphery of the cut. Precisely at the periphery this model exhibits an elastic singularity but at distances more than a few microns from the periphery realistic values of dilation and tilt can be derived which agree quite well with observations. To explain the additional contrast where

the abrading wheel enters the cut, a line source of additional compressive stress is placed at this region of the periphery and is superimposed upon the stress produced by the surface layer covering the abraded area as a whole. This extra stress doubtless is due to a concentration of cracks where the wheel, loaded with abrasive particles, first causes these particles to hit the surface of the specimen. A concentration of microcracks at this region of the periphery is also to be expected since during the course of abrasion the resultant stress due to friction will be here most strongly tensile. The elastic strains revealed by the topographs are very intense: within the region covered by microcracks they may approach 1%. The small lattice tilts detectable by X-ray topography also extend to a long distance outside and below the cut: tilts of more than 1" of arc may exist up to distances of about 75 microns outside or below the periphery of the cut. The X-ray topographic studies suggest that the process of abrasion of diamond can be explained satisfactorily by a mechanical model involving brittle fracture alone: a crazing of the abraded area with microcracks and the continuous plucking of fragments from it. No evidence for graphitization or plastic deformation has been obtained.

2.2. Synthetic Diamond.

The literature on the morphology and imperfection content of man-made diamond is not extensive; references to the relatively small number of important papers relating to these topics may be found in R13 (Kamiya and Lang 1965b). Bovenkerk first described the variations in morphology that occur as a result of variations in conditions of synthesis: the habit of well-formed diamonds may vary from octahedral through cubo-octahedral to almost pure cubic, and the cubic faces possess a smoothness and flatness never exhibited by the occasionally observed cube faces of natural stones. In X-ray diffraction studies the most striking phenomenon to be reported is the 'satellite' diffraction pattern studied by Lonsdale and co-workers. This is the pattern of a face-centered cubic phase, lattice parameter 3.539\AA , which appears to be a carbon-nickel phase deriving from the nickel impurity that is included in many synthetic diamonds. By taking X-ray photographs using standard single-crystal techniques Lonsdale and co-workers found that the crystallites producing this satellite pattern were in parallel

orientation with the diamond matrix. To discover more about the nature and distribution of the crystallites responsible for the satellite pattern, topographic studies are required. In this problem and in others to do with synthetic diamond it was clear that X-ray topography could yield useful information, particularly in view of the wide experience already gained in studies of natural diamond. Consequently, a comprehensive topographic study was undertaken to examine the characteristics of both the most perfect man-made diamonds and also the much more common and imperfect specimens. This work has been fully reported (Kamiya and Lang 1965b, R13) so only a few aspects of it will be touched upon here.

As regards technique, the experiments were fairly demanding. The crystals examined ranged from about 100 to 500 microns in diameter. Reflections from crystals near the smaller limit of this size range are not always easy to locate. When making adjustments to the specimen such as changing the setting of the arcs of the goniometer head, and when rotating the specimen about the goniometer axis, it is necessary to check frequently that the specimen remains properly bathed in the incident X-ray beam. Complications arise from twinning of the specimen (this is very frequent in synthetic diamonds) and from the presence of gross misorientations. A useful innovation was the development of the technique of taking stereo-pairs of absorption topographs using a selected, strictly monochromatic radiation. A perfect crystal of germanium, translated to and fro, was used to produce a uniform beam of the required monochromatic radiation (such as Cu K α and Cu K β , the latter radiation being much more strongly absorbed by nickel than the former. The absorption topographs were taken with the specimen set at any desired angle with this monochromatic beam. Thus stereo-pairs with any desired convergence angle could be produced; and any particular plane in the specimen could be brought parallel to the monochromatic beam.

Among the findings, the following may be noted. The better synthetic diamonds were, at least in some parts, relatively perfect. The familiar pattern of dislocation bundles radiating from a central nucleus could be recognised, and in favourable cases it appeared that individual dislocations could just be resolved. Where flat areas were present on the specimen surface, absorption topography revealed a nickel-rich film on

such areas, and diffraction contrast showed that this film was producing appreciable strain in the crystal underlying it. The absorption topographs detected nickel-rich impurity present internally in two states of agglomeration: as roughly globular inclusions ranging from 2 to 15 microns in diameter which produced little strain in the diamond matrix, and as finely divided material (less than 1 micron in diameter) which did produce strain in the matrix. In one case this finely divided material lay in a well-defined sheet which appeared to be the trace of the outward motion of a crystal edge during growth. This edge was of the $\langle 110 \rangle$ type that would be formed at the junction of two $\{111\}$ -type faces that have an included angle of $70\frac{1}{2}^\circ$.

The reflections of the satellite pattern could also be divided into two groups. One group was produced by relatively large crystallites. These were only roughly parallel to the diamond matrix since they were in some cases misoriented up to 6° from the matrix. The other group arose from quite small crystallites closely parallel to the matrix. Tentatively, the large inclusions were associated with the former group of reflections, and the finely divided inclusions with the latter group; but this relationship was not proved.

The rounded shape and general absence of matrix strain associated with the larger inclusions suggested that they had been incorporated as molten droplets. This absence of 'grown-in' stress at the larger inclusions, and the presumably rounded form of the internal surfaces of the diamond enclosing the globules, should prevent the build up of excessive stress concentrations at these inclusions when the diamond is subjected to external load. It may even be that these cavities in the diamond act as 'crack stoppers', inhibiting the propagation of cleavage through the crystal. This may be the explanation of the reputed better resistance to cleavage of synthetic diamond compared with the natural material.

2.3. Silicon.

2.3.1. The origin of dislocations in melt-grown silicon.

Since the complete configuration of dislocations within a large single crystal can be mapped by X-ray topography, this method of investigation is the one best equipped for providing information from which the origin of the dislocation configuration can be deduced. It is helpful that the method provides data on both the spatial configuration of a dislocation line and on its Burgers vector, and that it shows, moreover, the spatial relationship between any dislocation line and the local orientation of the growth front and of the external surfaces of the crystal. Some of the earliest X-ray topographic studies were performed on silicon crystals grown by the Czochralski method. The topographs of such crystals often revealed bands due to varying amount of oxygen impurity and other signs of instability both of growth rate and impurity content. Some such crystals, however, did show relatively large volumes free from dislocations. In view of the greater purity of crystals grown by the floating-zone method it was considered desirable to make a survey of dislocations in a crystal grown by this method. The first X-ray investigation of this type is here summarised, a full report having already appeared in the literature (Jenkinson and Lang 1962, R2). It should be borne in mind that at the time this work was performed the floating-zone technique was still under development. Although the material produced was of high purity (the X-ray topographs bore witness to the high degree of lattice perfection apart from dislocations), sufficient control of thermal conditions had not yet been achieved to keep thermal stresses in the specimen low enough to avoid plastic deformation. Thus the dislocation density was by no means negligible: in parts of the crystal remote from the seed the density was locally in excess of 10^5 lines per cm^2 .

The investigation had the following main aims: to record the density and spatial arrangement of dislocation and to identify the dominant Burgers vectors at a series of positions along the length of the crystal, to examine the modes of dislocation motion and multiplication due to thermal stresses, to search for evidence of generation of dislocations in the process of solidification, and to analyse dislocation reactions.

Seven slices were cut from the crystal, covering a length of about 35 cm, and at least eight topographs (using different Bragg reflections) were taken of each slice. The dislocation configurations observed in all slices indicated a complex history of dislocation movement, with different slip systems having operated at different times and temperatures during the cooling of the crystal. Within about 1 cm of the seed the dislocation configuration was fairly simple and the density quite low. At about 2 cm from the seed there began to appear localised dislocation 'tangles'. These tangles were a notable feature of the dislocation configuration in all slices from parts of the crystal further from the seed. In such slices a three-zone distribution of dislocations across the ingot section had become established. Near the central axis of the ingot the tangles were found most profusely. The rim of the crystal section contained a relatively high density of glide dislocations with fairly straight segments. Between the core of the ingot and the rim was a zone of relatively low dislocation density, with the dislocation-line segments being generally more curved than in the rim. It was possible to analyse the distribution of Burgers vectors in the simpler tangles. The shape and location of the tangles indicated that they were associated with the mutual intersection of active slip planes, and that they were composed mainly of a pile-up of dislocations gliding in two or more intersecting slip systems. This conclusion was supported by the Burgers vector analyses possible in the simpler cases. Evidence was obtained that the heart of the tangle consisted of one or more Lomer reactions. Such reactions produce relatively immobile dislocations which would impede the movement of others and could initiate a local piling-up of dislocations. It is clear that the growth of tangles will involve a rapid build-up of dislocation density and will lead to work-hardening. Indeed, if an extrapolation from these observations at fairly low dislocation density is made, it suggests that the growth of tangles nucleated by Lomer reactions is an important part of the process of work-hardening in face-centered cubic crystals, and will be initiated when two mutually intersecting slip systems become simultaneously active.

Regarding dislocation sources, the X-ray topographs showed that internal multiplication during glide certainly occurred. The commonest

cause of increase in dislocation-line length arose from the cross-slip of screw components. Lack of stable pinning of loop ends prevented repetitive operation of sources of the Frank-Read type: rarely were more than one or two turns of a Frank-Read spiral observed. There was evidence that surface sources of dislocations were active. No evidence was found for the generation of dislocations by a vacancy disc collapse mechanism, or by growth accidents at the advancing growth front. The increase of dislocation-line length during glide and the trapping of dislocations in the crystal through their mutual interference appeared to account quite adequately for the density of dislocations observed.

2.3.2. Dislocation configurations in a very lightly deformed silicon crystal.

In specimens of silicon such as that described above in Section 2.3.1., in which most of the plastic deformation probably took place at a temperature within a couple of hundred degrees of the melting point, it is notable how curved are the dislocation lines involved in this high-temperature slip, and how easily cross-slip has occurred. The dislocations are not at all closely confined to their slip planes. At lower temperatures the tendency for dislocation lines to lie parallel to $\langle 110 \rangle$ or $\langle 112 \rangle$ is stronger, and at the lowest temperatures at which plastic deformation occurs the $\langle 110 \rangle$ directions are dominant. However, it is quite difficult to produce specimens containing a low density of dislocations with well developed linear segments parallel to $\langle 110 \rangle$. The technique for producing such specimens was beautifully developed by the late W. C. Dash. He started with bars about 2 to 3 mm square in cross-section and about 20 mm long which had a very low or zero density of grown-in dislocations. By twisting such bars in a narrow range of temperatures between that at which brittle fracture always occurred and that at which dislocations moved and multiplied too readily, he produced specimens in which slip had occurred on but a few planes, widely separated spatially. Several bars deformed in this manner by Dash have been examined X-ray topographically. The non-destructive character of the X-ray examination, and its ability to survey quickly large volumes of specimen, were useful in these experiments. Several well-developed internal dislocation sources of the Frank-Read type were discovered. One found in a bar which had probably been dislocation-free

before twisting was chosen for detailed examination. The aim of the study was to determine fully the three-dimensional configuration of the dislocations involved in the operation of the source, taking advantage of the fact that the X-ray method does not suffer from the limited depth of focus of the optical microscope, and that when a penetrating radiation such as Ag K α is used dislocations within a depth range of about 2 mm are clearly seen. By identifying Burgers vectors of dislocations as well as displaying the dislocation geometry it was possible to gain some idea of the conditions which brought the source into operation and the circumstances that subsequently caused its operation to cease. This analysis has been reported already (Authier and Lang 1964, R8). The presence of long straight dislocation segments in the specimen, some segments being pure screws, others 60° dislocations, gave opportunities for studying certain aspects of the diffraction contrast produced by dislocations. One such investigation involved the determination of the sense of pure screw dislocations (Lang 1965a). Other observations, involving the long-range strain fields of dislocations and their interaction with Pendellösung fringes (Kato and Lang 1959), provided valuable confirmation of some of Kato's theories (see Kato 1963a and Section 4 of this Report). A few points arising from the analysis of the dislocation geometry were as follows. The orientation of dislocation lines along $\langle 110 \rangle$ directions was shown not to be as strict as a cursory view of the configuration would suggest. departures from $\langle 110 \rangle$ directions amounting to several degrees were found. The configuration showed that 60° segments had travelled faster than pure screw segments. A variety of interactions between dislocations which had intersected each other, or which were still effectively in contact, was noted. Some such interactions enabled the relative sense of the Burgers vectors of the dislocations to be determined.

2.4. Germanium

2.4.1. Dislocation configurations in melt-grown crystals.

X-ray topography of germanium presents a problem not present in the case of silicon and diamond, in that germanium, being of moderately high atomic number, absorbs X-rays quite strongly. The identification of Burgers vectors from the diffraction contrast effects produced by dislocations is simplest, and the contrast is strongest, when the absorption is low. For this reason it is preferred to work in the range where the product of linear absorption coefficient, μ , and crystal thickness, t , is in the range $\mu t \leq 1$. For AgK α radiation values of μ for diamond, silicon and germanium are, respectively, 1.4, 8 and 183. The corresponding values of t , in mm, for which $\mu t = 1$ are 7.1, 1.25 and 0.054. Early topographic experiments with germanium specimens a few tenths of a millimeter thick showed quite different types of dislocation diffraction contrast from that observed with silicon. This difference was soon realised to be due to the much higher absorption in the case of germanium, and not to be due to any intrinsic difference between the two elements. Indeed, by comparing topographs of a germanium crystal about $\frac{1}{2}$ mm thick taken using AgK α (for which $\mu t \sim 10$) with those using W K α (for which $\mu t \sim 1$) it was proved that similar dislocation contrast was obtained to that found in silicon under the conditions $\mu t \sim 1$ (Lang 1959b). In the range of crystal thicknesses for which μt lies between about 2 and about 5 it was found that the dislocation contrast could be either positive (i. e. an excess of diffracted intensity from the dislocations compared with the matrix), or negative, and the type of contrast depended upon the position of the dislocation line within the crystal and upon the degree of edge or screw character of the dislocation. In particular, it was found that there could be a reversal of contrast of a given dislocation between topographs taken with $hk\bar{l}$ and $\bar{h}\bar{k}l$ reflections. It was believed that this contrast reversal could be used to find the sense of the dislocation Burgers vector. This belief was confirmed by an extended series of theoretical and experimental investigations which showed how X-ray topographic observations could be used to determine both the sense and the orientation of Burgers vectors (Hart 1963). These investigations were carried out mainly on specially prepared germanium

specimens and made use of both the dislocations present in the 'as-grown' specimen and dislocations deliberately introduced by controlled plastic deformation. The specimens were prepared in the form of thin wedges with smooth and flat surfaces. The wedge shape enabled the variation of dislocation contrast with specimen thickness to be studied on one and the same specimen. (Variation of diffraction contrast with X-ray wavelength and linear absorption coefficient was also studied by comparing topographs taken with Ag K α , Mo K α and Cu K α radiations.) The need for smoothness of the specimen surface arose both from the high X-ray absorption in germanium and the relatively small extinction distance (~ 10 microns); the topograph would exhibit a mottled appearance, at least at the thin end of the wedge, if the specimen surfaces were not smooth to within a few microns. The work on the diffraction contrast of dislocations will be described more fully in Sections 4.1 and 4.2; here an account will be given of some of the features discovered in the configuration of 'grown-in' dislocations in germanium.

The germanium crystals used were provided by the Royal Radar Establishment, Malvern. They were grown by the Czochralski method. Typical crystal dimensions were: length 8 cm, maximum diameter 2.5 cm. Their resistivity (intrinsic) was 50 ohm-cm at room temperature. The crystals were grown with careful control of temperature gradients to reduce the amount of plastic deformation produced by thermal stresses. The growth axis of the crystal was a $\langle 110 \rangle$ direction. For convenience in the following discussion this is taken to be $[1\bar{1}0]$. With this growth direction it is found that most dislocations grow out of the crystal and that at distances of a few crystal radii from the junction with the seed (or from the crystal 'shoulder' where plastic deformation is most prone to occur) the dislocations remaining are few in number and are mainly long and straight, parallel to the growth axis. It had been believed, on the basis of the work by Tweet (1958) and Dash (1959), that these long axial dislocations were pure screw, or possibly of 60° type. In the present work it was found that all of these dislocations were pure edge. It is believed that they were formed by a Lomer reaction between dislocations gliding on (111) and $(1\bar{1}\bar{1})$ slip-planes. If, while combining, they intersect the growth interface of

the crystal then they could be grown into the crystal indefinitely as long pure edge dislocations parallel to $[1\bar{1}0]$. To try and check this hypothesis, crystal sections were cut at closely spaced intervals and topographically surveyed. In this way it was hoped to trace these edge dislocations back towards the seed to see if they originated at Y-shaped nodes, the stem of the Y being parallel to $[1\bar{1}0]$ and its two arms lying respectively on the (111) and $(\bar{1}\bar{1}\bar{1})$ slip-planes with the appropriate Burgers vectors. It was found that the pure edge dislocations ran back into regions of fairly high dislocation density in which it was not possible positively to identify the expected reactions. There was, however, strong circumstantial evidence for the Lomer-reaction origin of these pure edge dislocations and for their having been grown into the crystal in the manner proposed. In this connection it could be seen that these edge dislocations were older than some of the glide dislocations and that they had remained immobile during later stages of plastic deformation. They had in fact acted as obstacles to the movement of the later-moving dislocations. Indeed, they could initiate tangles such as those observed in silicon (Jenkinson and Lang (1962)).

2.4.2. Deformation of germanium.

Crystals of germanium, originally dislocation-free or nearly so, have been deformed deliberately. This was done not for the purpose of studying the plasticity of germanium but to produce dislocation configurations suitable for working with in the investigation of the diffraction contrast in dislocation images. However, in the course of the work a good insight was obtained into the mode of multiplication and movement of dislocations in germanium near the threshold of plastic deformation. For the study of dislocation images it was required to produce configurations satisfying the following conditions: 1, the dislocations must be well separated from each other spatially, 2, they should have long linear segments (but these could be pure screw, 60° , or pure edge), and, most important, the sense of the Burgers vectors should be known. The latter condition could not be satisfied by generating dislocations from internal sources which would produce segments of opposite Burgers-vector sense

in roughly equal lengths. Early experiments with crystals pulled in tension did not produce dislocation configurations satisfying any of the above listed conditions, even though surface indentations were made on the crystal after etching and prior to pulling in the hope of restricting the sources of dislocations to the neighbourhood of these indentations. On the other hand, very satisfactory dislocation configurations were produced by three-point bending of bars at 510 to 520°C. The bars were 15 mm long and 2.5 mm by 4.0 mm in cross section. The bend axis was parallel to the side 4.0 mm wide. This axis was the $[11\bar{2}]$ direction and the specimen was oriented so that the (111) plane made about 50° with the face 4.0 mm wide. After grinding to shape, the bar was carefully chemically polished. Then surface reflection X-ray topographs were taken to check that all surface damage had been removed. Just before inserting in the bending jig, scratches were made with a diamond point parallel to the long dimension of the bar and along the center lines of the faces which were to become respectively convex and concave. These scratches then became the only sources of dislocations in the crystal. After bending, surface reflection topographs were again taken to find the distribution of dislocation outcrops. At suitably chosen places slices parallel to active slip-planes were cut out from the bar. After grinding and polishing to a final thickness of 80 to 100 microns the slices were surveyed by transmission topography and the glide dislocation images were studied in detail. It is difficult to restrict slip to one system only in this method of deformation, but locally one system would be dominant, and slices could be cut from the bar which contained a single system only. These slices showed arrays of dislocation, well spaced apart, with straight segments up to several hundred microns long. These segments were either pure screw or 60° in character. Also, as was particularly desired, the great majority of dislocations within a given group had Burgers vectors of the same orientation and sense. Some of the diffraction contrast phenomena observed will be described in Section 4. A full account of this work has been prepared (Hart 1963) and will be published in due course.

2.4.3. Heavily-doped germanium.

Practical interest in phenomena connected with impurity distribution in semi-conductor crystals stems from the importance of producing uniformly highly doped materials such as are required in Esaki diodes. Although the melt may be kept well stirred, it is found that crystals may take up the doping element in a very non-uniform way. This happens especially when 'cellular growth' occurs. Further redistribution of impurity may occur behind the solidification front. Occluded drops of dope-rich material may migrate before solidifying, and precipitation of segregated impurity may occur in part of the crystal. The interaction between the grown-in dislocations and the impurity cell structures, the distribution of stresses and dislocations produced by precipitates, and the tracks of migrated droplets can all be investigated by X-ray topography.

Crystals with the following compositions have been studied:

- Ge + 10^{-3} wt. % In,
- Ge + 10^{-3} wt. % Ga,
- Ge + 5×10^{-3} wt. % Sb,
- Ge + 3×10^{-2} wt. % Sn.

The following effects were observed. The walls of impurity cells can be detected by diffraction contrast due to the strain gradients associated with the excess impurity in the walls. In the specimens studied there was no nucleation of dislocations in the walls, and comparatively little interaction between the walls and the grown-in dislocation distribution. When precipitation had occurred, intense local strain was produced. When thin specimens were prepared, local lattice rotations near precipitates of more than one minute of arc were observed. Some precipitates had punched out prismatic dislocation loops and more complicated dislocation shapes, in all the $\langle 110 \rangle$ directions radiating from the precipitate.

Besides diffraction topography, absorption topography was also applied. In the case of the tin-doped specimen, the extra concentration of tin in the impurity cell walls could be detected by absorption contrast. This contrast is greatest when the wall is seen edge-on. Under these

conditions it is possible to make quantitative estimates of the concentration of the tin impurity in them. The figure derived was $\frac{1}{2}$ to 1%, that is about thirty times the average tin concentration in the crystal. Precipitates more than a few microns in diameter could also be seen well by absorption contrast. Stereo-pairs of absorption topographs displayed in a striking manner the distribution of precipitates and showed their spatial relationship with the impurity cells.

2.5. Indium Antimonide

2.5.1. Determination of the absolute configuration of the structure.

The reasons for undertaking topographic studies of indium antimonide were threefold. Firstly, like silicon and germanium, very pure specimens could be obtained with very low dislocation density. Thus the crystals silicon, germanium and indium antimonide, which form a series of increasing electron density, could be used for studying the variation in the form of dislocation images with increasing X-ray structure factor. Secondly, indium antimonide can be plastically deformed at temperatures as low as about 200°C. This facilitates experiments in which small, controlled deformations are introduced. Thirdly, indium antimonide, unlike silicon and germanium, is a polar structure. Consequently, the atomic structure at the core of a dislocation will depend upon the sense of the Burgers vector; and there is the interesting possibility to be investigated that dislocations of opposite sense exhibit different glide behaviour.

Experiments concerned with the polarity of the structure will be discussed first. Consider the formation of a surface parallel to an octahedral plane in the diamond or InSb structure. If the surface is formed by cleavage it would be expected to be that which breaks the minimum number of bonds per unit area. If the surface is formed by solution or evaporation then it would be expected to be that with the minimum number of unsatisfied bonds per unit area. In both cases the expected surface is that which cuts the bonds directed normal to the octahedral surface. The crystal surface thus formed consists of a double layer of atoms. In the elements possessing the diamond structure all these atoms are of course

of the same species; but in the case of InSb there are two alternatives, viz., that either indium or antimony atoms lie uppermost. As a consequence, a difference in chemical reactivity between a (111) surface and its inverse $\bar{1}\bar{1}\bar{1}$ will be exhibited. This difference can be revealed by several etchants. It is found, for example, that a CP4 type etch will produce dislocation etch pits on one octahedral surface of InSb but not on its inverse. Although differentiation between surfaces indexed as (111) and $\bar{1}\bar{1}\bar{1}$ can be effected quite reliably by etching techniques, the absolute configuration of the structure, i. e. whether, in the indexing convention used, the (111) surface exposes indium or antimony atoms, cannot be determined by etching. This information can be obtained by X-ray diffraction, using anomalous dispersion. In the present work an improved anomalous dispersion experiment was performed (Hart 1963) which established unambiguously the absolute configuration of the structure in the specimens used relative to their external morphology. These anomalous dispersion experiments make use of the phase shift on scattering which occurs when the wavelength of the scattered radiation is near an absorption edge of the scattering atom. By choosing a wavelength for which this phase shift occurs more strongly for one of the atom species in the InSb structure than for the other, an observable difference in integrated reflection from (111) and $\bar{1}\bar{1}\bar{1}$ faces can be produced. The sign of the difference can be related directly to the absolute configuration. In the present experiments radiation produced directly in the X-ray tube was employed in order to obtain a beam sufficiently strong for reliable intensity measurements of diffracted beams to be made. Choice of radiation was restricted to the characteristic radiations of elements which could be used as target materials in the demountable X-ray tube. There were two possibilities, chromium $K\alpha_1$ or tin $K\beta_1$. Anomalous dispersion effects produced by the chromium radiation involve the L electrons in both indium and antimony, and the resultant effect is small: the ratio of moduli of structure amplitudes for the 111 and $\bar{1}\bar{1}\bar{1}$ reflections is 0.96. With $\text{Sn}K\beta_1$ radiation, on the other hand, there is a relatively large difference in the anomalous dispersion effects in indium and antimony. The wavelength of $\text{Sn}K\beta_1$ radiation lies between the K absorption edges of

indium and antimony. On the other hand, $\text{SnK}\alpha_1$ radiation has a wavelength longer than the K absorption edges of either element: no phase shift on scattering is then produced by either atom. Integrated reflection measurements made with $\text{SnK}\alpha_1$ can thus be used for standardisation purposes. The 333 and $\bar{3}\bar{3}\bar{3}$ reflections were compared rather than 111 and $\bar{1}\bar{1}\bar{1}$ because the contributions of the K electrons are relatively more important with higher-order reflections. A complication arises from absorption of the X-ray radiation, particularly of $\text{SnK}\beta_1$, and the consequent strong dependence of the integrated reflection upon the obliquity of the prepared crystal face with the Bragg planes reflecting. Fortunately this affects reflections of $\text{SnK}\alpha_1$ and $\text{SnK}\beta_1$ by about the same amount at a given crystal setting, and obliquity effects can be substantially eliminated by repeating experiments with the directions of incident and diffracted rays interchanged with respect to the crystal. The calculated ratio of structure amplitudes for symmetrical reflection was 1.21. The mean of experimental measurements was 1.18 with an estimated error of $\pm 4\%$. Using the orientation convention introduced by Dewald, and recommended by Hulme and Mullin (1962), in which the surface with indium uppermost is called (111) , it was confirmed that CP4 etch produces dislocation etch pits on the $(\bar{1}\bar{1}\bar{1})$, antimony face, but not on the (111) , indium face.

The tin target for the demountable X-ray tube was prepared by dipping a standard copper target into molten tin. The target face was then ground until a layer of tin only about 10 microns thick remained. It was calculated that the total power input into the focal area would have to be reduced to about 25 watts if the focal area was to be 1,400 microns by 150 microns and the peak surface temperature was not to exceed 120°C . This temperature was considered to be the maximum that could be used to avoid excessive sublimation of the tin. Some change in the configuration of the electron beam focussing components was required to produce roughly the standard focal size with a tube current of only 0.4mA; but with this modification it was possible to run the tube continuously at 50kV and 0.4 mA with no deterioration of the target during the course of

the experiments.

2.5.2. Deformation of indium antimonide

The indium antimonide used was grown by a horizontal zone-melting technique in a sooted silica boat and was provided by the Royal Radar Establishment, Malvern. The technique used for plastic deformation was similar to that employed in the case of germanium (see Section 2.4.2); but in the case of indium antimonide the peak temperature was only 230°C . As in the case of germanium it was possible to restrict the dislocation sources to surface scratches introduced before bending, and dislocations belonging to different slip systems were spatially separated in the plates cut from the deformed bars. The dislocation images showed significant differences from those found in germanium: they were generally sharper and showed more intense positive contrast at the center of the image. These differences arise because indium antimonide has structure factors about 50% greater than those of germanium, but only half the absorption coefficient for MoK α and AgK α radiations.

The dislocations produced had straight segments, though not so straight as those produced in germanium. Pure screw and 60° dislocations dominated the dislocation population. It was found that the dislocation loops generated by the deformation were much more elongated than in the case of germanium, the pure screw segments being about ten times longer than the 60° segments. It was hence concluded that in indium antimonide, under the conditions of the experiment, 60° dislocations move with about ten times the speed of pure screw dislocations.

If atomic models of dislocation core structures are constructed they show that in pure indium antimonide there should be two types of 60° dislocation, depending upon whether the extra half-plane is terminated by indium or antimony atoms. Dislocations expected to be of these two types can be identified on the topographs if both the absolute configuration of the specimen and the sense of the Burgers vectors is known. Both these quantities were determined in the experiments here reviewed (Hart 1963). In the presence of an impurity attracted more to one type of dislocation than to the other, a difference in glide properties might arise. A survey

of the dislocation populations in the deformed specimens was undertaken to look for such an effect, but within experimental error none was found.

2.6. Lithium Fluoride.

2.6.1. Origin of dislocations in lithium fluoride.

The first step required in the investigation of the lattice imperfections in lithium fluoride was the development of an appropriate specimen preparation technique. If a proper study of internal structures is to be made it is essential that the specimen surfaces be free from imperfections that would mask the diffraction image from the material beneath. Scratches and percussion damage, which generate not only local dense concentrations of dislocations but also appreciable long-range strains, must be removed by chemical polishing; but after this treatment there remains the problem of adequate removal of the reaction products, a matter which involves difficulties with reactive surfaces like those of lithium fluoride. Very often films of material are left on the surface which adhere to it strongly and introduce strains clearly visible on the X-ray topograph. An extreme case may be cited in which a lithium fluoride crystal, initially apparently quite clean and strain-free, developed in the course of a few weeks a dendritic surface growth which was optically detectable by its birefringence and was strongly visible on the X-ray topographs by the strain it produced in the underlying crystal.

Although crystals of lithium fluoride several millimeters thick are easily penetrated by MoK α and AgK α radiations, it is desirable to examine specimens not greater than $\frac{1}{2}$ to 1 mm thick if a clear picture of the dislocation distribution is to be obtained; and in practice the specimens used were cleavage plates parallel to $\{100\}$ chemically polished to a thickness of about 0.3 mm. If the specimen is thicker than this, the images of dislocations located near the X-ray entrance surface of the crystal have a pronounced 'tail' which reduces the precision with which they can be located. (This tail can be seen in the images of some segments of the 'random' dislocations appearing in Figure 2, following page 33.) The three chemical polishes used were, (a) concentrated sulfuric acid, (b) fluoboric acid, HBF $_4$, about 40% concentration, and (c) a weak ammonium

hydroxide solution. Etch (c) was found to be too slow and variable for convenient use; etch (b) was fast, removing surface material at the rate of about 30 microns per minute, but was prone to leave a strained surface layer. Etch (a) was found most convenient for general use. Its average rate of removal of material was about 7 microns per minute, but this became much faster as agitation was increased. In order to remove reaction products, the technique was adopted of quickly rinsing the crystal in a series of solutions of decreasing concentration of sulfuric acid, finishing up with pure water at the termination of the polishing operation.

Material from several sources was studied. Some specimens had fairly low dislocation densities but showed relatively poor dislocation contrast. It was possible to improve the dislocation contrast sometimes by annealing. The best material, both for low dislocation density and for good dislocation contrast, was obtained from the University of Aberdeen. Only minor changes in dislocation configurations were produced by annealing, even at temperatures up to 600°C. Annealing at higher temperatures usually introduced fresh dislocations due to accidental deformation. The dislocation population could be divided into random dislocations distributed in sub-grains, and dislocations aligned in low-angle boundaries. The more perfect the crystals, the sharper was this division. Dislocation densities in sub-grains varied widely, but there was a general tendency for a reduced density to be observed within a hundred microns or so of the low-angle boundaries. The dislocations within the sub-grains were always markedly curved, though a slight tendency for segments to lie in $\langle 100 \rangle$ directions was observed. A notable feature in many crystals was the profusion of large loops, up to 100 microns in diameter. Their orientation varied, and was not confined to the $\{110\}$ slip-planes. Accompanying the loops, horse-shoe shapes of bowed-out dislocation segments were present. In regions of low density of dislocations, Burgers vectors of individual dislocations were easily determined by finding in which reflections the dislocation image vanished. No evidence was found for dislocations with Burgers vectors other than the expected $\frac{1}{2} \langle 110 \rangle$. Sets of concentric loops were never observed, and no Frank-Read dislocation mills were found.

Dislocation nodes and reactions were rare. Stable pinning points appeared to be absent, which explains the absence of Frank-Read sources. The dislocation multiplication that had undoubtedly taken place appeared to have been all by the process of multiple cross glide, occurring under conditions when much climb and cross glide were taking place. In most specimens the distribution of Burgers vectors among their possible directions was fairly uniform; but some cases were found when this was far from so, one or two of the possible directions being strongly dominant. Further information on the nature and origin of the grown-in dislocation configuration was gained by examination of a boule about 8 cm in diameter and 10 cm high grown at the University of Aberdeen. Samples were taken from various places in the boule and the density and dominant Burgers vectors in these were compared. The findings were that in most parts of the crystal the dislocation density and configuration within sub-grains was determined by the plastic deformation occurring there as a result of cooling stresses. The dislocation density on the axis of the boule was higher than nearer the periphery. This appeared to be due to mutual interference of dislocations belonging to various slip systems intersecting near the axis. Near the axis, in the regions of higher density, some rearrangement of the sub-grain dislocations had occurred with a tendency to produce polygonal 'walls' of dislocations. In some places evidence for sub-grain boundary migration was apparent. The last centimeter or so of the crystal to solidify had a higher imperfection content; its most striking feature was a dendritic impurity segregation which was visible both optically and on the X-ray topographs. Before the horizon at which clearly visible segregation was reached, however, an increasing density of very small precipitates was revealed by diffraction contrast.

A low density of dislocations distributed in sub-grains was generally found to be associated with a low density of dislocations aligned in low-angle boundaries, except in cases where the former density was higher owing to appreciable plastic deformation having taken place late in the history of cooling of the crystal, after the network of low-angle boundaries had become stable. Individual dislocations become resolvable in low-angle boundaries when their separation is about 3 microns. This corresponds to

a misorientation across the boundary of about $20''$ of arc. At all lower misorientations the individual dislocations can be seen distinctly. At higher misorientations the low-angle boundary appears as a continuous band of enhanced diffracted intensity, modulated only by the Pendellösung fringes which correspond to depth contours of the low-angle boundary surface from the crystal faces. (Pendellösung fringes are discussed in Section 3.1.) However, these larger misorientations can be directly measured fairly easily by noting the change in setting for peak reflection when a finely collimated beam is reflected by the sub-grains on either side of the low-angle boundary. A single such measurement gives only one component of misorientation, that about the goniometer axis; several crystal settings must be used to characterise the misorientation fully. Correspondingly, when the dislocation density in the low-angle boundary is low, topographs of several different Bragg reflections must be taken in order to show up all the dislocations in the low-angle boundary and determine their Burgers vectors. Such analyses have been performed on some low-angle boundaries and it has been possible to compare the misorientations calculated from the dislocation structure with that found directly from angular settings of the goniometer. Satisfactory agreement between the two measurements was obtained (Martin 1965). The segment of low-angle boundary shown in Figure 2 is typical of those that have been analysed. Note that the dislocation alignments are somewhat variable in density and direction; it is necessary to average dislocation spacing over about 20 dislocations to get a reliable figure for density in the boundary. In the upper part of the field, the dislocation structure is simple, but when the boundary bends downwards in the right of the Figure, the boundary partakes more of the character of a crossed grid of dislocations. In this reflection only one set of dislocations in the grid is visible. Two questions of interest in the study of low-angle boundaries are, firstly, is the dislocation structure the simplest that will give the observed misorientation; and, secondly, is a fixed misorientation strictly conserved along a low-angle boundary? The answers found were, to the first question, generally 'yes'. Indeed, there is a marked preference for the simplest structure, the pure tilt boundary, at any rate among the boundaries whose individual dislocations

are well resolved. The answer to the second question is 'no'. When a given low-angle boundary is examined over a length of up to 1 to 2 mm it is found that the dislocation density and Burgers vector distribution will change along the boundary, so that the resultant misorientation will not remain constant but will gradually change, possibly by several seconds of arc. This implies that the sub-grains on either side of the low-angle boundary are slightly warped. Such a finding need not cause surprise. A non-isotropic distribution of Burgers vectors of the dislocations within the sub-grains would give rise to an overall warping of the sub-grain.

Most of the crystals studied were free from diffraction-contrast-producing precipitates; but in some crystals grown at the University of Aberdeen such were present at a low concentration in the bulk of the crystal. It is likely that there are precipitates decorating the low-angle boundaries, but a low density of such precipitates would be difficult to see directly. However, interesting examples have been found in which a certain amount of low-angle boundary migration has occurred during and following the epoch of precipitation. In such cases the low-angle boundaries have a zone of precipitates extending on one side of them, indicating the volume which had been swept by the migrating boundary. An example is shown in Lang 1964c (R10). This observation proves that the low-angle boundaries have migrated, and it also gives an indication of the stage in the history of the specimen when precipitation occurred.

2.6.2. Radiation damage.

A wide range of experiments has been performed involving radiation damage of lithium fluoride (Lang 1963b, Martin 1965). The damage has been produced both by X-rays and by thermal neutrons. With both radiations, the progressive development of damage with increasing dose has been followed, and the changes produced by annealing in various ways, after various doses, have been recorded. X-ray damage will be discussed first. Limited areas of lithium fluoride plates were irradiated at room temperature by the full radiation from crystallographic X-ray generators, run at 30kV to 45kV peak. The irradiated area was defined by an aperture

in a lead or tantalum shield placed close to the specimen. Topographs were taken before and after various doses. Small doses that produced a very pale straw colour in the irradiated region caused a faint increase in diffracting power from the margin of the irradiated area. Higher doses, which produced a more definite yellow colour in the irradiated area, produced a more marked enhancement of intensity at the margin of the area, but still no change in the diffraction contrast within the irradiated area. The colour, and the enhanced diffraction from the margins, could be completely removed by annealing for 2 hours at 430°C . A notable feature of this enhancement around the boundary of the irradiated area is that the intensity is a maximum when the normal to the Bragg plane (i. e. the diffraction vector) makes a large angle with the periphery of the irradiated area, and is zero when it is parallel to the periphery. This relationship was tested with apertures of various shapes. Now diffraction contrast is produced by a strain gradient within the triangular region enclosed between the paths of incident and diffracted rays which leave the point of incidence of the X-ray beam on the crystal surface facing the X-ray tube. It appears that at low doses of X-radiation the irradiated volume expands isotropically, long-range order is maintained, and dislocation contrast remains good. Only at the margins of the irradiated volume, where the expanded crystal is constrained to match the unchanged surrounding crystal, is diffraction contrast produced by the strain gradient locally present. It is estimated that strain gradients as low as 10^{-3} to 10^{-4} per cm can be detected by diffraction contrast.

A marked change in the X-ray diffracting properties of the whole irradiated region is produced when the dose is raised sufficiently to turn the crystal a deep brown. This dose was achieved by irradiation for 160 hours with a peak voltage of 45kV, a tube current of 18 mA, and the specimen placed about 5 cm from the X-ray tube focus. The irradiated area now diffracted strongly, behaving more like an imperfect crystal, and diffraction contrast from individual dislocations was largely lost. An anneal at 450°C for two hours restored the dislocation diffraction contrast, though some overall intensity enhancement remained. The very strong intensity enhancement at the margins of the irradiated area was still quite

strong after this anneal. A further anneal at 780°C removed the enhancement at the margins completely, but it also caused a re-arrangement of the dislocations within sub-grains, in irradiated and non-irradiated regions alike.

The findings resulting from the experiments involving neutron irradiation of lithium fluoride can briefly be summarised as follows. Crystals irradiated with 10^{16} nvt showed comparatively little change in crystal perfection after irradiation provided that they were examined by symmetrical transmission, i. e. with the Bragg planes normal to the specimen plate. When asymmetric transmission was used, the entire topograph showed enhanced diffracted intensity and the contrast of low-angle boundaries and individual dislocations was much reduced. This curious phenomenon was interpreted as being due to a gradient of inter-planar spacing in a direction normal to the crystal surface, in its surface layers. Such a gradient would have no component to disturb the regular lattice periodicity in symmetrical transmission, but would have so in asymmetric transmission. Loss of helium and/or fluorine from surface layers may be the cause of the gradient.

Specimens irradiated with 10^{17} nvt still gave quite fair dislocation contrast in symmetrical transmission although the diffracted intensity from dislocation-free parts of the crystal was several times higher than in the unirradiated material. The angular range of reflection was significantly broadened: the reflection curve had developed marked 'tails'. At doses above 10^{17} nvt a drastic decrease in lattice perfection is suffered, the integrated intensity rises to a high value and the reflection curve is so broadened that the α_1 and α_2 components of the K α doublet can no longer be resolved. At this and all higher doses the crystal has become effectively completely imperfect as regards diffraction behaviour. An annealing sufficient to produce bleaching does not restore dislocation contrast. Not much improvement in the long-range lattice perfection occurs until a temperature of about 700°C is reached. Specimens irradiated to 5×10^{17} nvt and 10^{18} nvt were given anneals at temperatures such as 750° and 775°C for 24 hours and then slowly cooled. They then contained a high density of

cavities with cube surfaces. A considerable redistribution of the dislocations had occurred. In specimens which had been irradiated to 5×10^{17} nvt the cavities were especially dense in the low-angle boundaries revealed by X-ray topography, but those irradiated to 10^{18} nvt contained a uniform distribution of cavities with no preferential concentration of them on low-angle boundaries. The X-ray topographs show that there is definitely no long-range strain associated with the cavities in the annealed crystals. A careful comparison of dislocation positions mapped by X-ray topography with cavity positions mapped by optical microscopy showed that there was no demonstrable tendency for cavities to be located on dislocation lines.

2.7. Magnesium Oxide.

Magnesium oxide crystals from three sources have been studied: 1, crystals grown from the melt in an arc furnace in H.H. Wills Physics Laboratory, 2, crystals, some colourless, some slightly yellow, grown by the Norton Company, Worcester, Massachusetts, and 3, crystals obtained from Semi-Elements Inc., Saxonburg, Pennsylvania. The crystals grown in this laboratory showed a moderate dislocation density, about 10^5 lines per cm^2 , but dislocation contrast was rather poor, and there was evidence for the presence of a fair amount of precipitation. The Norton crystals exhibited on the whole a much higher lattice perfection. Some specimens possessed large sub-grains with a very low dislocation density within them. A notable feature of the better Norton crystals was the polygonal arrangement of walls of dislocations within the sub-grains. The walls divided the sub-grains into cells almost free of dislocations. Indeed, some of these cells, virtually dislocation-free, were several hundred microns in diameter. The mutual misorientation of cells within a sub-grain was of the order of one second of arc. Typical misorientations between sub-grains were 1 to 2 minutes of arc. Some low-angle boundaries with a misorientation of several minutes were present. Within the sub-grains the dislocation contrast was high and no precipitates were evident. However, even in the best Norton crystals, the low-angle boundaries were found to be decorated with impurities. In less perfect Norton crystals many dislocation loops 10 to 50 microns in diameter were present,

together with some well-developed helical dislocations.

The most extensive study was performed on some peculiar crystals obtained from Semi-Elements Inc. This work was done in collaboration with the Metallurgy Division, Atomic Energy Research Establishment, Harwell, and an account of it has been published (Lang and Miles 1965, R16). A complete topographic survey and a detailed Burgers vector analysis was made of a specimen of magnesium oxide which was one of a batch which exhibit strings of small light-scattering bodies when examined under the microscope. Ultramicrographs and X-ray topographs together confirm that the light-scattering bodies are decorating dislocations. All dislocations were found to be thus decorated and hence no dislocation movement had occurred, or fresh dislocations been introduced, following the epoch of decoration. In this specimen the average sub-grain size was quite large, an average diameter being about 2 mm, and the angle between sub-grains was quite low, of the order of ten seconds of arc. The number of dislocations within the sub-grains was quite low, but the total length of dislocation line was considerable because this crystal showed in an extreme form the phenomenon of extension of dislocation-line length through dislocation climb, an example of this process being the changing of straight dislocations into helices. A notable feature of the dislocation geometry was that these line extensions were nearly confined in a plane, so that the dislocation was looped back and forth many times. Considerable effort was made to try and determine the sense as well as direction of the Burgers vectors, since this would show whether climb had occurred through the absorption of interstitials or of vacancies. Unfortunately, experimental conditions militated against this determination, and the diffraction evidence was inconclusive. However, it was possible through the X-ray topographic analyses to decipher some of the history of the development of this unusual dislocation configuration.

2.8. Aluminum

X-ray topographic studies of single crystals of aluminum have been conducted intermittently over a period of several years. The crystals most studied were prepared by the strain-anneal method. Details of their

preparation, and the chief results of the investigation, have now been reported (Authier, Rogers and Lang 1965, R18). Also studied were crystals grown directly from the melt in a graphite-coated quartz boat held in a travelling furnace. The melt-grown crystals were found to have dislocation densities at best only locally as low as 10^4 lines per cm^2 . However, it appears from recent work that, with a sufficiently careful technique, melt-grown crystals can be prepared with dislocation densities as low as those achieved in strain-anneal grown crystals. Revelation of the very low densities present in some parts of the latter crystals (for densities as low as a few tens per cm^2 were discovered) was a striking outcome of the X-ray topographic investigation.

A difficulty accompanying work with very pure aluminum is its extreme softness and liability to accidental deformation. Many cases were observed in which many dislocations had invaded a volume originally containing but a few, for only a very small stress was required to produce a catastrophic multiplication of dislocations. Sequences of topographs taken before and after slight deformations were of interest in showing how the fresh dislocations spread through the crystal and interacted with the pre-existing dislocation configuration. The feasibility of performing investigations of this movement under deliberately produced stresses was demonstrated; but for the purpose of investigating the grown-in dislocations such movements had to be prevented, and special techniques for specimen handling and mounting were developed with this end in view.

The risk of gross mechanical deformation of the specimen is lessened when the specimen is relatively thick: in the investigation specimens 1 to $1\frac{1}{4}$ mm thick were used. In order to penetrate such thick specimens without undue loss of X-ray intensity by absorption it was necessary to employ Ag K α radiation. For the better resolution of details of the dislocation structure it would have been desirable to use a soft radiation such as CuK α (this follows from the discussion given in Section 1.3.3.), and it is hoped to perform such experiments in due course. However, the main features of the dislocation configuration were well displayed by the topographs taken with Ag K α radiation. The Burgers

vectors of dislocations were unambiguously determined; the condition for dislocation invisibility, that $\underline{g} \cdot \underline{b} = 0$, applies well under the conditions of low absorption with aluminum specimens and Ag K α radiation (\underline{g} is the diffraction vector, \underline{b} is the dislocation Burgers vector). Stereo-pairs and section topographs enabled the spatial configuration of the dislocations to be clearly seen. Two noteworthy results of the investigation were the following. Firstly, a dominant feature of the dislocation configuration is the occurrence of long lines of coaxial loops. The axes of the loops all lie exactly along $\langle 110 \rangle$ directions and the Burgers vectors of the loop dislocations lie parallel to the loop axis. Thus they are prismatic loops. Loop diameter ranges upwards from 1 micron (the threshold of visibility) to about 50 microns. Figures-of-eight and helices also occur. As many as 40 loops have been counted on a single axis, and the total length of the axis can be more than a millimeter. Several possible origins for these loops were investigated. It was concluded that they could satisfactorily be accounted for by the climb of screw segments into helices through absorption of vacancies, and the subsequent interaction of the helix with itself or with a neighbouring dislocation to convert the helix into a set of coaxial loops. These sets of loops, so it was concluded, revealed the position of long, straight, screw segments of dislocations which had constituted a major component of the dislocation population grown into the crystal at the recrystallisation front.

The second major observation was that in unstrained specimens there was an extremely low dislocation density within 200 to 300 microns of the crystal surface. This was attributed to loss of dislocations at the crystal surface during annealing, the loss having occurred chiefly at the highest temperatures (500 to 550 $^{\circ}$ C) at which the specimen was held. The configuration adopted by the few remaining dislocations in this surface layer supported the explanation of the low density as being due to loss from the surface. This finding has obvious relevance to the problem of producing aluminum crystals with very low dislocation density. It also affords a clear demonstration that only by X-ray topography, using specimens about 1 mm thick, can a fair picture of the dislocation configuration in the bulk material be obtained, in the case of pure aluminum.

2.9. Corundum and Ruby.

Pure single crystals of corundum, $\alpha\text{-Al}_2\text{O}_3$, are colourless. Addition of Cr_2O_3 impurity imparts a red colour, and the crystal becomes a ruby. Single crystals of $\alpha\text{-Al}_2\text{O}_3$ grown by three methods have been studied: (a) 'flame-grown' crystals, i.e. crystals grown by the Verneuil process. (b) crystals grown from the vapour, and (c) flux-grown, chromium-doped crystals. Findings concerning these will be discussed in the above order.

The crystals grown by the Verneuil process were examined in the form of discs about 1 cm in diameter and $\frac{1}{2}$ to 1 mm thick. They exhibited a considerable degree of lattice imperfection. Not only were low-angle boundaries with angles of several tenths of a degree present, but within each sub-grain the lattice was wavy with misorientations ranging up to about a tenth of a degree. Bands of more imperfect and misoriented material appeared to have resulted from the annealing of slip bands. The dislocation density was of the order of 10^6 lines per cm^2 and individual dislocations were resolved with difficulty locally in section topographs and limited projection topographs.

Crystals grown from the vapour were relatively perfect. The dislocation density was quite low. Localised diffraction contrast was produced by inclusions, and evidence of variations of impurity content was presented by strain concentrated in layers parallel to the growth layers of the crystals.

The flux-grown crystals, which were chromium doped and ruby-coloured to various depths, covered a range of lattice perfection. The imperfection present, together with its variation from point-to-point within a given crystal, and as between different crystals, appeared to arise mainly from strain due to non-uniform incorporation of impurity during growth. On the topographs there appeared lines of enhanced diffracting power of two types. One type was clearly due to dislocations, present singly or in bundles. The visibility of individuals was low; bundles of dislocations appeared as a mass of faint, wispy lines. More clearly visible were lines of imperfections running parallel to growth steps on the crystal surface, and others trending in the same directions and doubtless

representing buried growth steps. An indication of the nature of the latter type of line was obtained by microradiography of crystals grown from a lead-containing flux. The good correlation between lines of strain seen on the diffraction topographs and lines of occluded lead-rich material revealed by the microradiographs showed that incorporation of flux constituents had taken place on an appreciable scale. It appeared that flux constituents had piled up in front of advancing growth layers until a whole line of such impurity was overwhelmed by the growing material and was incorporated into the crystal.

A phenomenon of interest observed in some of the more perfect flux-grown platelets was repeated sectorial twinning. The platelets were parallel to the basal plane ((0001) in hexagonal Miller-Bravais indices). In one case a platelet was divided into six 60° sectors, adjacent sectors being twinned with respect to each other; and in another case the platelet was divided into four 90° sectors, with a similar twin relationship. X-ray topographs were taken in which the whole crystal was able to satisfy the Bragg condition, and also in which one or other only of the sets of twins was Bragg-reflecting. In this way the structure of the twin boundaries could be studied. They appeared to be relatively perfect, and they did not show stacking-fault-type fringe contrast.

2.10. Quartz

2.10.1. Defects in oscillator-grade quartz.

Experience accumulated from the examination of many specimens suggests that when a crystal of alpha quartz appears by the standard methods of visual examination to be of sufficiently high quality for use in the manufacture of oscillator plates then X-ray topography will show that the bulk of it has a highly perfect lattice; and that in such specimens individual defects such as inclusions, dislocations, and twin boundaries will be resolvable easily and visible with strong diffraction contrast. It follows that high-quality quartz is excellent specimen material for use in studying the diffraction effects of individual lattice imperfections in nearly perfect crystals. Added interest, but also increased difficulty of interpretation, arises from the fact that quartz can contain a variety of lattice defects not

present in the simple crystals with the diamond structure which also are available in a highly perfect state.

The variety of lattice defects in quartz which has been observed, and studied with varying degrees of thoroughness, includes (a) individual dislocations, (b) growth stratifications, (c) inclusions and precipitates, (d) twin boundaries and (e) fault surfaces other than twin boundaries and growth stratifications. These will now be discussed in the order in which they are listed above. The accounts presented will be qualitative only, and will not attempt to recite the mass of experimental evidence accumulated. The analysis of this evidence is in most cases still in progress, and in some problems there still remain gaps in the evidence waiting to be filled. Where crystallographic description of planes, zones, etc. is required, it will be given by reference to hexagonal axes, and the full Miller-Bravais indices will be quoted. It is necessary to bear in mind that some confusion has reigned concerning the orientation of the Miller-Bravais axes of alpha quartz. The history of this confusion, and recommendations for correct practice in notation have been given by Lang (1965b). All that need be here said is that indices of the major rhombohedron of quartz, r , are the form $\{10\bar{1}1\}$, and of the minor rhombohedron, z , are $\{01\bar{1}1\}$.

Quartz specimens have been examined in the shape of ground, polished and etched plates, ranging in area from 10 mm square to 20 mm square and in thickness from 0.3 mm to 1.5 mm. Plate orientations roughly or precisely parallel to the AT and BT oscillator plate cuts were generally used: the AT cut is 3° off a minor rhombohedral plane and the BT is 11° off a major rhombohedral.

Dislocations. Grown-in dislocations in quartz may be 'clean' or 'dirty'. The dirty dislocations are those obviously decorated by precipitation of impurity. The decoration may so modify the strain-field of the dislocation as to make inapplicable the usual rules for variation of dislocation visibility with angle between diffraction vector and Burgers vector. Sometimes exceptionally strong diffraction contrast arises from the strain in the quartz matrix produced by precipitates on the dislocations. Of

special interest are dislocations which are only obviously decorated along part of their length, and in which the precipitated phase is visible optically. It can then be demonstrated that the 'needles' familiar in optical examination of quartz are decorated dislocations. It has also been demonstrated that the etch tubes familiar in studies of the etching behaviour of quartz are located on dislocations both clean and dirty. Clean dislocations are defined as those whose visibility rules are not manifestly modified by strains introduced by precipitation, and upon which precipitates cannot be detected by any optical technique. This does not imply that the dislocation is free from impurity on an atomic scale, it is unlikely to be so clean. Dislocations are sometimes quite straight, sometimes they appear as long helices, and sometimes they are coiled in a very irregular fashion. Coiled dislocations are generally dirty. Clean, straight dislocations are chosen for study in experiments to determine Burgers vectors. Many topographs must be compared in order to determine the Burgers vectors with certainty. The most common Burgers vector is in the direction of one of the translation vectors in the basal plane; it can be assumed that its magnitude is equal to the unit translation, a , and is equal to $\pm 91\text{\AA}$. A minority of dislocations have a Burgers vector with a component parallel to the c -axis: they appear to have Burgers vector equal to the vector sum ($a + c$), 7.3\AA .

Growth stratifications. In common with many crystals, quartz exhibits bands of increased diffracting power in layers lying in surfaces which once were the external faces of the crystal at some stage in its growth. In some specimens such layers may be traced across more than one growth sector, say from a major rhombohedral growth sector, round the sector boundary, into a minor rhombohedral growth sector. If a section of the entire specimen could be examined, it is likely that a given layer could be traced completely round the crystal, covering all growing faces. These layers form a valuable record of the growth history, they can show, for example, how the relative development and relative rates of growth of the various faces varied during the development of the crystal. The identity of the impurities whose incorporation led to the change in cell dimensions which produced the strain-gradient which in

turn produced the diffraction contrast cannot be established by X-ray topography. Possibly electron-probe X-ray spectrographic micro-analysis might achieve identification. Some specimens are completely filled by growth stratifications, in others only a few discrete horizons are thus marked. In a region where no stratifications are visible in strong, low-order Bragg reflections, they may become visible in weak, high-order reflections. This results from the greater sensitivity of weak reflections to the 'interbranch scattering' which causes enhanced diffracted intensity in the low-absorption case (see Section 4). If at a particular horizon a strain gradient both strong and localised is present, strong interbranch scattering occurs at this horizon. Stacking-fault-type fringes are then produced which run as thickness contours in the wedge-shaped volume between the surfaces of the specimen plate and the growth horizon where the scattering has occurred. Careful observation is necessary to distinguish between a set of such fringes due to scattering at a single horizon, and the individual images of a set of regularly spaced growth horizons revealed by weak interbranch scattering. Even when the associated strain gradients are too low to produce increased diffracted intensity through interbranch scattering, growth stratifications may still be detected by the bending of Pendellosung fringes they produce in the section-topograph Pendellosung fringe pattern (this phenomenon also is discussed in Section 4). When regularly spaced growth stratifications occur throughout an appreciable volume of crystal they indicate a rhythm in the rate of growth. It is tempting to speculate that this rhythm may be a widespread, natural one, such as that due to earth tides.

Inclusions and precipitates. All the dislocations which originate in the crystal volume contained in the specimen plates examined by X-ray topography are observed to originate from lattice closure errors at inclusions incorporated during growth. It is likely that the great majority of dislocations found running through specimen plates, and whose point of origin is remote from the specimen examined, originated in this manner; though it should be noted, however, that an association of dislocation groups with the loci of junctions of fault surfaces such as those discussed below may indicate a more complex origin for some dislocations. On the

other hand, not all inclusions which make themselves visible by their strain fields do generate dislocations. Quartz is similar to diamond in this latter respect. An interesting case has been found in which certain growth horizons are marked by a relatively high incidence of inclusions only a minority of which produce bundles of dislocations that stretch out from the inclusion in the direction of advance of the growth surface. No case of the punching-out of dislocation loops by precipitates has been observed so far. Strong precipitation on the grown-in dislocations, with absence of detectable precipitates in dislocation-free regions, is a frequent occurrence.

Twin boundaries. The commonly observed twin boundaries in quartz are those separating twins which have been generated by the Dauphiné or Brazil Laws. The Dauphiné Law is a rotation of 180° about the c-axis: this reverses the piezoelectric polarity and is 'electric twinning'. The Brazil Law is a reflection in $\{11\bar{2}0\}$, i. e. in prism planes of Type II. This also changes the piezoelectric properties, and by changing the structural hand, the sense of optical rotation is also changed, and 'optical twinning' is produced. As long as Friedel's Law is obeyed (i. e. equal diffracted intensity from reflections hkl and $\bar{h}\bar{k}\bar{l}$), equal diffracted intensity will be produced by crystal volumes on either side of a Brazil twin boundary. The boundary itself is detectable on X-ray topographs because of the difference in phase of the amplitude of the diffracted waves produced by crystal on either side of the boundary. This phase jump may arise in part from an anomalous interplanar spacing at the boundary due to the abnormal crystal structure there, and in part from the reversal of phase resulting from the twinning operation of reflection performed on the non-centrosymmetric quartz structure. The latter contribution to the phase jump can be calculated from the known structure of quartz, using the familiar structure factor expression employed in X-ray structure analysis. The former contribution to the total phase jump, that due to the anomalous spacing, should then be determinable, within certain experimental limits and subject to the usual ambiguity of addition or subtraction of $2n\pi$. The determination can be made from studies of the variation of diffraction contrast of the boundary in different Bragg reflections. The type of

diffraction contrast produced by the boundary as that of the stacking-fault fringe pattern. If in any reflection the fringe system is vanishingly weak then the total phase jump for that reflection is $\pm 2n\pi$ (n being an integer or zero). In the case of Dauphiné twin boundaries, fringe systems also appear at the boundary, but there may also be large differences in intensity of reflection from the crystal volumes on either side of the boundary, and these occur under the usual conditions when Friedel's Law is obeyed. They arise because the reflections $hki\ell$ and $\bar{h}\bar{k}\bar{i}\bar{\ell}$, which are produced respectively by the two volumes related by the Dauphiné Law, may have quite different structure factor moduli, although their interplanar spacings (and hence Bragg angles) are the same. An extreme difference occurs with the pair of reflections $30\bar{3}1$ (very strong) and $\bar{3}031$ (very weak). Topographs taken with these two reflections may be used to detect small volumes of Dauphiné-twinning material. To produce a difference in diffracted intensity from crystal volumes on either side of a Brazil twin boundary, on the other hand, requires conditions under which Friedel's Law no longer applies. Such conditions can be achieved through anomalous dispersion, in the case of certain pairs of reflections; and if CrK α radiation is used the intensity difference may be quite easily detectable. The delineation of both Brazil and Dauphiné twinning by topographically recording different diffracted intensities from each member of the twin pair has been demonstrated by Lang (1965c). However, for the purpose of studying the phase jump and the topography of the composition surface at Dauphiné twin boundaries it is desirable to use reflections which produce equal diffracted intensities from crystal on either side of the twin boundary.

It is known that traces of Brazil twin boundaries revealed on crystal surfaces are usually straight, whereas those of Dauphiné boundaries are irregularly curved. This macroscopic difference has been confirmed by X-ray topography. Projection topographs show that Brazil twin boundaries may be flat and oriented parallel to low-index lattice planes such as the major and minor rhombohedral planes. If steps on a fine scale are distributed over Brazil twin boundaries then they occur on

a smaller scale than can be resolved by X-ray topography (less than about a micron in height). In the case of Dauphiné twin boundaries the situation is quite different. The X-ray topographs have revealed that Dauphiné twin boundaries lying in certain mean orientations are stepped on a fine scale, down to the topographic resolution limit. This fine structure is not described in the standard works of reference. Indeed, twin boundary steps on the scale of a few microns would escape notice in the usual method of delineating twin boundaries by etching crystal surfaces.

Regarding the phase jumps at twin boundaries, only a limited amount of data has so far been acquired. It has been found that the phase jumps evident in a given Bragg reflection depend upon the orientation of the twin boundary, in the case of both Brazil and Dauphiné twinning. In the latter twinning, the dependence of phase jump upon local boundary orientation is strikingly manifested. For example in a stepped Dauphiné twin boundary, diffraction contrast from one of the step surfaces may be strong and from the other be zero, in a given Bragg reflection. In the reflections from the basal plane, reflections 0003 and 0006, diffraction contrast from Dauphiné twin boundaries in all orientations is very weak or zero.

Other fault surfaces. The most surprising discovery accruing from X-ray topographic studies of good quality quartz crystals has been the prevalence of well-defined fault surfaces giving stacking-fault-type fringe contrast, such fault surfaces separating crystal volumes which are apparently highly perfect and which maintain parallel orientation with each other. The best developed fringe patterns are often exhibited by fault surfaces whose nature is at present little understood, for the surfaces now under discussion are not in general parallel to growth horizons. Neither are they identifiable as twin boundaries, though the possibility exists that some of them may be boundaries of thin twin lamellae. The unexplained fault surfaces may be flat or they may be irregular. The flat surfaces do not necessarily coincide with low-index planes; indeed, some flat surfaces are describable only by high indices. Some fault surfaces do have a simple topographic rationale: they lie in the boundaries of growth sectors (such as the boundaries between major and minor rhombohedral growth sectors,

for example). These sector-boundary fault surfaces appear in crystals which also show growth stratifications. It may be that they develop only above a certain impurity concentration. Another type of fault surface is also topographically understandable. These occur in synthetic quartz crystals and are found in material which has grown on a surface roughly parallel to the basal plane. (0001). They are associated with the mode of cellular growth on basal planes that gives rise to the rough external crystal surface known as the 'cobble' texture. Combined optical and X-ray topographic examination has shown that the fault surfaces lie in the boundaries between growth cells, and they consequently outcrop at the external surface at the grooves between cobbles. Since it is known that the degree of development of the cobble structure is proportional to the amount of aluminum impurity present, it is reasonable to suppose that the anomalous interplanar spacings that produce the fault surfaces in the cell boundaries are due to a local high concentration of the aluminum impurity. The relationship between these fault surfaces and the grown-in dislocation population has been studied: there is a tendency for dislocations to lie in, or close to, the fault surfaces.

Among the fault surfaces whose significance is not readily revealed by their topology on the topographs, several types may be distinguished. A rough division may be made into 'strong' and 'weak' surfaces. The strong surfaces give rise to an excess diffracted intensity in addition to that pertaining to the fringe system. This excess appears due to lattice curvature where the fault surface outcrops the surfaces of the specimen plate. Such curvature arises from the relief of stress in the fault surface. At the other extreme, the most 'weak' surfaces are those that are revealed only in high-order Bragg reflections. Another division may be made into those fault surfaces which may be revealed by etching and those that cannot. Some strong fault-surfaces are very rapidly etched out by both hydrofluoric acid and by strong alkali. Occasionally these strong, easily etched fault surfaces are visible optically as a faint film. A possible explanation of the fault surfaces in natural quartz that are not sector boundaries is that they mark boundaries of parallel crystal growths that have become included in the main crystal.

2.10.2. Amethyst quartz.

Alpha quartz is generally classed as amethyst on the basis of its colour, though this can range through quite a variety of tints, from a deep to a pale violet, or from a 'pure' violet to a reddish or brownish violet. Only rarely do large volumes of crystal exhibit a uniform tint, and it is common to find the coloration concentrated in bands parallel to the major and minor rhombohedral faces. These bands correspond to growth layers, and, as such, their distribution is generally similar to the growth stratifications that are found in good-quality quartz by X-ray topography (described above in Section 2.10.1), or which can sometimes be revealed by selective coloration after irradiation. A characteristic feature of amethyst coloration is its concentration in certain growth sectors. Commonly it is more intense in the major rhombohedral growth sectors. But the most remarkable property of amethyst is the occurrence in many specimens of regularly repeated Brazil twinning in the major rhombohedral growth sectors. This was first described by David Brewster in 1819, whose paper and drawings on the subject (published in 1823) remain to this day the best description of the phenomenon. The width of the twins ranges typically from about 50 microns to a few tenths of a millimeter. This polysynthetic twinning is also found in crystals which do not have the characteristic amethyst colour. Its manifestation both visually and in X-ray topographic examination does not appear to depend upon the colour of the crystal. An optical, X-ray topographic and microradiographic study was made on a basal-plane slice of crystal containing the amethyst structure of repeated twinning in the major rhombohedron growth sectors. The crystal was in fact colorless, and may have been a bleached amethyst. The results of this study have been published (Schlössin and Lang 1965, R14). A few remarks may be added here to supplement that paper, taking into account additional, more recent observations. It is notable that amethyst quartz, inspite of a high dislocation density and a relatively high impurity content, maintains excellent long-range parallelism of its crystal lattice. Direct measurement of angular settings for peak Bragg reflection across crystal sections up to 2cm in diameter, and, more sensitively, the observed straightness of Aufhellungen over these distances (see Section 3.2)

demonstrate that misorientations in these crystals do not exceed a second or so of arc. In comparison with oscillator-grade quartz the visibility of individual dislocations is poor unless they are strongly decorated. This poor visibility of individuals, combined with the relatively high dislocation density, rendered it not feasible to attempt Burgers vector determination of individual dislocations. Where Brazil twin boundaries occur singly, as in the minor rhombohedral growth sectors, they can be detected topographically but do not show the fault-surface fringe pattern that they do in good crystals. In some of the more perfect parts of amethyst crystals (i. e. in parts of minor rhombohedral growth sectors) weak Pendelösung fringes may be seen.

Once again, as in the studies of synthetic diamond (Section 2.2.), and of ruby (Section 2.9.), microradiography has proved an informative companion technique to diffraction topography. The excess concentration of iron impurity in the major rhombohedral growth sectors was demonstrated, and, within the latter sectors, its concentration in the imperfect lamellae featured in the diffraction topographs was also revealed.

The fine details of the X-ray diffraction contrast associated with the twin lamellae in the major rhombohedral growth sectors is best interpreted as being due to a rather high density of decorated dislocations. The degree of decoration depends upon the distance from the twin boundary. The diffraction contrast is most intense in the general vicinity of the twin boundaries, but examples have been found where the diffraction contrast has a bimodal distribution with its central minimum located just at the boundary (as far as can be determined with a resolution of a few microns). The lines best described as 'brush marks', which are strongly believed to be decorated dislocations, take a sinuous course passing through the twin lamellae. Their orientation is determined both by their location in the growth sector and by the order of change of hand at the twin boundary (i. e. dextro to laevo, or vice versa).

The evolution of the system of polysynthetic twinning during the growth history of the crystal may be divided for convenience into the 'juvenile', 'mature', and 'senile' stages. It is in the mature stage that

the structure is most beautifully developed. Then the twin boundaries depart little from the $[0001]$ zone and are most easily studied both optically and X-ray topographically. Polysynthetically twinned amethyst crystals are often terminated by a cap of normal untwinned growth which may be colorless. A change to such a mode of growth, which may invade the growing surfaces irregularly, together with the decay of the regular twinning system, is characteristic of the senile stage. There is reason to believe that the juvenile stage is relatively brief compared with the mature stage; its details have not yet been studied by X-ray topography.

2.11. Organic Crystals.

The X-ray topographic experiments that have been performed so far on organic crystals do not amount to more than a preliminary reconnaissance of the field, but they have provided pointers to a likely profitable area for future X-ray topographic activity. Two out of the three crystal species examined were found to produce specimens in which at least some parts of the crystal had quite perfect lattices so that strong diffraction contrast was produced from groups of dislocations and other localised centers of strain. This observation is of interest in showing that crystals composed of large molecules can be free of lattice defects just as simple structures and crystals of the elements can be. The low absorption of X-rays is one feature that makes organic crystals convenient for topographic study, but this advantage is offset by several difficulties. The extreme softness of organic crystals makes them greatly prone to deformation, and they are difficult to mount rigidly for examination without deforming them by the adhesion of wax or cement. In addition, their large coefficients of thermal expansion increase the probability of drift off the angular setting for peak reflection during exposure. Most organic crystals deteriorate under X-irradiation, but it has not yet been determined how long such crystals will maintain their lattice perfection under the relatively low radiation level involved in X-ray topography. The fact that good topographs have been obtained is encouraging. Another difficulty with organic crystals is their generally low values of integrated reflection

compared with those given by the simplest structures. Not only does this weak reflecting power require long exposure times, but it also means that images of individual dislocations are very wide and hence the topographic resolving power for separating dislocation images is poor. (This inverse relationship between strength of reflection and width of dislocation images is discussed in Section 4.2).

The first organic material studied was a very large single crystal of sucrose. It measured 30 mm X 20 mm X 10 mm and was examined in transmission through its 10 mm thickness using AgK α radiation. Strong diffraction contrast was observed from lineage structures, but it was not possible to resolve individual dislocations. Some interesting growth features were seen; for example, in one part of the crystal there appeared a discontinuity in texture at a certain growth horizon following which a columnar texture developed.

The second organic material studied was the high-explosive RDX (Cyclotrimethylenetrinitramine). Many crystals were studied one to two millimeters in diameter. In the better specimens a pattern of linear defects radiating from the center of the crystal was observed. These were interpreted as grown-in dislocations radiating from the crystal nucleus. The dislocation pattern was very similar to that exhibited by many diamonds. In fact topographs of RDX could well have been taken for those of not very perfect natural diamonds. The interpretation of the linear defects as dislocations was reinforced by an examination of the fine structure of the dislocation images. In both projection topographs and section topographs they were found to have the double-peak profile evident under certain diffraction conditions in dislocation images in diamond, silicon and other simple structures. The whole dislocation image intensity profile will be wider, and hence its double peak more easily resolved, in reflections whose structure factor is small, such as the reflections from RDX. Dynamical diffraction effects such as Pendellösung fringes, and the disturbance of the fringe pattern by long range strains, were also observed in RDX crystals. These observations clearly indicate that, at least in part, these specimens behave as perfect crystals.

Crystals of hexamethylenetetramine have also been examined. These molecular crystals have a body-centered cubic lattice with cell edge equal to 7.02\AA . They exhibited images of individual dislocations and also Pendellösung fringes, both with good diffraction contrast.

3. X-RAY DIFFRACTION PHENOMENA IN PERFECT CRYSTALS

3.1. Pendellosung Interference.

Suppose a plane wave of monochromatic X-rays falls upon a perfect crystal at an angle that exactly satisfies the Bragg condition for certain lattice planes that are steeply inclined to the crystal surface. Then, with Bragg planes so oriented, both the Bragg reflected waves and the incident waves are directed into the crystal. Now it is an immediate consequence of the assumption of a 'perfect' crystal, which, by definition, maintains throughout its volume an ideal periodicity of its lattice, that the coherent addition of the contributions of reflections from individual Bragg-reflecting planes to the resultant amplitude of the Bragg-reflected wave can build up this amplitude to a value comparable to that of the incident X-ray beam, and such build-up may occur within a short distance from the surface at which the incident X-ray beam enters the crystal. For example, in the case of the 220 reflection in silicon, using Ag K α radiation, the amplitude of the wave reflected by a single Bragg plane is the fraction

$$r(= \frac{1}{7 \times 10^{-4}})$$

of the incident amplitude, when the Bragg condition is satisfied. Thus it may be estimated that after reflection at 70,000 Bragg planes, which correspond to a crystal thickness of only 1.4 microns, the amplitudes of incident and diffracted waves would be about equal in magnitude. The exact calculation of the amplitude ratio of diffracted to incident waves, which must be in dynamical equilibrium with each other to conserve energy, is provided by the dynamical theory of diffraction. (Good English-language summaries of this theory have been written by James (1948) and Batterman and Cole (1964)). The result that might be anticipated from the idea of dynamical equilibrium between incident and diffracted waves, that beyond some depth below the X-ray entrance surface the energy flow in a crystal exactly satisfying the Bragg condition is equally divided between the directions of incident and diffracted waves, is found to be true only when an average is taken over a depth interval ξ_g , known as the extinction distance (or extinction period). Within one extinction period, the energy-flow direction makes a complete oscillation between the one extreme of flowing purely along the incident beam direction and the other of purely along the

diffracted beam direction. When the Bragg plane is normal to the X-ray entrance surface of the crystal, i.e. when diffraction conditions are those of the 'symmetrical Laue case', the relation between ξ_g , q , and the interplanar spacing d is

$$\xi_g = \frac{\pi d}{q} \quad (1),$$

and for the case cited above, the 220 reflection of Ag K α by silicon,

$$\xi_g = 44 \text{ microns.}$$

When Bragg reflection occurs in a perfect crystal, waves travelling in the incident and diffracted beam directions are each split into two component waves with slightly different phase velocities, one velocity being slightly greater and the other slightly less than the phase velocity as given by the usual expression for the refractive index. Thus the incident and diffracted waves in the crystal each contain two slightly different wavelengths. It is the interference between these slightly different waves that causes the energy flow to oscillate between the incident and diffracted beam directions. This oscillation is analogous to the transfer back and forth of kinetic energy between a pair of coupled pendulums: the solution to the dynamical diffraction problem obtained by Ewald in 1917 which displayed the oscillation was consequently termed by him the 'Pendellosung'- the pendulum solution. The various waves propagating in the crystal at or near Bragg reflection are conveniently represented in reciprocal space (k -space) by wave vectors drawn to the wave surface (dispersion surface, constant-frequency surface) appropriate to the frequency of the monochromatic X-radiation used in the diffraction experiment. (A certain convention for drawing these vectors has been found useful in discussing diffraction problems, is generally accepted, and is described in the reviews by James (1948) and Batterman and Cole (1964).) A measure of the difference in wavelengths between the component waves in the pair of waves travelling either in the incident or diffracted beam directions is given by the degree of splitting of the dispersion surface at the Brillouin zone boundary corresponding to the Bragg reflection which is active. Indeed, in the symmetrical Laue case, the extinction distance, ξ_g , is just the reciprocal of the minimum separation, D , of the two

branches of the dispersion surface at the Brillouin zone boundary in reciprocal space. In terms of familiar quantities, this separation is given by

$$D = \left(\frac{e^2}{mc^2} \right) \frac{\lambda F}{\pi V \cos \theta} \quad (2),$$

θ being the Bragg angle and V the volume of the unit cell. (Actually a complication arises through the two states of polarisation of the X-rays, the σ state in which the electric vector is perpendicular to the plane of incidence and the π state in which it lies in the plane of incidence. The expression (2) applies to the σ state: the dispersion surface for the π waves has a minimum separation of its branches equal to CD , where $C = |\cos 2\theta|$. The topic of polarisation is more fully discussed below, and in Hart and Lang (1965), R15). The extinction distance is the depth periodicity of the Pendellösung oscillations, measured normal to the X-ray entrance surface of the crystal. The distance D is measured parallel to the Brillouin zone boundary, i.e. parallel to the Bragg plane. Hence for asymmetric transmission, when the Bragg plane is not normal to the X-ray entrance surface, the simple relation between ξ_g and D for the symmetrical Laue case,

$$\xi_g = 1/D \quad (3a)$$

must be modified for the asymmetric Laue case to be

$$\xi_g = (\cos \theta_0 \cos \theta_g)^{\frac{1}{2}} / \cos \theta \quad (3b),$$

where θ_0 and θ_g are the angles between the normal to the X-ray entrance surface and the direct and diffracted beams, respectively.

X-ray Pendellösung phenomena were first studied by Kato and Lang (1959). They took topographs of wedge-shaped specimens of perfect crystals. On the topograph image of the wedge, fringes appear parallel to the wedge axis. The fringes correspond to intersections of the X-ray exit surface of the wedge with the depth contours given by the Pendellösung oscillation of energy flow between the direct and diffracted beam directions. Indeed a comparison between the usual 'diffracted-beam' topographs and 'direct-beam' topographs of the same specimen demonstrated that the fringe patterns in the two types of topograph were complementary. A recognisable manifestation of Pendellösung phenomena in any part of a

crystal is taken as a criterion of crystal perfection: it can only occur when direct and diffracted waves have comparable amplitudes, and a good measure of coherence between the diffracted rays is maintained over a distance of the order of an extinction distance. Conversely, when any interface or imperfection occurs in a perfect matrix so that phase relations are abruptly disturbed and 'interbranch scattering' occurs, the intensity scattered into the diffracted beam will depend upon the local phase of the Pendellösung oscillation. Hence a depth-dependent periodic intensification of blackening will occur in topograph images of the imperfection, and it is a familiar feature in images of low-angle boundaries, fault surfaces of any type, and also of dislocations.

When the Pendellösung fringe spacing on topographs of well-defined wedges is measured, all the quantities are known, or can easily be determined, which relate this fringe spacing with the extinction distance, and hence with D . Then, from equation (2), the magnitude of the structure factor F can be determined absolutely. The technique of accurate, absolute measurement of structure factors by measurement of Pendellösung fringe spacings has been developed to a high degree of refinement by Professor Kato and his colleagues. In studies of crystal imperfections such as have been described in this Report, Pendellösung fringes have been found very useful in a more prosaic application, the reverse of that just outlined. This is the determination of specimen thickness from the order of Pendellösung interference, the structure factor being known. Such a measurement requires knowledge of the relation between the extinction distance and the specimen thicknesses for maxima and minima of Pendellösung fringes on projection topographs. A number of interesting and significant theoretical points are involved in this relation; just one of these need be mentioned here. It was the manifestation of 'hook-shaped' Pendellösung fringes in section topographs of wedge-shaped crystals that demonstrated that the accepted 'plane incident wave' diffraction theory for perfect crystals did not apply in the practical conditions of topographic experiments. The explanation of these fringes was obtained through the 'spherical incident wave' theory developed by Kato (1961) (summarised by Kato (1963a)). One result of Kato's calculations was the demonstration that for integrated intensities,

as recorded on projection topographs, the plane wave theory and the spherical-wave theory make similar predictions. The expression for the integrated intensity, as a function of specimen thickness, takes a fairly simple form when it is assumed that X-ray absorption in the specimen is negligible, the geometry is that of the symmetrical Laue case, and no distinction need be made between the contribution of waves in the σ and π polarisation states. (This last assumption is valid when $|\cos 2\theta|$ is little less than unity). The integrated intensity, R , from a perfect crystal of thickness t may be written

$$R = \frac{1}{2}\pi Dd \int_0^{2\pi tD} J_0(x) dx \quad (4)$$

A plot of R versus the upper limit of the integral (such appears in the text by Zachariasen (1945)) shows a steep rise, initially linear, up to the first maximum, followed by oscillations whose amplitude decays proportionally to $(tD)^{-\frac{1}{2}}$. Table 3.1.A. gives the intensities (normalised) of the maxima and minima, and the specimen thicknesses at which they occur (expressed as multiples of the extinction distance), calculated from equation (4).

Table 3.1.A.

Relative intensities and specimen thicknesses for Pendellösung maxima and minima on projection topographs, zero absorption, symmetrical Laue case.

Interference order	Normalised intensity ($R/\pi Dd$)	Specimen thickness (t/ξ_g)
1st max	0.735	0.382
1st min	0.334	0.878
2nd max	0.634	1.377
2nd min	0.385	1.876
3rd max	0.603	2.376
3rd min	0.466	2.876
4th max	0.586	3.376
4th min	0.419	3.876
5th max	0.576	4.376
5th min	0.428	4.876

It will be observed that the first Pendellosung maximum occurs at a specimen thickness just larger than $\frac{1}{3} \xi_g$, but that after the first Pendellosung minimum the fringe depth period departs negligibly from ξ_g . For determining the actual specimen thickness, Table 3.1.A is used together with the calculated value of the extinction distance. Some typical values of the extinction distance, for the symmetrical Laue case, are listed in Table 3.1.B.

Table 3.1.B.

Representative values of extinction distance (symmetrical Laue case).

Crystal, reflection, radiation.	ξ_g , microns
Diamond, 220, MoK α	48
" " CuK α	27
Silicon, 220, MoK α	36
" 440, "	60
LiF, 111, MoK α	59
" 200, "	33
α -Quartz, 10 $\bar{1}$ 1, MoK α	45
" 0003, "	205
α -iron, 110, AgK α	13
" " CoK α	5.7

In many different studies of crystal imperfections it has been found most useful to be able to measure the thickness of a non-uniform specimen at any point by means of the Pendellosung fringe contours. For the lower orders of interference, as listed in Table 3.1.A., and with the lower values of extinction distance among those given in Table 3.1.B., it is quite possible to measure specimen thickness within a range of plus or minus one or two microns. This is better than could be obtained by a mechanical thickness gauge, and is, moreover, achieved without any damaging physical contact with the specimen.

When the specimen absorbs X-rays appreciably, an enhanced transmission occurs in the vicinity of the Bragg reflection due to the

Borrmann effect. (This is discussed further in Section 4.1.) The formula for the integrated intensity becomes more complicated than that given in equation (4); an expression for it which can be easily compared with equation (4) has been given by Hart and Lang (1965). The positions of Pendellosung maxima and minima are not significantly altered by absorption. However, the relative modulation of the diffracted intensity by Pendellosung fringes is less than that in the non-absorbing case as calculated from equation (4) and recorded in Table 3.1.A. Although the average level of transmitted intensity falls off with increasing specimen thickness at a rate less than that expected from attenuation by normal absorption, $\exp(-\mu t \sec \theta)$, through operation of the Borrmann effect, the oscillatory components of R , both for σ and π waves, do have this normal attenuation. Since the visibility of Pendellosung fringes is used as a qualitative indication of crystal perfection, and could possibly be used as a quantitative 'perfection index', it is important to take into account the influence of the Borrmann effect on the Pendellosung modulation of diffracted intensity.

There is another effect which can modify Pendellosung fringe visibility profoundly. This arises from the polarisation factor, $C = |\cos 2\theta|$. The fringe systems due to the σ and π waves have Pendellosung periods in the ratio 1 to $\cos 2\theta$, and the observed intensity is the sum of the intensities of the two fringe systems. For higher Bragg angles, the σ and π fringes will get out of step every few Pendellosung periods, and the resultant fringe system has a complicated profile with periodic 'fading' of fringe visibility. Even when $\cos 2\theta$ differs not greatly from unity, as in the 220 reflection of MoK α by silicon ($\cos 2\theta = 0.93$), the large number of orders of Pendellosung interference that can be observed in such perfect crystals (orders up to 45 - 55), allow fading to zero of fringe visibility to occur four or five times, the interval between visibility minima being 14 Pendellosung fringes. Clearly this fading is important whether the fringes are being used in accurate determinations of F or as indications of lattice perfection. The theoretical and experimental aspects of polarisation fading have been discussed in detail by Hart and Lang (1965), R15. In this work it was demonstrated experimentally that fringes free from fading

could be obtained by the use of a plane-polarised incident X-ray beam. Such a beam can be obtained by reflection at a single crystal, choosing a Bragg angle as close as possible to 45° for which $\cos 2\theta = 0$.

3.2. Coherent Simultaneous Reflection.

The aim of crystal structure determinations by X-ray diffraction is to find the distribution of electron density throughout the unit cell of the crystal. This distribution can be represented by a three-dimensional Fourier series, and it will become determined when the amplitudes and phases of the Fourier components are known. The X-ray structure factors are the required Fourier components. But as long as the structure factor, F , is derived from a measurement of intensity of a Bragg reflection, or even from a measurement of a Pendellösung fringe spacing, only its modulus $|F|$ can be found, the phase remaining undetermined. This is the essence of the 'phase problem' that has been a central theme in X-ray crystallography for fifty years. There are certain ways of finding experimentally the phases of at least some Bragg reflections given by a structure. The most successful of these methods employs the 'isomorphous replacement' of one atom in the structure by another of considerably different X-ray scattering power, and analyses the changes in intensities of X-ray reflections that are produced thereby. Another method uses 'anomalous dispersion' and observes the change in relative intensities of X-ray reflections when different X-ray wavelengths are used close to an absorption edge of one of the atoms in the structure: near the edge the phase and modulus of the scattering factor of the atom concerned will depend upon the wavelength. It will be noted that both the 'isomorphous replacement' and the 'anomalous dispersion' methods depend upon the existence of certain conditions in the crystal chemistry and, in the latter method, the presence of an atom within a limited range of atomic numbers. Now there does exist a possible method of phase determination quite independent of the chemical nature of the crystal. This makes use of the interactions between Bragg reflections when two reflections take place simultaneously. The relative phases of the two reflections are determinable from the way the interaction takes place. However, this interaction must be a genuine dynamical interaction between the amplitudes of all the waves

concerned, and not merely a redistribution of intensities. Various attempts reported over the years to secure information about relative phases by studying simultaneous reflection phenomena have clearly failed because essential conditions for coherence were not achieved. The experimental conditions for observing genuine coherent dynamical interactions are extremely stringent, as was pointed out some years ago (Lang 1957c). The advent of the topographic techniques described in this Report, with their precise control of angular and spatial relationships, and the possibility of relating positions on a topograph to particular angular settings of the crystal, made feasible a successful experiment to determine directly the relative phases of X-ray reflections. The novel X-ray method used was to observe the perturbation of the Pendellösung interference pertaining to a given reflection when the angular setting of the crystal came close to satisfying the Bragg condition for another reflection. This perturbation was manifested on the topograph by a displacement of the Pendellösung fringes on either side of an 'Aufhellung' line on the topograph which marks the locus of points which simultaneously satisfy the Bragg condition for two reflections (Lang 1957c). In crystals of low dislocation density, with reasonably smooth surfaces, the effect is clear and the interpretation straightforward. An outline of the theory and an account of the experiment has been published (Hart and Lang 1961, R1). The displacement of Pendellösung fringes in the vicinity of the occurrence of simultaneous reflection has been observed in silicon, germanium, indium antimonide and quartz. These are, of course, well-known structures. The application of the method to unknown structures would require their crystals to possess volumes perhaps some hundreds of microns in diameter which diffracted X-rays as perfect crystals do. Obtaining such crystals may not be insuperably difficult, in view of the topographic experience indicating the large measure of perfection of fairly complex organic crystals grown from solution. For the time being, however, the experiment remains of academic interest; but its interest is a genuine one, as being the first direct determination of X-ray reflection phase relationships by a general method applicable in principle to all crystals, achieved nearly fifty years after the problem of phase determination began to vex crystallographers.

4. DIFFRACTION CONTRAST FROM IMPERFECTIONS IN NEARLY PERFECT CRYSTALS.

4.1. Diffraction Contrast without Interbranch Scattering.

In section 3.1. the expression was given, equation (4), for the variation with crystal thickness of the integrated reflection produced by a perfect, non-absorbing crystal in the symmetrical Laue case. The initial linear rise in intensity corresponds to the situation when the amplitude of the diffracted wave is much less than that of the incident wave and multiple reflection within the crystal may be ignored as in the calculation of intensity from an ideally mosaic crystal. Thus, up to a certain thickness, the ideally perfect and the ideally mosaic crystal cannot be distinguished on the basis of a difference in integrated reflection. Gross misorientations can be detected by their effect on the angular range of reflection, but lattice defects such as dislocations and stacking faults do not give rise to any diffraction contrast until the crystal thickness is sufficient to make the intensity as given by equation (4) fall significantly below that given by a prolongation of the initial linear region. The intensity indicated by the latter prolongation would be that reflected by a thick, non-absorbing ideally mosaic crystal, in the absence of secondary extinction. The transition from 'thin-crystal' diffraction behaviour to that of the thicker crystal can often be observed experimentally in very thin, tapering specimens of a moderately perfect crystal. The topograph image is completely featureless until a thickness of about $1/3$ the extinction distance is reached, fair diffraction contrast from imperfections appears at the first Pendellösung maximum, and at the first Pendellösung minimum stronger diffraction contrast is manifested than at any other thickness, in the non-absorbing case. The data in Tables 3.1.A and 3.1.B enable the minimum specimen thicknesses at which diffraction contrast should be observable to be estimated, and actual observations confirm these estimates. Examples of minimum thicknesses are, 12 microns with silicon, 220 reflection, using MoK α radiation, and 2 microns with iron, 110 reflection, using CoK α radiation. The latter, low value of thickness is of potential interest since it is within the range of thicknesses accessible for study by transmission electron microscopy, using high voltage electron microscopes

operating in the $\frac{1}{2}$ to 1 MeV range.

In thicker specimens, those whose thickness ranges upwards from a few extinction distances, a variety of diffraction contrast phenomena can appear which are not observed in thin-film transmission microscopy. They bear witness to the fact that there are complexities in the X-ray diffraction situation from which the electron microscope experiments are free. Such complexities are in part responsible for the less developed state of X-ray diffraction contrast theory compared with that worked out for electrons (the latter theories are reviewed by Hirsch et al. 1965). There are, however, compensating simplifications, some of them very valuable, which attend the X-ray experiments. Notable among these is the ease with which it can be arranged that a single desired Bragg reflection, and that one only, is active in producing the topograph image.

One important difference between the electron and X-ray diffraction situations is the different ratio of angular range of illumination to angular range of reflection that applies with these two radiations. The angular range of reflection of 100 kV electrons by a perfect crystal is about 10^{-2} radians for strong reflections; but the range of illumination of the specimen, as determined by the condenser aperture and focussing adjustment, does not usually exceed about 10^{-3} radians. Thus the incident electron beam acts effectively as a plane incident wave: if the illuminated region of the specimen is oriented, as a whole, exactly at the Bragg setting then a locally distorted part of the illuminated region will no longer be able to satisfy the Bragg condition fully. On the other hand, in the X-ray case, with a typical angular range of reflection of only 10^{-5} radians, and the illumination range defined by the incident-beam collimating system to be about $1'$ of arc, i.e. 3×10^{-4} radians, the angular range of illumination is more than adequate to generate the full integrated reflection both from a perfect matrix and from an incoherently reflecting slightly misoriented region within it. Experiment and theory (Kato and Lang 1959, Kato 1961) confirm that this is so, and show, moreover, that the divergent incident beam excites coherently all the diffracted waves within the perfect crystal's angular range of Bragg reflection, and thus acts as a coherent spherical

incident wave.

Another important difference between the electron and X-ray cases arises from the combined effect of the great difference in specimen thicknesses used (typically 1mm with X-rays and 10^{-4} mm with electrons) and the difference in Bragg angles (typically about 10^0 in the X-ray case and about 1^0 in the electron case). Thus in the electron case all incident and diffracted rays produced by an incident ray impinging at a given point on the specimen surface are contained within a column parallel to the Bragg planes about 20 Å in diameter, a dimension comparable with the resolution limit of the electron microscope; whereas in the X-ray case, with the figures quoted above, the separation at the exit surface of incident and diffracted rays that have originated at a given point on the entrance surface may be several tenths of a millimeter, a thousand times the X-ray topographic resolution limit. Thus diffraction calculations designed to find the resultant wave disturbance at a given point on the exit surface, which in the electron case can be carried out one-dimensionally within a column such as that just described, must in the X-ray case be expanded into two-dimensions to cover the triangular area enclosed between the directions of incident and diffracted rays.

The manner of distribution of energy-flow of X-rays within the triangle contained between the incident and diffracted ray directions assumes great importance in all investigations of X-ray diffraction contrast. The distribution in the case of an undistorted, perfect crystal has been calculated by Kato (1960); its essential feature is that rays comprising a given pair of incident and diffracted waves propagate normal to the tangent plane at the point on the dispersion surface that defines the wave vectors of the pair of waves. Exactly at the Bragg angle, rays belonging to both the branches into which the dispersion surface is split propagate parallel to the Bragg planes since both branches intersect the Brillouin zone boundary normally. Some way off the peak of the curve of Bragg-reflected intensity versus angle of incidence of a plane wave on the crystal, the wave vectors corresponding to the waves excited in the crystal end on the dispersion surface some distance away from the Brillouin zone boundary. It then

follows from the shape of the dispersion surface that the ray from one branch will propagate nearly in the direct beam direction and from the other nearly in the diffracted beam direction. Thus, when the whole angular range of reflection is excited by the divergent incident beam, the whole energy-flow triangle is filled with a fan of rays. The dynamical diffraction theory for the perfect crystal shows how the ratio of amplitudes of direct and diffracted waves on a given branch of the dispersion surface depends upon the distance from the Brillouin zone boundary of the wave-vector-defining point on the dispersion surface (briefly, the wave-point). It also shows how the distribution of energy between the two branches of the dispersion surface is determined by matching the wave disturbances on either side of the X-ray incidence surface. (A re-matching must be made, it should be noted, at any surface where phase relations between direct and diffracted waves are abruptly changed).

Now if the crystal has zero X-ray absorption, rays associated with all wave-points will propagate without attenuation. When absorption is present, it is found that attenuation is a function of position of the wave-point on the dispersion surface. In the case when the concentrations of absorbing power and of scattering power in the unit cell are generally coincident (which happens to be so in all simple structures) it is found that rays associated with the branch of the dispersion surface corresponding to a phase velocity closer to the value in vacuo suffer less than the normal absorption, whereas those associated with the other branch are more strongly absorbed than normally. The difference in absorption between rays belonging to the two branches is a maximum for wave-points on the Brillouin zone boundary. Hence, after some passage through the crystal, rays belonging to one branch only (that commonly called branch 1) will survive, the rays belonging to the other branch (branch 2) being completely absorbed. Moreover, with strong absorption, it is only branch 1 rays travelling closely parallel to the Bragg planes, which are of all rays those which suffer minimum absorption, which survive. This selective, and anomalously high, transmission of one narrow bundle of rays out of the whole fan of rays which start out within the energy flow triangle describes, in essence, the Borrmann effect. In specimens which have μ greater than unity the

Borrmann effect has an important influence on the character of topograph images: that it should change the intensity profile across section topographs follows from the narrowing of the energy-flow fan with consequent peaking of intensity in the center of the section topograph (Kato 1960). The influence of the Borrmann effect on the images of imperfections will be described below and in Section 4.2.

In a perfect crystal, when once the energy of the spherical incident wave has been distributed among the fan of rays within the crystal by matching disturbances inside and outside the crystal at the X-ray entrance surface, the rays propagate independently through the crystal in straight lines, the amplitudes of a given bundle associated with an element of one branch of the dispersion surface remaining independent of those associated with other elements, of either branch. When the crystal is distorted, this pattern can change in two ways, depending upon the degree of distortion. The problem of finding the ray paths in weakly distorted crystals was investigated by Penning and Polder (1961) and later by Kato (1963b, 1964). Penning and Polder showed that the rays are bent, the change in wave vector accompanying the bending being in the direction of the spatial gradient of the component of distortions that changes the local degree of satisfaction of the Bragg condition. The situation is analogous to the bending of a ray of light in a medium of slowly varying refractive index, and the phenomenon in the X-ray case is often referred to as 'energy-flow refraction'. As long as the distortion is slight, a narrow ray bundle bends without spreading. Its energy, which may be regarded as associated with its corresponding element (i. e. wave-point) on the dispersion surface, is conserved (apart, of course, from losses due to absorption). As the ray bends, its wave-point migrates along the branch of the dispersion surface to which it belongs, and this results in a redistribution of energy on this branch but no interchange of energy between this and the other branch. The changes in energy-flow pattern which arise solely from this 'adiabatic' wave-point migration give rise to the diffraction contrast that occurs without 'interbranch scattering'. If, on the other hand, the distortion affecting satisfaction of the Bragg condition is severe, or an interface such as a stacking fault is encountered, there takes place a

redistribution of energy between the two branches of the dispersion surface. This is the type of redistribution termed 'interbranch scattering'. Three types of diffraction contrast phenomenon involving only adiabatic wave-point migration will now be briefly described. They appear under conditions of low, moderate and high absorption, respectively.

When the energy-flow refraction theories of Penzling and Polder (1961) and Kato (1963b, 1964) are applied to problems of bent crystals they show that if the Bragg reflecting planes are curved the branch 1 rays are curved in the same sense as the Bragg planes, the branch 2 rays in the opposite sense. Then as long as the absorption of rays of both branches is negligible, and the overall bending of the crystal is small, little or no effect of the bending upon the integrated intensity of the reflection is produced except that resulting from the change in order of the Pendellösung interference. This latter change occurs because of the change in phase difference between the branch 1 and branch 2 waves that interfere at the specimen X-ray exit surface consequent upon the change in wave vector that accompanies the wave-point migration along the trajectory. Consequently, the observed modifications of integrated intensity are limited to the range between maxima and minima of intensity in the vicinity of the mean order of Pendellösung interference, as given by equation (4), Section 3.1. The effect of crystal distortion is to increase the order of Pendellösung interference in the X-ray case (Kato 1963a, 1963b, 1964). This increase is often observed experimentally. The projection topograph Figure 4 of Authier and Lang (1964, R8) shows it well. On section topographs the displacement of Pendellösung fringes by distortions such as those due to dislocations is even more evident, see Figures 2 and 3 of Lang (1964c, R10).

As soon as even a moderate amount of absorption is present, the different attenuations of the branch 1 and branch 2 waves enlarges the range of intensity variation that a given bending may produce, and, most important,

makes the change in integrated intensity depend upon the sense of curvature of the Bragg planes. This sense-dependence is most readily observed by noting local differences in topograph image intensity between the $hk\ell$ and $\bar{h}\bar{k}\bar{\ell}$ reflections. Such differences, termed 'local failure of Friedel's Law', were first observed on topographs of silicon and calcite by Lang in 1958. They formed the subject of an intensive theoretical and experimental study by Hart (1963) and have also been treated theoretically by Kato (1963c). A useful application of the 'local failure of Friedel's Law' is the determination of the sense of Burgers vectors of dislocations, and it has been employed in several studies (Hart 1963, Lang and Polcarová 1965, and see Section 2.4.1.). Now the intense positive diffraction contrast produced by dislocations arises from interbranch scattering in the strongly distorted crystal surrounding the dislocation. There is, however, surrounding the region where interbranch scattering occurs, a relatively large volume of weakly distorted crystal where only wave-point migration takes place. In the range of specimen absorptions corresponding to μt values between about 2 and 5, the intensity of the central part of the dislocation image is much reduced, largely because interbranch scattering feeds energy from the weakly attenuated branch 1 to the strongly attenuated branch 2 rays. The outer parts of the image, produced by bent but not scattered rays, may then predominate in the production of the overall contrast of the dislocation image, and even a marked reversal in overall contrast between the $hk\ell$ and $\bar{h}\bar{k}\bar{\ell}$ images of the dislocation may be observed. Interpretation is simplest in the case of reflections from the slip-plane of edge dislocations. When reflection is obtained from the concave side of the planes, the dominant, strongly transmitted, branch 1 rays, which have curvature in the same sense as the Bragg planes, are bent round into the diffracted beam direction, and at the crystal exit surface they split so that most of their energy travels in the diffracted beam direction, with little in the direct beam direction. Hence this reflection shows the excess diffracted intensity. More generally, the rule for finding the sense of the edge component of the Burgers vector of a dislocation from the difference between its $hk\ell$ and $\bar{h}\bar{k}\bar{\ell}$ images is as follows: in the reflection which shows extra intensity the extra half-plane lies on the side of the dislocation image

closer to the direct beam.

When the X-ray absorption is quite high, so that only a narrow bundle of branch 1 rays is able to travel through the crystal, any bending of the rays away from a direction close to the Bragg plane will involve some loss of anomalous transmission. Thus the overall contrast of a dislocation will be negative: it will appear as a light line on a darker background. The redistribution of energy arriving at the specimen X-ray exit surface due to the bending of the rays passing close to the dislocation may generate one or more fringes on either side of the light line marking the center of the dislocation image. The intensity distribution across the dislocation image produced in these conditions has been calculated by Kamiya (to be published) using the theories of Kato (1963b, 1964). Calculations of a similar sort have been performed by Taupin (1964) using a theory equivalent to that developed by Takagi (1962, R3).

The methods for dealing with problems of the distorted crystal that apply the notions of ray optics are valuable in showing physically how the energy-flow pattern is modified by the distortion (Penning and Polder 1961, Kato 1963a, b, 1964). They can be applied only as long as the distortion is so small that a narrow ray bundle will propagate through the crystal without appreciable spreading. They have been applied so far to experimental situations where no interbranch scattering occurs.

Diffraction theories which use the model of the lamellar crystal (Kato 1963c) are analogous to the treatments of distorted crystals developed for electron microscopy (Hirsch et al 1965) and have a common origin in Darwin's diffraction theories. The useful picture of ray trajectories in X-ray diffraction is lost in such theories, but there is no limit to the degree of distortion they can handle provided the distortion is a function only of distance normal to the lamellae. (A problem coming within the latter limitation would be that of a pure screw dislocation normal to the Bragg plane).

The theory of Takagi (1962, R3) gives a more complete picture of the multiple scattering process than the lamellar theories, and is not restricted to the type of distortion it can handle. It is, however, restricted

in the degree of distortion to which it is applicable. Moreover, with strain fields such as those of a dislocation in arbitrary orientation, the quantity of calculation that would be required to build up the topograph image, involving one two-dimensional mesh for every image point, is quite prodigious. This problem illustrates the great complications involved in complete X-ray diffraction contrast investigations.

4.2. Diffraction Contrast with Interbranch Scattering

It is the intense, localised, positive diffraction contrast produced by dislocations, precipitates, inclusions, ring-cracks, etc. that is taken advantage of in X-ray topographic investigations of the distribution of imperfections in nearly perfect crystals. There are several ways of considering the manner by which this strong contrast is generated. At the simplest level, it is easy to see that if a certain sharply bounded volume of crystal is misoriented with respect to the perfect crystal matrix by an amount greater than the angular range of reflection of the perfect crystal (typically only about 10^{-5} radians, or $2''$ of arc) then such a misoriented volume will Bragg reflect independently of the matrix. It can make use of incident radiation coming from areas of the X-ray tube target other than those that can be 'seen' by the perfect crystal, and the waves diffracted by it are incoherent with those diffracted by the perfect crystal. Indeed, a strongly distorted region may be considered as consisting of a series of zones, each of which accepts for Bragg reflection radiation from a different area of the target, which it diffracts independently of the other zones. Since the angular range of incidence of X-radiation on any point of the crystal is typically about thirty times the angular range of reflection of the perfect crystal, there is an evident possibility that strong positive diffraction contrast can be generated by the addition of the intensities independently reflected by misorientated zones. No similar mechanism for producing strong positive contrast operates in electron microscopy, for which, as pointed out in Section 4.1., the illumination is effectively a plane wave. In the X-ray case diffraction contrast can be reasonably explained by this simple mechanism when distortion is severe, but experimental evidence shows that in the cases of the imperfections chiefly of interest (such as dislocations) this model of independent reflection by perfect matrix and by

locally imperfect zones is oversimplified. The chief evidence against the simple picture is the presence of the 'extinction shadows' of reduced diffracted intensity that accompany the excess diffracted intensity of the localised image of the imperfection. Such shadows can be seen associated with the 'random' dislocations in the projection topograph of a slice of lithium fluoride, Fig. 2 of this Report, following page 33. They are seen, too, associated with the dislocation images in Fig. 1 of Authier and Lang (1964, R8). In section topographs, such as Figs. 2 and 3 of Lang (1964c, R10), they are strongly in evidence. This shadowing shows that the lattice imperfection has intercepted and diverted some of the waves participating in the dynamical balance of direct and reflected waves that occurs in the close vicinity of exact satisfaction of the Bragg condition, and which gives rise to the rays that propagate within the energy-flow triangle. This diversion process is describable by 'interbranch scattering'. Within the triangle of energy flow, most of the energy (in the low-absorption case) is flowing in directions close to the incident beam, and hence is associated with wave-points on the dispersion surface where the normal to the dispersion surface is close to this direction. A transfer of such energy from one branch of the dispersion surface to the other branch will carry it to wave-points where the dispersion-surface normal is directed more towards the diffracted-beam direction, with the production of stronger rays flowing in the direction of the diffracted beam. Interbranch scattering is, of course, the mechanism whereby diffraction contrast is produced by stacking faults, and by twin boundaries such as those of Brazil and Dauphiné twinning in quartz (see Section 2.10.i.). With such defects the situation is relatively simple because the orientation of the lattice is the same on either side of the boundary. In the case of dislocations, on the other hand, the situation is complicated by the great distance over which the energy-flow is perturbed, due to the form of the strain-fields of dislocations. As the X-rays approach the dislocation, wave-point migration (as described in Section 4.1.) first occurs. This may produce a substantial redistribution of energy on each branch of the dispersion surface prior to interbranch scattering. Following the interbranch scattering, a further redistribution of energy by wave-point migration occurs as the X-rays pass into less

strongly distorted crystal. A proper quantitative account of this succession of processes which together contribute to the final distribution of energy on the X-ray exit surface of the crystal would clearly be difficult, and has not yet been achieved. However, some predictions can be made from this model of wave-point migration, interbranch scattering, and further wave-point migration that account qualitatively for some aspects of dislocation image contrast, such as the asymmetric bimodal intensity profile of certain dislocation images (Lang 1965a).

For a given X-ray wavelength and Bragg reflection, interbranch scattering will occur when a certain critical curvature of the Bragg plane is exceeded. The integral of Bragg-plane curvature between two points along the X-ray trajectory gives the mutual tilt of the Bragg planes at these points. If the Bragg-plane curvature is substantially confined within a distance roughly equal to the extinction distance, and the integral of the curvature over that distance is such as to produce a Bragg-plane tilt greater than a certain critical value, then it does not appear to matter greatly with regard to the production of interbranch scattering whether the curvature is uniformly distributed or concentrated at a given horizon. In the strain-fields of dislocations, which give rise to lattice-plane curvatures that increase rapidly as the dislocation is approached, it appears that it is the magnitude of the tilt away from the matrix orientation reached at a point near the dislocation that can be taken as the criterion for commencement of interbranch scattering and hence for a sharp rise of diffracted intensity above that given by the perfect matrix (assumed to be weakly absorbing). If the critical tilt is reached a relatively long distance from the dislocation core then there will be a relatively large volume of crystal in which interbranch scattering takes place, and the integrated excess intensity from the dislocation will be high. If, on the other hand, the critical tilt is not reached at all along the X-ray trajectory, or only at a point so close to the dislocation core that interbranch scattering can occur within a volume of less than, say, a micron in diameter, then the dislocation will be invisible. The notion that dislocation visibility and dislocation image width depend upon local lattice tilt has been applied in numerous studies to determine the Burgers vector and type (i. e. edge or screw) of dislocations

in cases when X-ray absorption is low (e. g. Lang 1959b, Jenkinson and Lang 1962). It appears to account well for the observation that images of pure edge dislocations lying in the Bragg plane and normal to the plane of incidence are about 1.75 times as wide as images of pure screw dislocations normal to the Bragg plane, with the same value of $\underline{g} \cdot \underline{b}$ (\underline{g} is the diffraction vector, \underline{b} is the dislocation Burgers vector). This is the ratio expected from calculations of tilts in the dislocation strain fields.

Frank and Lang (1965) have discussed the variation of strength of X-ray topograph images of dislocations as a function of $\underline{g} \cdot \underline{b}$ and the dislocation type and orientation. Experimentally it is found that overall visibility (i. e. integrated excess intensity) depends approximately quadratically on the value of $\underline{g} \cdot \underline{b}$, and is zero or very weak if $\underline{g} \cdot \underline{b} = 0$ in the low-absorption case. Prediction and experiment agree that pure screw dislocations are invisible in reflections from all planes that contain \underline{b} ; pure edge dislocations are invisible in a single reflection only, that from the plane normal to the dislocation line, and mixed dislocations never completely vanish.

Experiment suggests that the critical value of tilt is about equal to the angular width, $2\Delta\theta_{\frac{1}{2}}$, at half maximum intensity of the perfect-crystal reflection curve. In the symmetrical Laue case, and negligible absorption, the simple relation applies:

$$2\Delta\theta_{\frac{1}{2}} = 2d/\xi_g \quad (1).$$

The extinction distance ξ_g is given by equation (2) and (3a) of Section 3.1. and d is the interplanar spacing. It is useful to bear in mind that for the perfect crystal the angular width, $2\Delta\theta_{\frac{1}{2}}$, is also a measure of the integrated reflection. The tilt criterion suggested above is easily applied to the case of the pure screw dislocation making an angle ψ with the Bragg plane normal. The dislocation image width, W , is then given by the two alternative expressions

$$W = b \cos \psi (2\pi c \Delta\theta_{\frac{1}{2}})^{-1} \quad (2a)$$

$$\text{and} \quad W = \underline{g} \cdot \underline{b} (2\pi c)^{-1} \xi_g \quad (2b).$$

If the dislocation width, W , is measured between the points where the excess intensity rises sharply above that of the matrix (clearly rather a subjective measurement) the value of the constant c found appropriate is 0.8 for dislocations in pure silicon, in the low-absorption case. For such unavoidably imprecise quantities as W the value of c might as well be taken as unity, and this is the value used in Table 4.2.A. This Table gives values of W , and some other relevant quantities, for various types of dislocation in diamond and in iron. The figures agree well with the observations (Frank and Lang 1965, Lang and Polcarová 1965).

Table 4.2.A.

Dislocation image width (W), extinction distance (ξ_g) and angular width of reflection ($2\Delta\theta_{\frac{1}{2}}$) in the symmetrical Laue case, negligible absorption, for diamond and α -iron.

Crystal	Diamond		Iron	
Reflection	220		110	
Radiation	Mo K α	Cu K α	Ag K α	Co K α
ξ_g (μm)	48	27	13	5.7
$2\Delta\theta_{\frac{1}{2}}$ (seconds)	1.1	1.9	6.4	15
W , pure screw, $\underline{g} \cdot \underline{b} = 1$, (μm)	8	4.3	2.5	1.1
" " " $\underline{g} \cdot \underline{b} = 2$, "	16	8.6	-	-
W , pure edge, $\underline{g} \cdot \underline{b} = 2$, "	27	15	-	-

REFERENCES

- Amelinckx, S., 1964, The Direct Observation of Dislocations, New York: Acad. Press.
- Ashby, M.F. and Brown, L.M., 1963, Phil. Mag. 8, 1083, 1649.
- Authier, A. and Lang, A.R., 1964, J. Appl. Phys. 35, 1956.
- Authier, A., Rogers, C.B., and Lang, A.R., 1965, Phil. Mag. 12, 547.
- Batterman, B.W. and Cole, H., 1964, Rev. Mod. Phys. 36, 681.
- Berman, R. (ed.), 1965. Physical Properties of Diamond, Oxford: Clarendon Press.
- Booker, G.R., 1964, Discussions of the Faraday Society 38, 298.
- Burhop, E.H.S., 1952, The Auger Effect, Cambridge: The University Press.
- Compton, A.H. and Allison, S.K., 1960, X-Rays in Theory and Experiment, New York: Van Nostrand.
- Dash, W.C., 1959, J. Appl. Phys. 30, 459.
- Ehrenberg, W. and Spear, W.E., 1951, Proc. Phys. Soc. Lond. B64, 67.
- Elliott, R.J., 1960, Proc. Phys. Soc. Lond. 76, 787.
- Evans, T. and Phaal, D.H., 1962, Proc. Roy. Soc. A 270, 538.
- Frank, F.C., 1956, Proc. Roy. Soc. A 237, 168.
- Frank, F.C. and Lang, A.R., 1965, in Physical Properties of Diamond, ed. Berman, Oxford: Clarendon Press, Chap. III.
- Freeman, G.P. and Van der Velden, H.A., 1952, Physica, 18, 1, 9.
- Hart, M., 1963, Ph.D. Thesis, University of Bristol.
- Hart, M. and Lang, A.R., 1961, Phys. Rev. Lett. 7, 120.
- Hart, M. and Lang, A.R., 1965, Acta Cryst. 19, 73.
- Hirsch, P.B., Howie, A., Nicholson, R.B., Pashley, D.W. and Whelan, M.J., 1965, Electron Microscopy of Thin Crystals, London: Butterworths.
- Hulme, K.F. and Mullin, J.B., 1962, Solid State Electronics, 5, 211.
- James, R.W., 1958, Optical Principles of the Diffraction of X-Rays, London: Bell.
- James, P.F. and Evans, T., 1965, Phil. Mag. 11, 113.
- Jenkinson, A.E. and Lang, A.R., 1962, in Direct Observation of Imperfections in Crystals, ed. Newkirk and Wernick, New York: Interscience, p. 471.

- Johnston, W.G., 1962, Progress in Ceramic Science, Vol. II.
(ed. J.E. Burke) Oxford: Pergamon Press.
- Kamiya, Y. and Lang, A. R., 1965a, Phil Mag. 11, 347.
- Kamiya, Y. and Lang, A.R., 1965b, J. Appl. Phys. 36, 579.
- Kato, N., 1960, Acta Cryst. 13, 349.
- Kato, N., 1961, Acta Cryst. 14, 526, 627.
- Kato, N., 1963a. in Crystallography and Crystal Perfection,
ed.G.N. Ramachandran, London: Academic Press. p.153.
- Kato, N., 1963b. J. Phys. Soc. Japan 18, 1785.
- Kato, N., 1963c, Acta Cryst. 16, 276, 282.
- Kato, N., 1964, J. Phys. Soc. Japan 19, 67, 971.
- Kato, N., and Lang, A. R., 1959, Acta Cryst. 12, 789.
- Lang, A.R., 1957a, Acta Cryst. 10, 839.
- Lang, A.R., 1957b, Acta Met. 5, 358.
- Lang, A. R., 1957c. Acta Cryst. 10, 252.
- Lang, A.R., 1958, J. Appl. Phys. 29, 597.
- Lang, A.R., 1959a, Acta. Cryst. 12, 249.
- Lang, A.R., 1959b, J. Appl. Phys. 30, 1748.
- Lang, A.R., 1963a. Brit. J. Appl. Phys. 14, 904.
- Lang, A.R., 1963b, J. Phys. Soc. Japan 18, Suppl. II, 332.
- Lang, A.R., 1964a. Proc. Roy. Soc. A 278, 234.
- Lang, A.R., 1964b, Proc. Phys. Soc. London 84, 871.
- Lang, A.R., 1964c. Discussions of the Faraday Society 38, 292.
- Lang, A.R., 1965a. Z. f. Naturforschung 20a, 636.
- Lang, A.R., 1965b. Acta Cryst. 19, 290.
- Lang, A.R., 1965c. Appl. Phys. Lett. 7, 168.
- Lawn, B. , Kamiya, Y. and Lang, A.R., 1965, Phil. Mag. 12, 177.
- Lang, A.R. and Miles, G.D., 1965, J. Appl. Phys. 36, 1803.
- Lang, A.R. and Polcarová, M. 1965, Proc. Roy. Soc. A 285, 297.
- Martin, K.J., 1965, Ph D. Thesis, University of Bristol.
- Newkirk, J.B. and Wernick, J.H., 1962, Direct Observation of
Imperfections in Crystals, New York: Interscience.
- Nye, J.F , 1949, Proc. Roy. Soc. A 198, 190.
- Penning, P. and Polder, D., 1961, Philips Res. Rep. 16, 419.

Powell, C.F., Fowler, P.H. and Perkins, D.H., 1959, The Study of Elementary Particles by the Photographic Method, London: Pergamon Press.

Ramachandran, G.N., 1946, Proc. Indian Acad. Sci. 24A 65.

Schlössin, H.H. and Lang, A.R., 1965, Phil. Mag. 12, 283.

Seal, M., 1966, Phil. Mag. 13, 645.

Shah, C.J. and Lang, A.R., 1963, Mineralogical Mag. Lond. 33, 594.

Takagi, S., 1962, Acta Cryst. 15, 1311.

Takagi, M. and Lang, A.R., 1964, Proc. Roy. Soc. A 281, 310.

Taupin, D., 1964, Ph.D. Thesis, University of Paris.

Tweet, A.G., 1958, J. Appl. Phys. 29, 1520.

Zachariasen, W.H., 1945, Theory of X-Ray Diffraction in Crystals, New York: Wiley.

LIST OF REPRINTS

- R1. Direct Determination of X-ray Reflection Phase Relationships through Simultaneous Reflection.
M. Hart and A. R. Lang, Phys. Rev. Letters 7 (1961) 120.
- R2. X-ray Diffraction Topographic Studies of Dislocations in Floating-Zone Grown Silicon.
A. E. Jenkinson and A. R. Lang in "Direct Observation of Imperfections in Crystals", ed. Newkirk and Wernick (1962, New York: Interscience), 471.
- R3. Dynamical Theory of Diffraction Applicable to Crystals with any Kind of Small Distortion.
S. Takagi, Acta Cryst. 15 (1962) 1311.
- R4. An Unusual Distribution of Precipitates in a Diamond.
C. J. Shah and A. R. Lang, Mineralogical Mag. (London) 33 (1963) 594.
- R5. Recent Studies of Lattice Defects by X-ray Diffraction Topography.
A. R. Lang, J. Phys. Soc. Japan, 18 Suppl. II (1963) 332.
- R6. Applications of 'Limited Projection Topographs' and 'Direct Beam Topographs' in X-Ray Diffraction Topography.
A. R. Lang, Brit. J. Appl. Phys. 14 (1963) 904.
- R7. Dislocations in Diamond and the Origin of Trignons.
A. R. Lang, Proc. Roy. Soc. A. 278 (1964) 234.
- R8. Three Dimensional X-Ray Topographic Studies of Internal Dislocation Sources in Silicon.
A. Authier and A. R. Lang, J. Appl. Phys. 35 (1964) 1956.
- R9. X-Ray Bragg Reflexion, 'Spike' Reflexion and Ultra-violet Absorption Topography of Diamond.
M. Takagi and A. R. Lang, Proc. Roy. Soc. A 281 (1964) 310.
- R10. Crystal Growth and Crystal Perfection : X-Ray Topographic Studies.
A. R. Lang, Discussions of the Faraday Society, 38 (1964) 292.
- R11. A Proposed Structure for Nitrogen Impurity Platelets in Diamond.
A. R. Lang, Proc. Phys. Soc (Lond) 84 (1964) 871.
- R12. On the Structure of Coated Diamonds.
Y. Kamiya and A. R. Lang, Phil. Mag. 11 (1965) 347.
- R13. X-Ray Diffraction and Absorption Topography of Synthetic Diamonds.
T. Kamiya and A. R. Lang, J. Appl. Phys. 36 (1965) 579.

LIST OF REPRINTS (Contd.)

- R14. A Study of Repeated Twinning, Lattice Imperfections and Impurity Distribution in Amethyst.
H.H. Schlössin and A.R. Lang, Phil. Mag. 12 (1965) 283.
- R15. The Influence of X-Ray Polarization on the Visibility of Pendellösung Fringes in X-ray Diffraction Topographs.
M. Hart and A.R. Lang, Acta Cryst., 19 (1965) 73.
- R16. X-Ray Topography of Decorated Dislocations in Magnesium Oxide.
A.R. Lang and G.D. Miles, J. Appl. Phys. 36 (1965) 1803.
- R17. An X-Ray Topographic Study of Planar Growth Defects in a Natural Diamond.
B. Lawn, Y. Kamiya and A.R. Lang, Phil. Mag., 12 (1965) 177.
- R18. On the Macroscopic Distribution of Dislocations in Single Crystals of High-Purity Recrystallized Aluminum.
A. Authier, C.B. Rogers and A.R. Lang, Phil Mag., 12 (1965) 547.

UNCLASSIFIED
Security Classification

DOCUMENT CONTROL DATA - R&D		
(Security classification of title, body of abstract and indexing annotation must be entered when the overall report is classified)		
1. ORIGINATING ACTIVITY (Corporate author) H.H. Wills Physics Laboratory, University of Bristol, Royal Fort, Bristol 2, England.		2a. REPORT SECURITY CLASSIFICATION UNCLASSIFIED
3. REPORT TITLE An Investigation of Crystal Imperfections by X-ray Diffraction.		2b. GROUP
4. DESCRIPTIVE NOTES (Type of report and inclusive dates) Scientific Final		
5. AUTHOR(S) (Last name, first name, initial) LANG, Andrew R.		
6. REPORT DATE 20th April, 1966	7a. TOTAL NO. OF PAGES 126	7b. NO. OF REFS 65
8a. CONTRACT OR GRANT NO. AF 61(052)-449	8b. ORIGINATOR'S REPORT NUMBER(S)	
a. PROJECT NO. 7021		
c. 61445014	9a. OTHER REPORT NO(S) (Any other numbers that may be assigned this report) ARL 66-0118	
d. 681306		
10. AVAILABILITY/LIMITATION NOTICES / Distribution of this document is unlimited.		
11. SUPPLEMENTARY NOTES	12. SPONSORING MILITARY ACTIVITY Aerospace Research Laboratories (ARZ) Office of Aerospace Research Wright-Patterson AFB, Ohio	
13. ABSTRACT High resolution X-ray topographic methods have been used to study lattice imperfections in many natural and man-made crystals. Individual lattice imperfections can be resolved in specimen thicknesses from a few microns to several millimeters. The topographic resolution obtainable is one micron. The effects on the resolution of X-ray geometry, mechanisms of diffraction contrast, photographic processes and statistical fluctuations are discussed. Lattice imperfections studied include dislocations, inclusions, precipitates, impurity layers, and fault surfaces such as stacking faults and twin boundaries. Both the direction and sense of dislocation Burgers vectors can be determined. Studies performed on natural diamond include the origin of dislocations and the correlation of dislocation outcrops with trigon pits; the correlation of lattice imperfections, ultra-violet absorption and 'spike' reflections in Type I and Type II diamonds; planar defects of stacking-fault type; abrasion of natural and polished faces; and the structure of coated diamonds. Synthetic diamonds have been studied by diffraction topography and microradiography. Configurations of grown-in dislocations and of dislocations deliberately introduced by plastic deformation have been studied in silicon, germanium and indium antimonide. The configuration and origin of dislocations have also been investigated in LiF, MgO, aluminium, Al ₂ O ₃ , quartz and some organic crystals.		

DD FORM 1473
1 JAN 64

Unclassified
Security Classification

14 KEY WORDS	LINK A		LINK B		LINK C	
	ROLE	WT	ROLE	WT	ROLE	WT
X-ray Diffraction Dislocations Inclusions Precipitates Stacking faults						

INSTRUCTIONS

1. **ORIGINATING ACTIVITY:** Enter the name and address of the contractor, subcontractor, grantee, Department of Defense activity or other organization (*corporate author*) issuing the report.

2a. **REPORT SECURITY CLASSIFICATION:** Enter the overall security classification of the report. Indicate whether "Restricted Data" is included. Marking is to be in accordance with appropriate security regulations.

2b. **GROUP:** Automatic downgrading is specified in DoD Directive 5200.10 and Armed Forces Industrial Manual. Enter the group number. Also, when applicable, show that optional markings have been used for Group 3 and Group 4 as authorized.

3. **REPORT TITLE:** Enter the complete report title in all capital letters. Titles in all cases should be unclassified. If a meaningful title cannot be selected without classification, show title classification in all capitals in parenthesis immediately following the title.

4. **DESCRIPTIVE NOTES:** If appropriate, enter the type of report, e.g., interim, progress, summary, annual, or final. Give the inclusive dates when a specific reporting period is covered.

5. **AUTHOR(S):** Enter the name(s) of author(s) as shown on or in the report. Enter last name, first name, middle initial. If military, show rank and branch of service. The name of the principal author is an absolute minimum requirement.

6. **REPORT DATE:** Enter the date of the report as day, month, year, or month, year. If more than one date appears on the report, use date of publication.

7a. **TOTAL NUMBER OF PAGES:** The total page count should follow normal pagination procedures, i.e., enter the number of pages containing information.

7b. **NUMBER OF REFERENCES:** Enter the total number of references cited in the report.

8a. **CONTRACT OR GRANT NUMBER:** If appropriate, enter the applicable number of the contract or grant under which the report was written.

8b, 8c, & 8d. **PROJECT NUMBER:** Enter the appropriate military department identification, such as project number, subproject number, system numbers, task number, etc.

9a. **ORIGINATOR'S REPORT NUMBER(S):** Enter the official report number by which the document will be identified and controlled by the originating activity. This number must be unique to this report.

9b. **OTHER REPORT NUMBER(S):** If the report has been assigned any other report numbers (either by the originator or by the sponsor), also enter this number(s).

10. **AVAILABILITY/LIMITATION NOTICES:** Enter any limitations on further dissemination of the report, other than those

imposed by security classification, using standard statements such as:

- (1) "Qualified requesters may obtain copies of this report from DDC."
- (2) "Foreign announcement and dissemination of this report by DDC is not authorized."
- (3) "U. S. Government agencies may obtain copies of this report directly from DDC. Other qualified DDC users shall request through _____."
- (4) "U. S. military agencies may obtain copies of this report directly from DDC. Other qualified users shall request through _____."
- (5) "All distribution of this report is controlled. Qualified DDC users shall request through _____."

If the report has been furnished to the Office of Technical Services, Department of Commerce, for sale to the public, indicate this fact and enter the price, if known.

11. **SUPPLEMENTARY NOTES:** Use for additional explanatory notes.

12. **SPONSORING MILITARY ACTIVITY:** Enter the name of the departmental project office or laboratory sponsoring (paying for) the research and development. Include address.

13. **ABSTRACT:** Enter an abstract giving a brief and factual summary of the document indicative of the report, even though it may also appear elsewhere in the body of the technical report. If additional space is required, a continuation sheet shall be attached.

It is highly desirable that the abstract of classified reports be unclassified. Each paragraph of the abstract shall end with an indication of the military security classification of the information in the paragraph, represented as (TS), (S), (C), or (U).

There is no limitation on the length of the abstract. However, the suggested length is from 150 to 225 words.

14. **KEY WORDS:** Key words are technically meaningful terms or short phrases that characterize a report and may be used as index entries for cataloging the report. Key words must be selected so that no security classification is required. Identifiers, such as equipment model designation, trade name, military project code name, geographic location, may be used as key words but will be followed by an indication of technical context. The assignment of links, rules, and weights is optional.